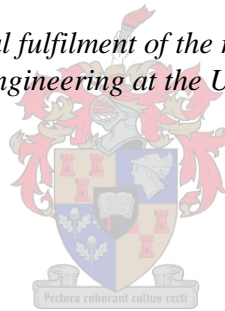


The behaviour of Strain-hardening cement composites under biaxial compression

by
Katiso Tokoloho Molapo

*Thesis presented in partial fulfilment of the requirements for the degree
Master of Science in Engineering at the University of Stellenbosch*



Supervisor: Prof. Gideon van Zijl
Faculty of Engineering
Department of Civil Engineering

December 2010

DECLARATION

By submitting this thesis electronically, I declare that the entirety of the work contained therein is my own original work, that I am the owner of the copyright thereof (unless to the extent explicitly otherwise stated) and that I have not previously in its entirety or in part submitted it for obtaining any qualification.

Katiso Tokoloho Molapo

NAME OF CANDIDATE

SIGNATURE OF CANDIDATE

22th day of November 2010

Copyright © 2010 Stellenbosch University

All rights reserved

SUMMARY

Reinforced concrete is susceptible to cracking. This makes it less durable than it would be had it been crack-free. Ingress of harmful substances into reinforced concrete through cracks – which causes corrosion of steel – is not desirable. This can be mitigated by the use of fibre reinforced-concretes or mortars showing strain hardening properties accompanied by improved ductility and multiple cracking under tensile loading. Such materials are called Strain-hardening cementitious composites (SHCC's).

At Stellenbosch University, work has been done in previous years on SHCC to determine its behaviour under various loading conditions. Some of the aspects of the material that have been studied are the behaviour under uni-axial tensile loading, uni-axial compression and shear. The behaviour of SHCC under biaxial stresses was investigated to enable the prediction of the material behaviour under complex stress conditions.

Square plate specimens of nominal dimensions 100 x 100 x 20 mm were cast and subjected to biaxial compressive loading at stress path angles of 0° , 15° , 30° and 45° ; which were equivalent to vertical/horizontal stress ratios of 0/1, 0.27/1, 0.58/1 and 1/1 respectively, at ages 23 to 33 days. Comparisons were made between specimens tested using steel platens and those tested using Vesconite sheets. Those tested using Vesconite yielded lower failure stresses. Vesconite was used to reduce the restraining effect of the frictional force between the specimens and the steel platens.

Poisson's ratios were calculated for specimens tested using steel and those tested using Vesconite. The values for Vesconite were found to be higher than for steel. Additionally, the values for the uni-axial case were different from those obtained for other stress ratios. This could have been due to the assumption made that plane stress was realised and that Elastic moduli in tension and in

compression was the same. The possibility of the existence of a triaxial stress state could render the calculated Poisson's ratios incorrect.

Shear slip type failure accompanied by wedging was observed. Vertical to near diagonal cracks were evident on the front faces of the specimens for the stress path angles of 0° to 45° respectively. The observed crack patterns showed closely spaced multiple micro-cracking on the narrow edges of specimens indicating Strain-hardening behaviour. The stress-strain curves also showed a slight indication of strain-hardening where tensile strains were measured.

OPSOMMING

Gewapende beton is vatbaar vir krake. Dit maak dit minder duursaam as wanneer dit kraak-vry is. Instroming van skadelike stowwe in gewapende beton deur middel van krake - wat korrosie van staal veroorsaak - is nie wenslik nie. Dit kan verbeter word deur die gebruik van veselversterkte beton of mortel wat vervormingsverharding eienskappe *toon*, vergesel deur verbeterde rekbaarheid en veelvuldige krake onder trekspanning. Sulke materiaal word Strain-hardening cementitious composites (SHCC's) genoem.

Die Universiteit Stellenbosch, het in vorige jare werk gedoen om SHCC se gedrag te bepaal onder verskillende belastingstoestande. Sommige van die aspekte van die materiaal wat bestudeer is, is gedrag onder uni-aksiale trek, uni-aksiale druk en skuif. Die gedrag van SHCC onder biaksiale spannings is ondersoek om voorspelling van materiaalgedrag onder komplekse spanningstoestande moontlik te maak.

Vierkantige plaat monsters van nominale dimensies 100 x 100 x 20 mm is gemaak en aan biaksiale drukkragte onderwerp, met spanningspad hoeke van 0° , 15° , 30° en 45° ; wat soortgelyk is aan die horisontale spanning verhoudings van 0/1, 0.27/1, 0.58/1 en 1/1 onderskeidelik, op ouderdomme 23-33 dae. Vergelykings is getref tussen monsters getoets met staal plate en diegene getoets word met Vesconite plate. Die proefstukke getoets met Vesconite het laer falingsspannings opgelewer. Vesconite is gebruik om die uitwerking van die wrywingskrag tussen die monsters en die staal plate te verminder.

Poisson se verhouding is bereken vir die staal en Vesconite monsters afsonderlik. Daar is gevind dat die Vesconite waarde hoër was as die vir staal. Daarbenewens het die waardes vir die uni-aksiale geval, verskil van dié vir ander spanningsverhoudings. Dit kan wees as gevolg van die aanname van vlakspanning en dat die Elastiese moduli in druk en in trek dieselfde is. Die

moontlikheid van die bestaan van 'n drie-dimensionele spanningstoestand, kan beteken dat die berekende Poisson's verhoudings onakkuraat is.

Skuif-glip tipe falings, vergesel deur vaswigting is waargeneem. Vertikale tot feitlik diagonale krake is duidelik sigbaar op die voorkant van die monsters vir spanningspadhoeke van $0-45^{\circ}$ onderskeidelik. Die waargeneemde kraakpatrone het nou gespasieerde, veelvuldige mikro-krake op die smal randte van die monsters, wat dui op vervormingsverharding. Die spanningsvervormingskurwes het ook effense aanduidings getoon van die vervormingsverharding waar trekvervorming gemeet is.

ACKNOWLEDGEMENTS

I would like thank the staff of the Structural division of the Civil Engineering department at Stellenbosch University for the continuous help and support. In particular, I would like to thank Amanda de Wet, Natalie Scheepers, Charlton Ramat, Arthur Layman, Dion Viljoen, Johan van der Merwe, Adriaan Fouche and Billy Boshoff.

I would also like to thank the following students: Willie Swanepoel, Christo Adendorff and Francis Labrousse.

I thank my colleague and friend Daniel Kraal for translating the summary from English to Afrikaans.

I would like to thank my employer Infraset for their financial support and allowing me time from work to do experiments.

Last, I would like to thank my supervisor Gideon van Zijl for guiding me through this research project, for his patience and for always being available when help was needed.

CONTENTS

	Page
DECLARATION	i
SUMMARY	ii
OPSOMMING	iv
ACKNOWLEDGEMENTS	vi
LIST OF FIGURES	x
LIST OF TABLES	xiii
1 INTRODUCTION	
1.1 Overview	1
1.2 Objective of the study	3
1.3 Layout of Thesis	3
1.4 Background Study and Literature Review	4
2 PROPERTIES OF FRC	
2.1 Introduction	7
2.2 Classification by strength	7
2.3 Classification by particle size	8
2.4 Behaviour of SHCC in Tension	8
2.5 Behaviour of SHCC in Compression	9
2.6 Behaviour of SHCC in Shear	9
2.7 Applications of FRC	9
2.8 Conclusion	10
3 EXPERIMENTAL DESIGN	
3.1 Introduction	11
3.2 Specimen Size and Geometry	11
3.2.1 Size	11
3.2.2 Geometry	12

3.3	Loading Platens, Brushes and Vesconite	20
3.4	Conclusion	26
4	EXPERIMENTAL PROGRAMME	
4.1	Introduction	28
4.2	Materials	28
4.2.1	Ordinary Portland Cement (CEM1-42.5N)	28
4.2.2	Fly ash	29
4.2.3	Fine sand	29
4.2.4	Super-plasticizer	29
4.2.5	Viscous agent	29
4.2.6	Fibres	30
4.3	Mixing and Casting of Specimens	31
4.3.1	Mix design	31
4.3.2	Apparatus	31
4.3.3	Batching procedure	32
4.3.4	Casting of specimens	33
4.4	Testing of Specimens	40
4.4.1	Biaxial specimens	40
4.4.2	Cylindrical specimens	48
4.4.3	Dumbbell specimens	50
4.4.4	Cubes	52
4.5	Conclusion	53
5	EXPERIMENTAL RESULTS	
5.1	Introduction	54
5.2	Cylindrical Specimens	54
5.3	Dumbbell Specimens	58
5.4	Cubic Specimens	60
5.5	Square biaxial Plate Specimens	62
5.6	Stress-strain relationships	66
5.7	Poisson's ratio	70

5.8	Conclusion	74
6	ANALYSIS AND DISCUSSION OF RESULTS	
6.1	Introduction	76
6.2	Failure Envelope	76
6.3	Biaxial Stress-strain Relationships	77
6.4	Observed failure patterns	78
6.5	Conclusion	81
7	RECOMMENDATIONS AND CONCLUSIONS	
7.1	Introduction	82
7.2	Observations	83
7.3	Recommendations	83
7.4	Conclusions	84
	REFERENCES	86
	BIBLIOGRAPHY	88
	APPENDICES	
A	SHCC FE MODELS SHOWING SHEAR STRESSES	90
B	STRESS-STRAIN CURVES FOR SHCC IN DIRECT TENSION	92
C	STRESS-STRAIN CURVES FOR SHCC IN DIRECT COMPRESSION	94
D	BIAXIAL RESULTS: GRAPHS OF VERTICAL LOADS AGAINST HORIZONTAL LOADS	96
E	BIAXIAL RESULTS: LOAD-DISPLACEMENT CURVES (INSTRON)	98
F	BIAXIAL TEST SETUP (PHOTOGRAPH)	100

LIST OF FIGURES

Figure	Page
1.1 Interaction of constituents for ECC	2
2.1 Typical tensile stress-strain curve for SHCC and Normal FRC	8
3.1 Nominal dimensions of the biaxial test specimen	12
3.2 Biaxial FEA models a) without chamfers and b) with chamfers	13
3.3 Free body diagram of FEA model	15
3.4 Effect of chamfer width on normal stresses along edge 1	16
3.5 Effect of chamfer width on normal stresses along edge 2	16
3.6 Dimensions of the biaxial SHCC specimen in millimetres	17
3.7a Normal stresses of model without chamfers (Diana 9.3)	18
3.7b Normal stresses of model with 1 mm chamfer (Diana 9.3)	18
3.7c Normal stresses of model with 2 mm chamfer (Diana 9.3)	18
3.7d Normal stresses of model with 2.5 mm chamfer (Diana 9.3)	19
3.7e Normal stresses of model with 3 mm chamfer (Diana 9.3)	19
3.8 Specimen loaded through solid steel platens increasing strength due to friction	20
3.9 Specimen loaded through steel loading brushes to reduce friction	21
3.10 Brush filament a) under compressive load P_{crit} and b) in bending due to δ	22
3.11 Critical loads and bending stresses for varying lengths of brush filament	23
3.12 Loading brushes a) prior to testing, b) as they are damaged, and c) after the damage has occurred	25
4.1 Dry raw materials for SHCC (Cement, Fly ash, PVA fibres, Philippi sand and Aqua beton	30
4.2 Biaxial test specimen mould	34
4.3 Cylindrical specimen mould	34
4.4 Dumbbell specimen mould with lid	34
4.5 Two biaxial specimen moulds on vibrating table	36

4.6	Casting of Cylindrical specimens	37
4.7	Casting of Dumbbell specimens	38
4.8	Dimensions of square specimens taken	40
4.9	Biaxial test frame	41
4.10	Illustration of applied load ratios	42
4.11	Biaxial test setup showing bearing system detail	43
4.12	Vesconite between loading platens and specimen to reduce friction	44
4.13	Preparation of speckle pattern for deformation measurement	45
4.14	Layout of Biaxial test equipment (cameras and specimen in plan view)	45
4.15	ARAMIS sections in global coordinate system	47
4.16	Apparatus for Cylindrical specimens	48
4.17	Apparatus for Dumbbell specimens	50
4.18	Zwick Z250 testing machine, Spider8 console and PC for Catman software	52
5.1	Mean compressive strengths of Cylindrical Specimens	56
5.2	Typical Load-displacement curve for Cylindrical Specimens	57
5.3	Mean tensile strengths of Dumbbell Specimens	59
5.4	Typical Load-displacement curve for Dumbbell Specimens	60
5.5	Mean compressive strengths of Cubic Specimens	62
5.6a	Normalised Biaxial stress envelope (using Cylinder strengths)	64
5.6b	Normalised Biaxial stress envelope (using Vesconite uni-axial strength)	66
5.7	Sections used for calculating strains	67
5.8	Stress-strain relationships for specimens loaded using steel platens	69
5.9	Stress-strain relationships for specimens loaded using Vesconite	69
5.10	Vertical strain against horizontal strain for specimens tested using steel	73
5.11	Vertical strain against horizontal strain for specimens tested using Vesconite	74
A1	Shear stresses of model without chamfers (Diana 9.3)	90

A2	Shear stresses of model with 1 mm chamfer (Diana 9.3)	90
A3	Shear stresses of model with 2 mm chamfer (Diana 9.3)	91
A4	Shear stresses of model with 2.5 mm chamfer (Diana 9.3)	91
A5	Shear stresses of model with 3 mm chamfer (Diana 9.3)	91
B1	Tensile stress-strain curves for Dumbbells from batch 1	92
B2	Tensile stress-strain curves for Dumbbells from batch 2	92
B3	Tensile stress-strain curves for Dumbbells from batch 3	93
B4	Tensile stress-strain curves for Dumbbells from batch 4	93
C1	Compressive stress-strain curves for Cylinders from batch 1	94
C2	Compressive stress-strain curves for Cylinders from batch 2	94
C3	Compressive stress-strain curves for Cylinders from batch 3	95
C4	Compressive stress-strain curves for Cylinders from batch 4	95
D1	Typical graph of vertical force vs horizontal force for stress ratio of 0 (0^0)	96
D2	Typical graph of vertical force vs horizontal force for stress ratio of 0.27 (15^0)	96
D3	Typical graph of vertical force vs horizontal force for stress ratio of 0.58 (30^0)	97
D4	Typical graph of vertical force vs horizontal force for stress ratio of 1.0 (45^0)	97
E1	Typical Load-displacement curve for stress ratio of 0 (0^0)	98
E2	Typical Load-displacement curve for stress ratio of 0.27 (15^0)	98
E3	Typical Load-displacement curve for stress ratio of 0.58 (30^0)	99
E4	Typical Load-displacement curve for stress ratio of 1.0 (45^0)	99
F1	Picture of biaxial setup	100

LIST OF TABLES

Table	Page
3.1 Applied distributed loads for FEA models	14
3.2 Comparison between brushes used	22
4.1 SHCC mix proportions	31
4.2 Loading rates for biaxial tests	42
5.1 Results obtained from testing of Cylindrical specimens	55
5.2 Summary of results obtained from Compressive tests	56
5.3 Results obtained from testing of Dumbbell specimens	58
5.4 Summary of results obtained from Tensile tests	59
5.5 Results obtained from testing of Cubic specimens	61
5.6 Summary of results obtained from crushing of cubes	62
5.7 Summary of Biaxial test results	63
5.8 Expressions for strains for specimens tested using steel	72
5.9 Expressions for strains for specimens tested using Vesconite	72
6.1 Typical crack patterns	80

CHAPTER 1

INTRODUCTION

1.1 OVERVIEW

Concrete is one of the most commonly used man-made construction materials in the world due to it being versatile and having a good track record. It has been used by some ancient civilisations such as the Egyptians and the Romans, who used it without reinforcing steel (Wikipedia, 2010). In modern day, concrete is often used with reinforcing steel bars to enhance its tensile properties. However, reinforced concrete is susceptible to cracking. This cracking makes it less durable than it would be had it been crack-free. Ingress of harmful substances into reinforced concrete through cracks, which causes corrosion of steel, is not desirable and can be mitigated by the use of fibre reinforced-concretes or mortars showing strain-hardening properties accompanied by improved ductility and closely spaced multiple cracking under simple tensile loading. These materials have acquired the name *Strain-hardening cement composites* (**SHCC**).

SHCC falls under a family of fibre-reinforced concretes (FRC) named Engineered Cement-based composites (ECC). They are designed by careful integration of raw materials, manufacturing process, micromechanics and intended structural performance of the structural element in which they are to be used as seen in figure 1 (Li, 2002). In SHCC, these components are integrated in such a way that the resulting material exhibits metal-like properties by being able to carry increased loading after the occurrence of the first crack. Contrary to normal reinforced concrete, which forms few wide cracks, cracks in SHCC are numerous and very small in width. This is a good characteristic in that ingress of harmful substances into the reinforced concrete element can be minimised or eliminated. Maalej and Li (1995) showed in their study, in which

they compared reinforced concrete beams without ECC and those with ECC, that strain-hardening ECC's are good in controlling cracks and in keeping their widths below design codes requirements under service loads.

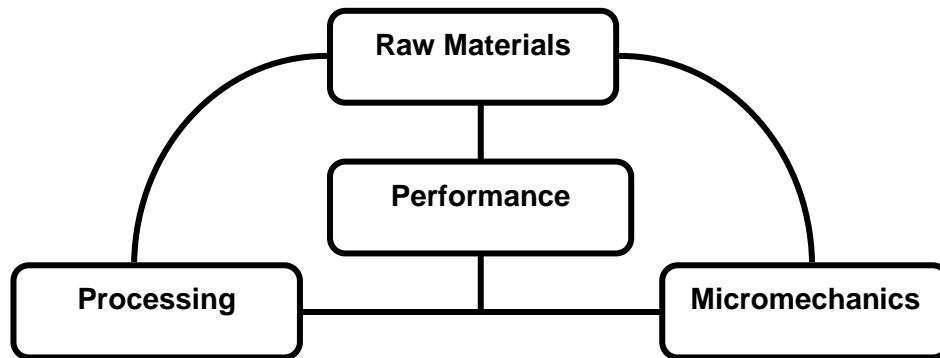


Figure 1.1: Interaction of constituents for ECC.

At Stellenbosch University, work has been done on SHCC material, and the following aspects have been studied: behaviour under simple uni-axial tensile stress; time-dependant behaviour such as creep and drying shrinkage; behaviour in shear; behaviour in bending; feasibility of the use in extrusion applications and bond strengths of overlays applied to different concrete substrates for repair applications. Computational models have also been developed to predict behaviour under simple uni-axial stresses.

However, at Stellenbosch University, the behaviour under biaxial stresses has not been studied and it is not known what the behaviour would be under complex stress conditions. In many instances where materials are used in structures, they are not only utilized to perform under simple uni-axial tension, uni-axial compression or pure bending; but are subjected to combinations of these functions in complex ways. One example is when the material is subjected to shear stresses in slabs and bridge decks. Shear is a clear manifestation of a biaxial stress state.

1.2 OBJECTIVE OF THE STUDY

The purpose of this study is to determine the behaviour of SHCC under biaxial stresses through physical testing. For other materials such as concrete and structural steel, provisions have been made in codes of practice by means of Yield or Limit Criteria to estimate behaviour under complex stresses. When using Yield criteria to predict behaviour, only simple uni-axial information (ie. stresses or strains) is needed. This is due to the ease with which uni-axial tests can be performed on materials as opposed to biaxial or triaxial tests. The biaxial test results obtained in this study will enable prediction of complex behaviour from simple uni-axial information. This research work was limited to biaxial compression only.

1.3 LAYOUT OF THESIS

This thesis consists of seven chapters. Chapter 1 is an introductory one in which information forming background to this research and literature review are discussed.

In chapter 2, the reader is introduced to the SHCC material by discussing its known properties and potential applications. Distinctions are made between different types of fibre reinforced concretes and mortars by strength, average aggregate particle size and intended performance. Furthermore, the behaviour of SHCC under simple uni-axial tensile loading and in shear is discussed.

In Chapter 3, the design of experiments is described. The reasons that led to the choice of the size and geometry of the biaxial test specimen are presented. This entailed the analyses of SHCC models using the FEA software Diana (version 9.3). Additionally, due the tendency of the solid steel loading platens to increase the specimen strength as a result of the frictional force between the

surface of the loaded specimen and loading platens, an investigation into the use of solid steel platens, steel loading brushes and Vesconite was undertaken.

Presentations of the Experimental Programme and results are made in chapters 4 and 5 respectively. In chapter 4, the following are discussed: the materials used to make the specimens, different types of specimens that were used in the study, the mixing and casting procedure, and the testing of specimens. The results obtained from the tests described in Chapter 4 are presented in Chapter 5.

The analysis and discussion of results are done in Chapter 6. The biaxial failure envelopes, the stress-strain relationships and failure patterns obtained and observed from the results are discussed. The end of the thesis is marked by the observations made, recommendations and conclusions in Chapter 7.

1.4 BACKGROUND STUDY AND LITERATURE REVIEW

Reinforced concrete has been used as the major building material around the world for many years. It is because of this that it has become a well known and better understood material. Even with this understanding, reinforced concrete still has some shortcomings: that is, it is weak in tension and susceptible to attack when used in harsh environments. Researchers around the world have developed tools for practicing engineers (or users) to better understand this material. These tools are in the form of codes of practice to give guidance on the use of materials and models to predict flexural, shear, buckling, uni-axial and biaxial behaviour, for instance. As new materials, ECC's and hence SHCC, will also have to be investigated to better their understanding.

In the early 1990's, a new breed of materials called Engineered Cement-based composites (ECC's) were developed at the University of Michigan. Through

careful design that involved integration of constituents and intended performance, these materials have proved to have superior qualities to normal fibre reinforced concretes (Li, 2002). Various groups of researchers have also looked at numerous aspects of material design, such as crack width, flexural behaviour, tensile behaviour and shear to mention a few.

At Stellenbosch University, work has been done to characterize simple uni-axial tensile, shear, flexural and time-dependent (eg. creep and drying shrinkage) behaviour of SHCC. Shang (2006) investigated the testing of SHCC in shear, and the modified Iosopescu test was developed. In the same study, the shear behaviour of reinforced ECC beams was compared to that of normal reinforced concrete beams. It was found that ECC can partially replace shear reinforcement in reinforced concrete beams.

Furthermore, computational SHCC models have been developed by Boshoff and van Zijl (2007, 2009). These models can be used to predict uni-axial tension and compression, shear and time-dependent behaviour of SHCC. The behaviour under the uni-axial stresses is adequately understood while time-dependent behaviour is undergoing further investigation. For the refinement of the behaviour under shear stresses, biaxial testing of SHCC, which was done in this study for the first time, will provide the necessary experimental data.

Behaviour of plain concrete under biaxial stresses was studied by several groups: Ehm and Schneider (1985) and Kupfer et al (1973). Several authors have also studied behaviour of different types of fibre reinforced concretes under biaxial stresses. In their study, Yin et al (1990) observed that the failure mode for fibre reinforced concrete under biaxial compression was shear slip type and not tensile splitting type observed in normal concrete. They also concluded that under biaxial stresses, fibre reinforced specimens failed at higher stress due to the resistance that the fibres were providing in the out-of-plane direction.

The following chapter will be on the known properties of SHCC. This was considered essential for the understanding of succeeding chapters.

CHAPTER 2

PROPERTIES OF FRC

2.1 INTRODUCTION

The purpose of this chapter is to introduce the reader to the properties of fibre reinforced concretes (FRCs) and SHCC. The classifications of FRC with respect to strength and particle size will be made. Furthermore, the behaviour of SHCC in tension, compression and shear will be discussed. Lastly, the applications of FRC and SHCC will be discussed.

2.2 CLASSIFICATION BY STRENGTH

Fibre reinforced concrete (FRC) can be classified into three groups: those with low percentage fibre volume V_f of less than 1%; those with moderate V_f (1-3%) for improved mechanical properties, impact resistance and fracture toughness; and the third class regarded as high performance FRC (also known as HPFRCC) with strain hardening properties usually derived from moderate to high fibre content. The material for which the biaxial behaviour is to be studied falls in the second class (low to moderate fibre content).

Initially, fibre reinforcement was introduced in plain concrete to improve its tensile strength and ductility. Through careful mix design and processing of materials, it has become possible to achieve high performance with low to moderate fibre volumes ranging between 1 % to 3 % (Li, 2002). SHCC is one of these composites with moderate compressive strength of 30 MPa with considerable ductility in tension (3-7% tensile strain). Ultra-high fibre reinforced concretes (UHPFRC) have flexural strength of 25-60 MPa, very high compressive strength of 180-240 MPa and high tensile strength (van Zijl, 2007).

2.3 CLASSIFICATION BY PARTICLE SIZE

Classification of fibre reinforced composites can also be made by aggregate particle size. Distinctions are made between fibre reinforced cements, fibre reinforced mortars and fibre reinforced concretes based on particle size of the aggregate used. For certain applications and intended performance of the hardened composite it is required that the matrix be made up of fine material. SHCC, which is very ductile accompanied by strain hardening and good crack control behaviour also requires such fine grained matrix.

2.4 BEHAVIOUR OF SHCC IN TENSION

In the early 1990's, a new breed of FRCs called ECC was developed. These materials behave in different ways from normal concrete. After the occurrence of the first crack, the material continues to form closely spaced multiple micro-cracks until failure occurs, when subjected to tensile loading as shown in figure 2.1. Also built into this property is ductility. Strain hardening ECC has strain capacity of 3-7% in tension and unlike normal FRC (figure 2.1), this is achieved with fibre content of about 2 % by volume (Li, 2002). The high ductility is achieved by careful material design (ie. by optimization of the microstructure) using models that account for interaction of fibre, matrix and interface (see figure 1.1).

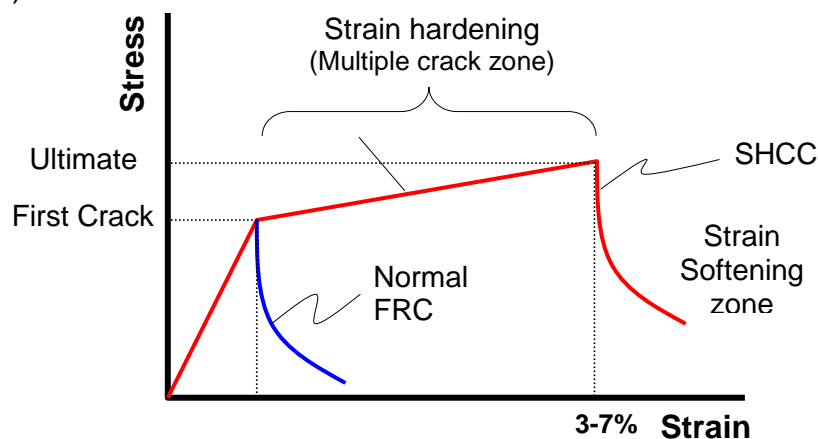


Figure 2.1 Typical tensile stress-strain curve for SHCC and Normal FRC

2.5 BEHAVIOUR OF SHCC IN COMPRESSION

The behaviour of normal concrete or mortar under compressive loading is not influenced very much by inclusion of fibres. While the inclusion of low to moderate fibre volumes can reduce bleeding, plastic shrinkage and settlement cracking in FRCs, care must be taken to control the amount of fibres used as this is known to entrain air into the composite. Entrained air has an effect of reducing the compressive strength and stiffness of the hardened FRC and hence SHCC material. SHCC does not show significant strain hardening behaviour in compression.

2.6 BEHAVIOUR OF SHCC IN SHEAR

Results obtained from experiments done on SHCC indicate that the material had improved ductility in shear (van Zijl, 2007). Multiple cracking was also evident for fibre volumes equal to or greater than 2%. This shows that even in shear, ingress of harmful substances can be minimised to ensure durability of the structural element in which SHCC is to be used. Additionally, it was found that the shear strength of SHCC exceeded its direct tensile strength.

2.7 APPLICATIONS OF FRC

The applications of FRCs can be classified into structural and non-structural ones. For the latter, the aim is to improve the performance of the hardened material with respect to aspects such as plastic shrinkage cracking, drying shrinkage, replacement of crack distribution steel in slabs, impact resistance and repairing of damaged concrete.

Structural applications of FRC include soil stabilisation, permanent formwork to be used in composite construction, various kinds of fibre boards used for dry walling or roofing, high performance bridge decks and high energy dissipation for earthquake prone regions.

2.8 CONCLUSION

The general properties of FRCs have been discussed. Classifications by strength and particle size were described. The behaviours of SHCC under tensile loading, compressive loading and in shear were also discussed. Lastly, the applications of FRC were separated into structural and non-structural ones. The following chapter will be on the design of experiments.

CHAPTER 3

EXPERIMENTAL DESIGN

3.1 INTRODUCTION

In this part of the thesis, focus is placed on the design of the experiments. It will be shown how the commercial finite element software Diana (version 9.3) was used to conduct Finite Element Analyses (FEA's) with the aim of selecting the geometry of biaxial specimens. The reasons that led to the choice of Vesconite over steel brushes and Teflon to reduce the restraining effect of the frictional force between steel platens and the specimen to be tested are also discussed.

The SHCC specimens to be used for biaxial tests were square plates (figure 3.1). Due to the likelihood of the loading platens in perpendicular directions to bear on one another during simultaneous application of vertical and horizontal compressive loads, it was decided to introduce chamfers at the corners of the specimens (figure 3.2). These chamfers were to help leave spaces between perpendicular platens. FEA's were conducted to investigate the effect of this change in geometry on the stresses and strains within the model.

3.2 SPECIMEN SIZE AND GEOMETRY

3.2.1 Specimen Size

In the applications for which strain-hardening cement composites (SHCC's) are to be used, it will be in thin layers. For example, in repair works or to protect reinforced concrete members. The plates of SHCC specimens to be tested under biaxial stress conditions were of nominal dimensions 100 x 100 x 20 mm. Other researchers have used 200 x 200 x 50 mm (Kupfer et al. 1973) and 150 x 150 x 40 mm (Hussein et al. 2000) for plain concrete. The compressive strength

of the SHCC material to be used was 30MPa. The amount of force required to cause failure of the two specimen sizes, namely 300 kN and 180 kN respectively for the 200 x 200 x 50 mm and 150 x 150 x 40 mm size specimens could be provided by the 500 kN hydraulic jacks available at Stellenbosch University. However, the testing frame stiffness required for such large forces was prohibitive. The required force to cause failure of a 30 MPa, 100 x 100 x 20 mm specimen is 60 kN.

The thickness of 20 mm was also decided upon because it was found desirable for ensuring that, during casting, the fibres were aligned in the plane in which the specimens were to be loaded. The plane in which the forces were to be applied is indicated by the arrows in figure 3.1. This is representative of thin layer applications.

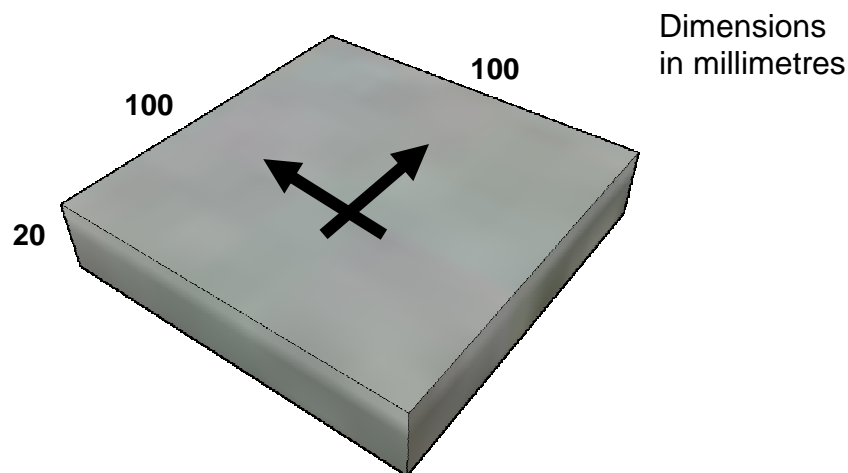


Figure 3.1 Nominal dimensions of the square biaxial test specimen

3.2.2 Geometry

Due to the potential of the perpendicular loading platens to bear on one another during biaxial testing – that is, to be in contact under biaxial compression conditions – it was decided to introduce chamfers at the corners of the

specimens (see figure 3.2). In order to find an acceptable value of the chamfer width, the effect of chamfer width on the biaxial behaviour of 100 x 100 x 20 mm SHCC Finite Element Models (FEM) was investigated. Diana (2009) FEA software (version 9.3) was used for this purpose.

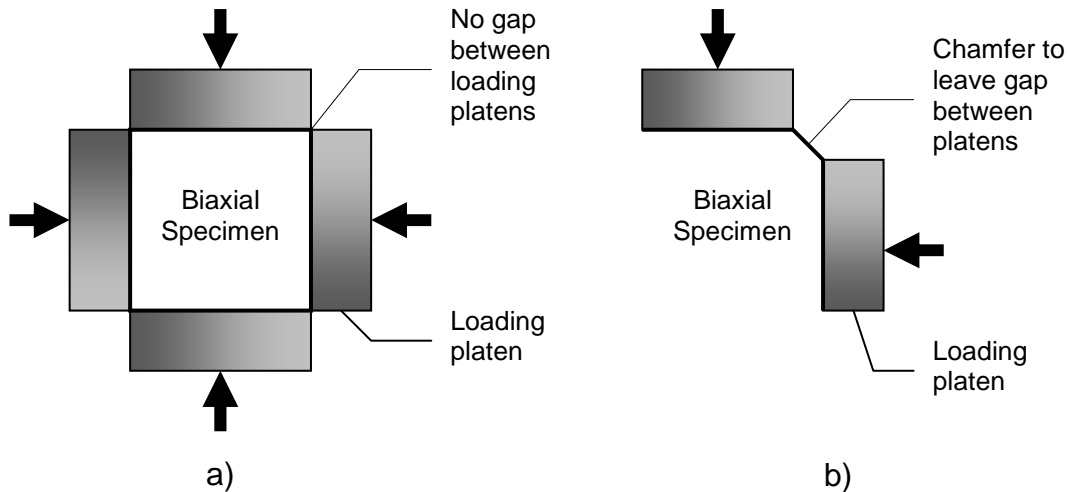


Figure 3.2 Biaxial FEA models a) without chamfers and b) with chamfers

Five models with the following chamfer widths were investigated: 0 mm (no chamfers), 1 mm, 2 mm, 2.5 mm and 3 mm. The biaxial load applied on each edge was uniformly distributed to give a stress of 30 N/mm^2 in both directions (ie. biaxial stress ratio of 1). This is equivalent to a total force of 60 kN ($\equiv 600 \text{ N/mm}$) in one direction for the model without chamfers. In order to avoid unfairness, the applied distributed loads for the models with chamfers were corrected to give the same total force of 60 kN. This is illustrated in table 3.1.

In table 3.1, it is shown that the lengths of load bearing edges decrease as the chamfer width is increased. That is, the length over which the distributed load was applied decreased with increasing chamfer width. If the distributed load of 600 N/mm was kept the same for all the models, then the total applied force would decrease as shown in column 3 of table 3.1. This problem was solved by correcting the distributed loads for each model as shown in the last column of the same table. For example, for the model with 1 mm chamfers the length of

the edge was 98 mm ($= 100 - 2 \times 1$); a distributed load of 600 N/mm results in a total force of 58.8 kN ($= 98 \times 600 \times 10^{-3}$). To correct this, the total load of 60 kN was divided by the edge length to obtain the corrected distributed load of 612.2 N/mm.

Table 3.1 Applied distributed loads for FEA models

Chamfer width (mm)	Length of edge (mm)	Uncorrected Total force (kN)	Corrected Distributed Load (N/mm)
0.0	100	60.0	600.0
1.0	98	58.8	612.2
2.0	96	57.6	625.0
2.5	95	57.0	631.6
3.0	94	56.4	638.3

The type of analysis done was plane stress analysis because it was assumed that during casting of biaxial specimens, the fibres would be aligned randomly in the plane of loading. The elements used were 8 nodes quadrilateral plane stress elements (CQ16M) and 6 nodes triangular plane stress elements (CT12M) at the chamfers. The material properties used were as follows:

- Elastic modulus, $E = 25 \text{ GPa}$;
- Poison's ratio, $\nu = 0.3$.

Furthermore, the material was assumed to be homogeneous and isotropic in the plane of the applied stresses. This assumption was valid because the casting of the specimens was going to be such that the fibres were randomly aligned in that plane.

The models were simplified by considering symmetry of the loading and that of the geometry. The supports along the lines of symmetry were such that the supported edges were restrained against movement in the direction perpendicular to it but free to move parallel to it. The free body diagram of the model is shown in figure 3.3.

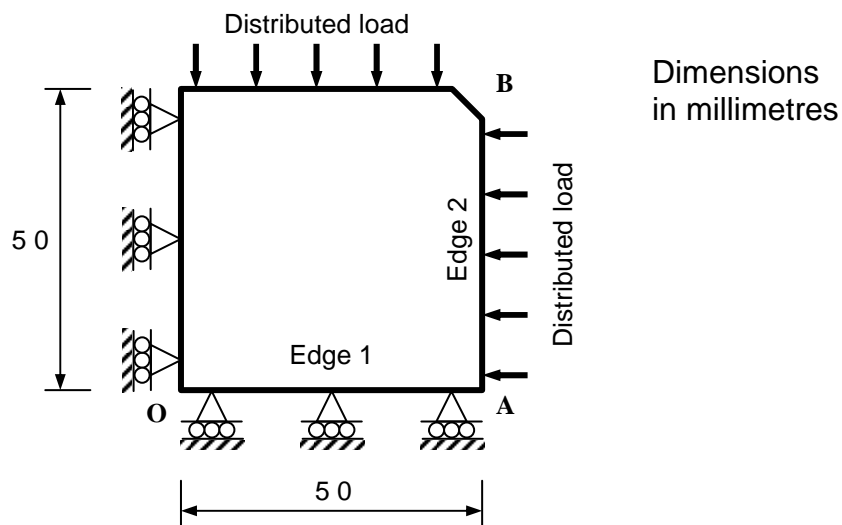


Figure 3.3 Free body diagram of FEA model

The normal stresses obtained from the analyses are presented on contour plots as shown in figure 3.7a–e. The stresses are shown by the values in the legend to the right of the contour plot in N/mm^2 . The graphs showing the stresses along edge 1 (OA) and edge 2 (AB) of the model as shown in figure 3.3 were plotted against distance measured from O-A and A-B in figure 3.4 and figure 3.5, respectively. The ordinate in figures 3.4 and 3.5 show normalised stresses; this was to make comparison of the effects of different chamfer widths easy. The stresses were normalised by dividing the values obtained from the analyses by the characteristic strength of the material, 30 N/mm^2 .

While the contour plots of the stresses still showed lack of uniformity in the vicinity of the chamfers, it was not clear what the actual values were. The

graphs in figures 3.4 and 3.5 gave very useful information in that they showed actual values and that the variation in stresses could clearly be seen.

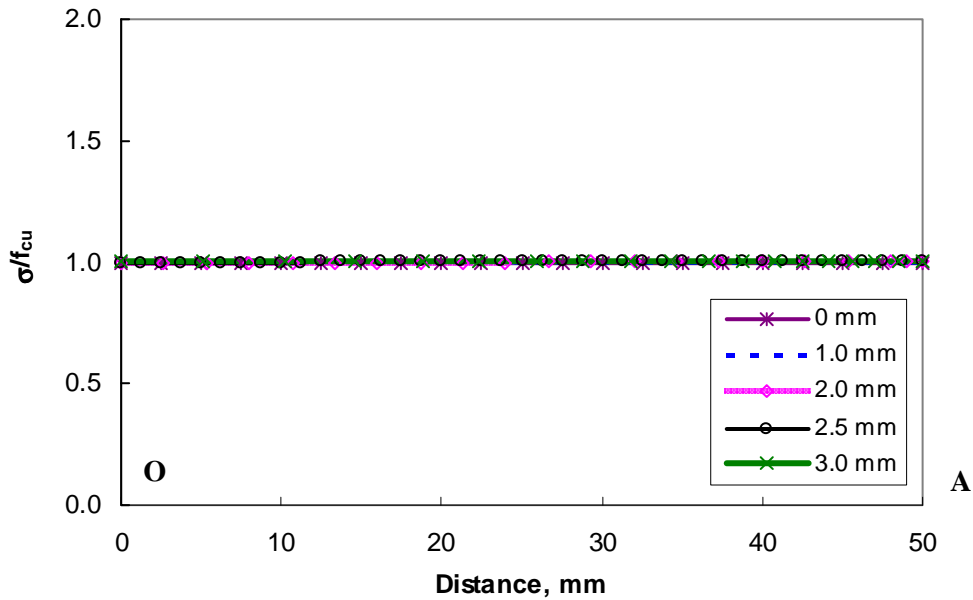


Figure 3.4 Effect of chamfer width on normal stresses along edge 1

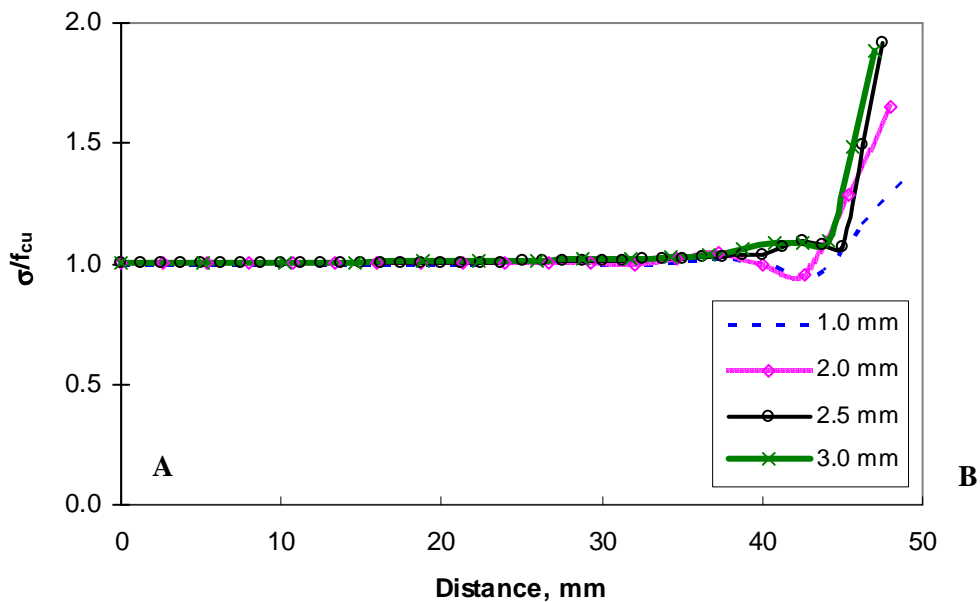


Figure 3.5 Effect of chamfer width on normal stresses along edge 2

Figure 3.4 shows no variation in the stresses along edge 1 for all the models, with the normalised stress over the entire edge being equal to unity. However,

along the edge with chamfer (edge 2), an increase in stresses in the area of the chamfers (see figure 3.5) was noticed. These were stress concentrations due to change of geometry at the chamfers. Even though the stress concentrations covered very small areas, they are not good because, in the real material, they can cause premature cracking around chamfer proximities of the specimen before the ultimate load is reached.

The normal stresses in the models with chamfers increased by 36 percent, 65 percent, 95 percent and 88 percent for models with chamfer widths of 1 mm, 2 mm, 2.5 mm and 3 mm, respectively. Although 1 mm chamfer yielded the smallest stress variations around the chamfers, it was not practical to work with because it was too small to serve the intended purpose of the chamfer. Since a 2 mm chamfer was the smallest that can realistically solve the platen contact matter, and the stress concentration factor clearly increases with increasing chamfer size, 2 mm was chosen as the width of the chamfer to be used as can be seen in figure 3.6.

A thorough study of mesh dependence must be conducted to confirm the outcome of FE models. However, this was not done in this thesis.

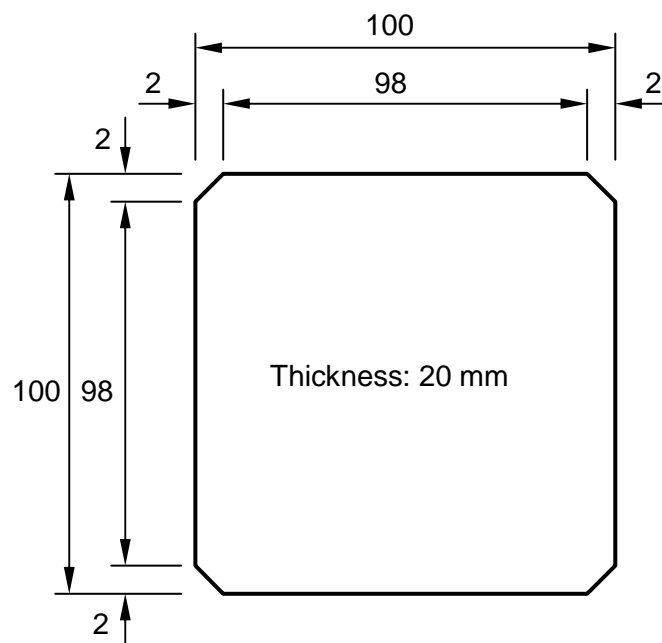


Figure 3.6 Dimensions of the biaxial SHCC specimen in millimetres

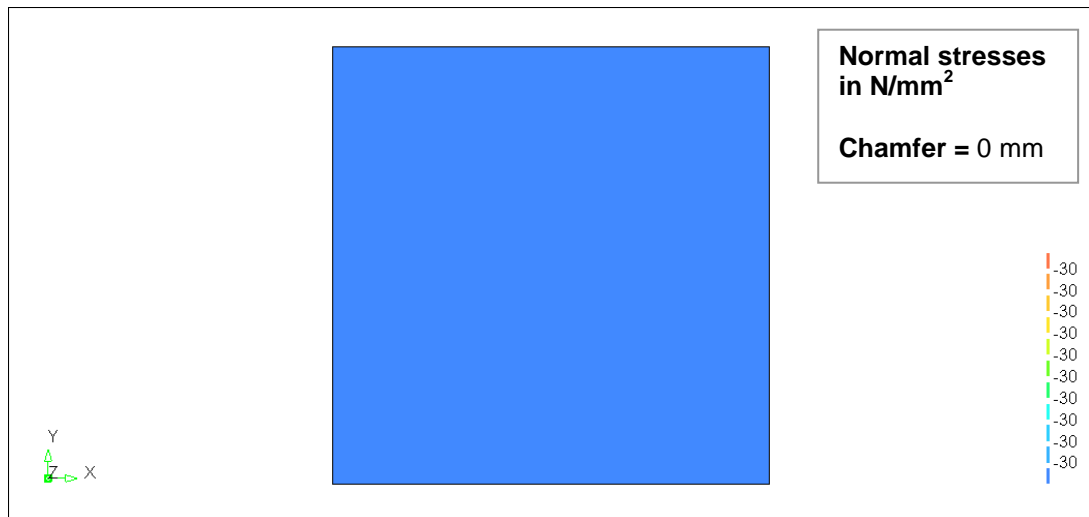


Figure 3.7a Normal stresses S_{xx} for model without chamfers (Diana 9.3)

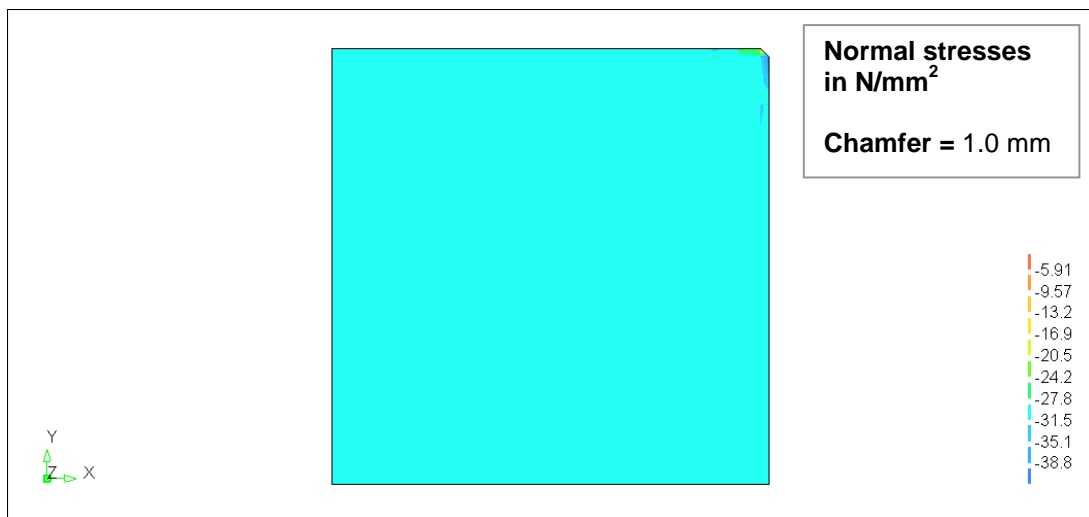


Figure 3.7b Normal stresses S_{xx} for model with 1 mm chamfer (Diana 9.3)

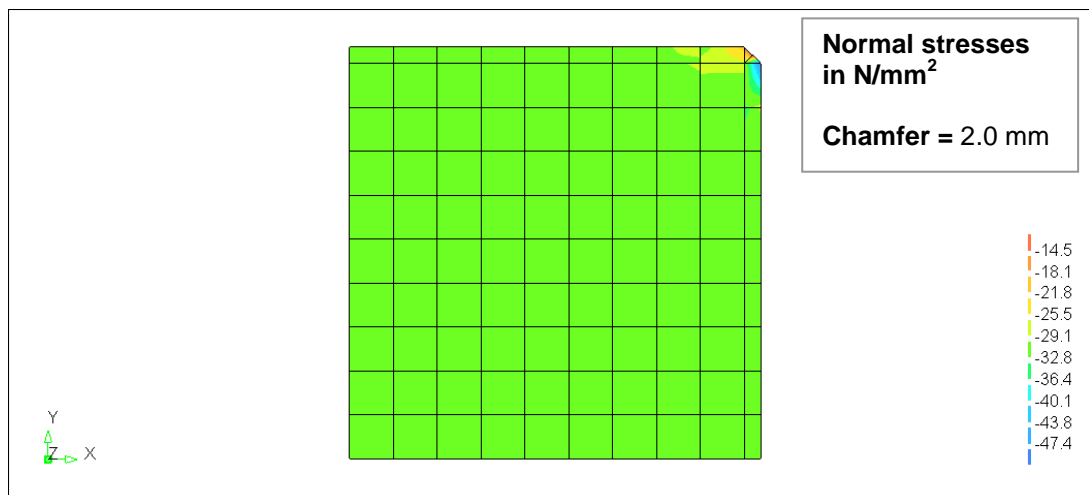


Figure 3.7c Normal stresses S_{xx} for model with 2 mm chamfer (Diana 9.3)

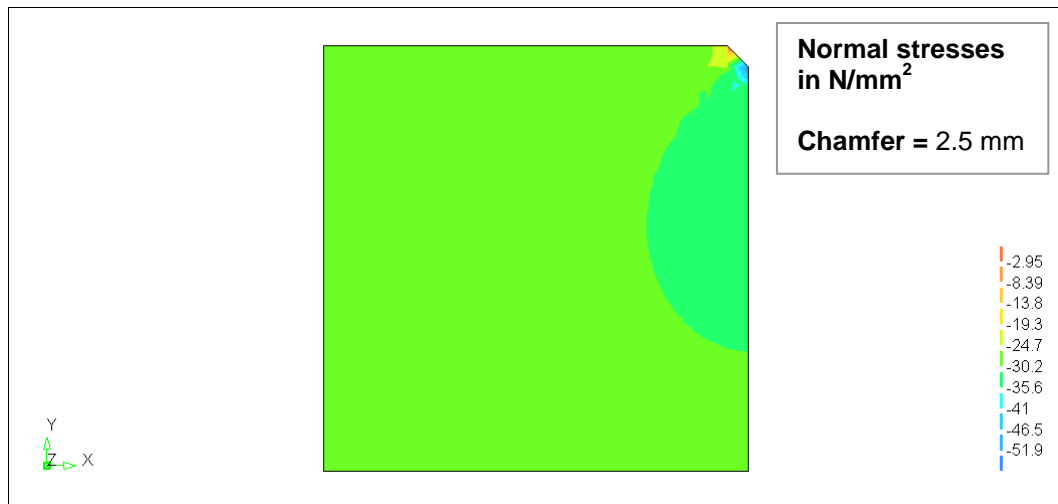


Figure 3.7d Normal stresses S_{xx} for model with 2.5 mm chamfer (Diana 9.3)

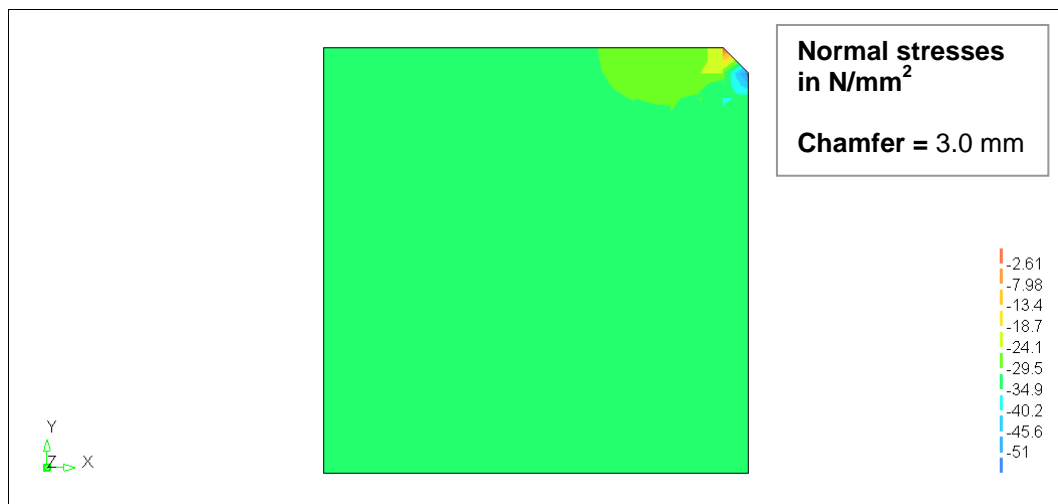


Figure 3.7e Normal stresses S_{xx} for model with 3 mm chamfer (Diana 9.3)

The contour plots of shear stresses for the five models are obtainable in the appendix section of this thesis. The shear stresses were also found to be negligibly small except around the chamfer areas.

3.3 LOADING PLATENS, BRUSHES AND VESCONITE

When tested under uni-axial compression, steel loading platens of the testing machines tend to increase the *true* strength of concrete. This is due to the restraining frictional force between the steel platens and the surface of the concrete. As a cube of concrete is compressed in one direction (uni-axial), it will shorten in the direction of the applied load and widen in the lateral direction to partially maintain its volume (see figure 3.8), due to the Poisson effect. It is this movement in the lateral direction that the friction between the steel platens and the concrete does not permit.

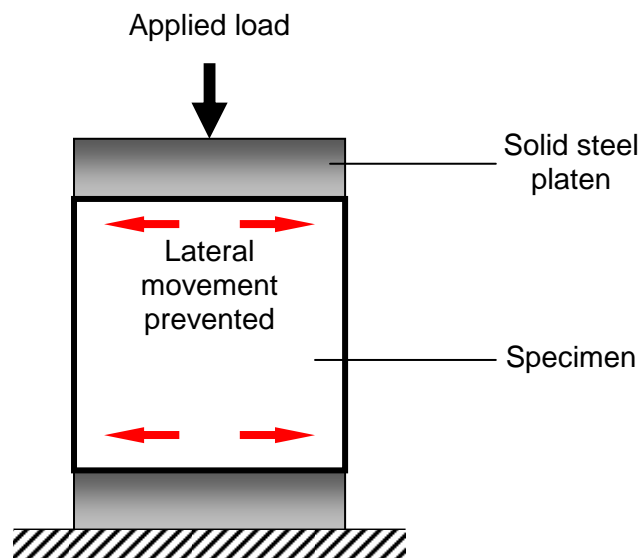


Figure 3.8 Specimen loaded through solid steel platens increasing strength due to friction.

Even though it was initially intended to use brushes to reduce the restraining effect of the frictional force between the specimen and the loading medium, 2 mm thick Vesconite sheets were used in the final experiments. However, it was decided to give information on why the use of brushes was considered.

In their study on behaviour of concrete under biaxial stresses, Kupfer and Gerstle (1973) found that the results of the strength of concrete obtained from

tests done using solid steel platens were higher than those obtained from test done using steel brushes (see figure 3.9). The reason for using the steel brushes to apply the loads was because they allow movement in the lateral direction, thereby lessening the restraining effect of the frictional force between the two surfaces in contact. Hussein and Marzouk (2000) also noticed the same pattern in their results when they conducted biaxial tests on high-strength concrete using similar kind of brushes.

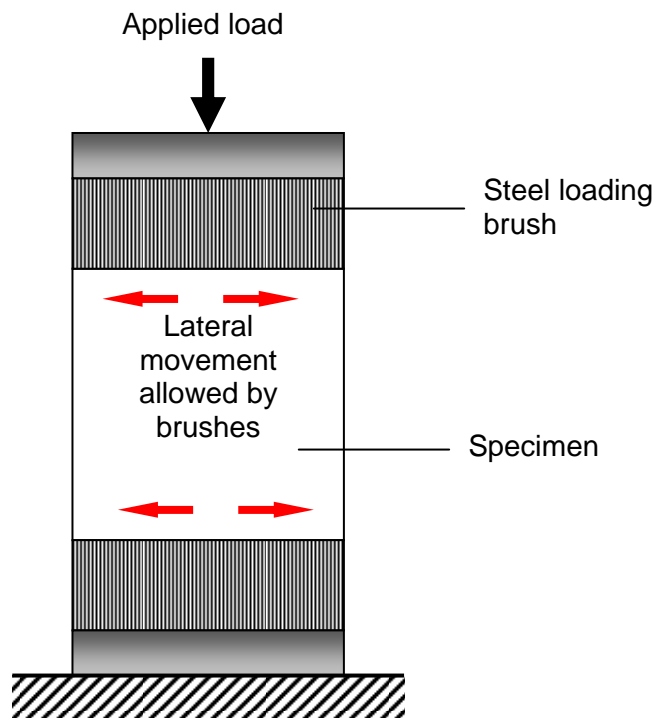


Figure 3.9 Specimen loaded through steel loading brushes to reduce friction

It was not clear how the brushes that were used by Kupfer and Gerstle were manufactured. However, Hussein and Marzouk's paper provided very clear information on the details of the brushes that they used. It was from this that guidance on the type of brushes to be used was found. Comparison between the properties of the brushes used in this study and those used by Hussein and Marzouk is made in table 3.2.

Table 3.2 Comparison between brushes used

	Hussein & Marzouk	Molapo
Type of steel	SAE 4140 steel	German no. 2312 AISI Equivalent : P20
Ultimate tensile strength (N/mm ²)	700	1000
Heat treatment	Annealing condition	Annealing condition
Brinell hardness number (BHN)	207	210
Overall dimensions (mm)	150 x 150 x 40	150 x 98.6 x 20.6
Size of filament (mm) (L x B x T)	75 x 5 x 5	100 x 5 x 5
Width of grooves (mm)	0.2	0.3

In deciding on the length of the filaments, an analysis was done in which the critical Euler buckling loads and maximum bending stresses were calculated for varying filament lengths, L . The critical loads (P_{crit}) were calculated based on fixed-free end conditions (figure 3.10 a). The maximum bending stresses for the same end conditions were calculated with the displacement δ of 2 mm at the free end (figure 3.10 b).

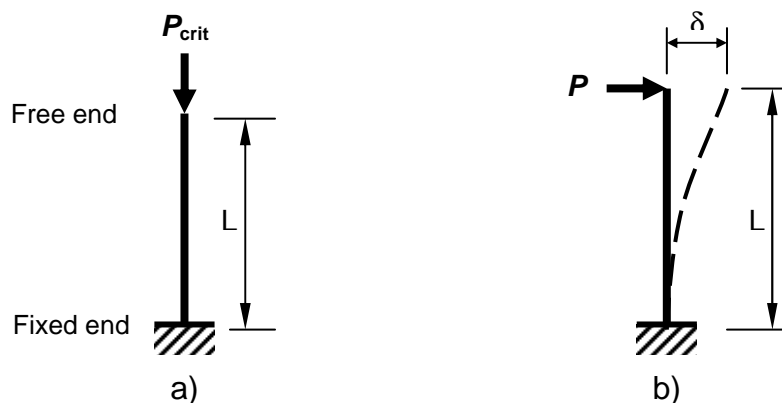


Figure 3.10 Brush Filament a) under compressive load P_{crit} and b) in bending due to δ

The results of the filament length analysis are shown in figure 3.11. The abscissa in figure 3.11 shows the length of the filament in millimetres, the left hand ordinate the critical compressive load in kilonewtons and the right hand ordinate the bending stress in MPa on logarithmic scale. The logarithmic scale was used because the two curves were lying on top of each other, thereby making it difficult for one to see the difference between them. Both curves show a decline in the critical load and bending stress with increasing filament length.

Since the SHCC material to be tested had high ultimate strain capacity of 3 to 5 percent, it was desirable to select a filament length that would result in a flexible filament and at the same time satisfying stability and strength requirements. The length of 100 mm was chosen. The critical load and bending stress corresponding to this length are 2.6 kN and 300 MPa, respectively. These two values were within the requirements of 0.79 kN per filament and 1000 MPa for the critical load and bending stress, respectively. The corresponding factors of safety against buckling and bending capacity were both 3.3. The maximum critical load of 0.79 kN was calculated by dividing the total force of 60 kN by 76 filaments (4×19).

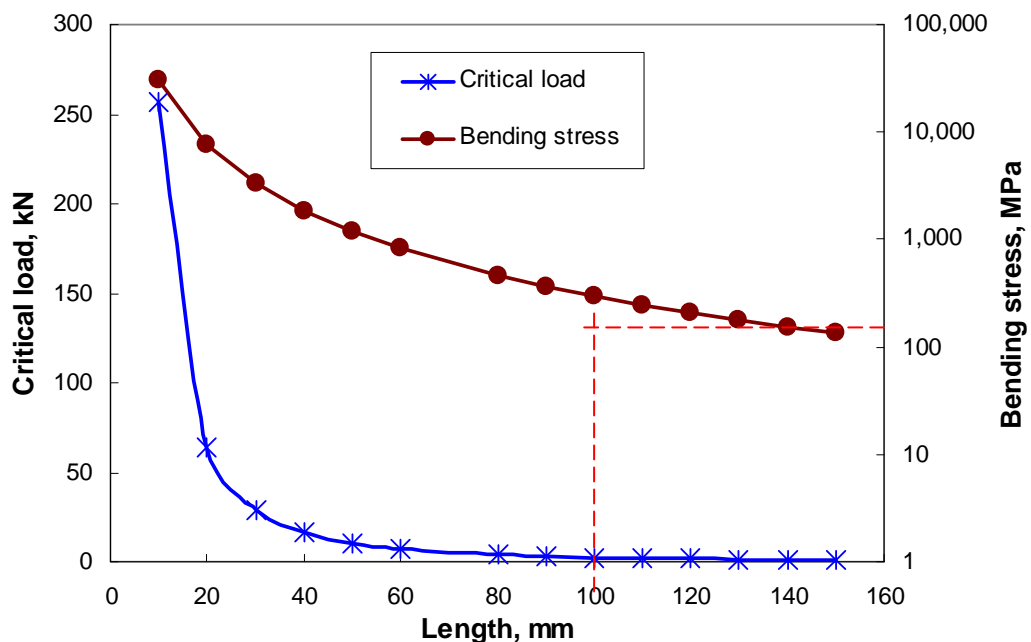
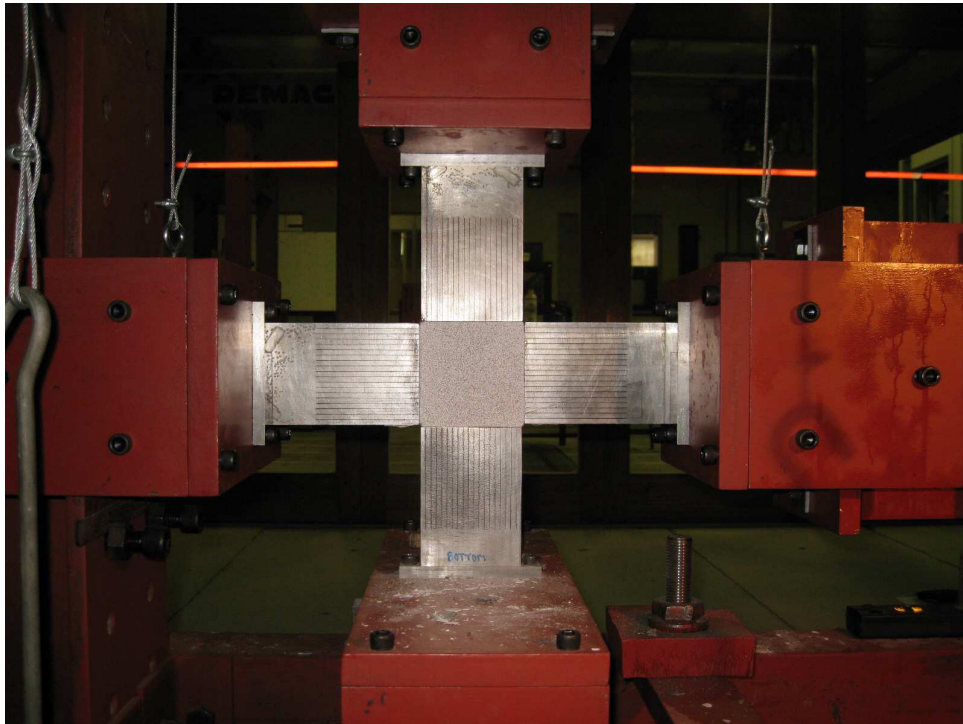


Figure 3.11 Critical loads and bending stresses for varying lengths of brush filament

Final brushes and specimen dimensions: Since the desired size of brush filaments was 5 mm by 5 mm and the specified gap between the filaments was 0.2 mm, the final overall dimensions of the brushes in cross-section were 98.6 mm wide by 20.6 mm thick. These were obtained by adding the 19 rows of filaments and their gaps (ie. $19 \times 5 + 0.2 \times 18 = 98.6$) in the width direction and 4 rows of filaments and their gaps (ie. $4 \times 5 + 0.2 \times 3 = 20.6$) in the thickness direction. The dimensions of the specimen were also changed to suit the new brush dimensions: the final specimen dimensions were 102.6 x 102.6 x 20.6 mm.

Trials using brushes: Biaxial test trials were conducted with the aim of setting control systems for the test as the new actuator system was used for the first time at Stellenbosch University to do this kind of experimentation. This involved determining the loading rates and setting limits for the actuators so that the problem of the brushes or platens touching each other as it is discussed in 3.2.2 was avoided. The two kinds of limits set in both directions were displacements and maximum compressive forces. The purpose of each limit was to trigger an event – in this case, to stop the test – once the limit was reached in order to avoid damaging the test equipment.

While the trials conducted achieved the purpose for which they were intended – to help set controls – an error occurred in which some of the brushes were damaged. The damage occurred because during one of the tests, the displacement limit for the vertical actuator was not set. This resulted in the actuator continuing to apply compressive loading onto the trial specimen beyond the displacement limit that had to trigger the end of the test thereby exceeding the critical buckling load and maximum bending stress of the brush filaments discussed previously in this section and shown in figure 3.11. This can be attributed to inadequate understanding of the actuator system which required that limits be set every time a test was carried out. The other problem of the brushes was that they clogged easily with concrete requiring to be cleaned after each test. The damaged brush is shown in figure 3.12.



a)



b)



c)

Figure 3.12 Loading brushes a) prior to testing, b) as they are damaged, and c) after the damage has occurred

Vesconite:

Although it was intended to use steel brushes to reduce the restraining effect of the frictional force between the specimen surface and the loading platens, brushes were found to be problematic. They clogged easily with crushed concrete and got damaged due to plastic deformation as explained previously. The issue of non-uniform lateral deformation, which has as secondary effect non-uniform axial force transfer, was also of concern. This meant that alternatives needed to be considered.

As alternatives to using steel brushes, thin sheets of Teflon and Vesconite were considered. Teflon is used in the construction industry as the preferred material for low friction bridge support bearings and on masonry walls supporting concrete slabs where frictional forces are to be minimised to allow lateral movement. However, the Teflon sheet available locally was found undesirable mainly due to the low stiffness. Trials indicated poor dimensional stability; since it deformed easily under compression, and splitting failure of the Teflon sheets was observed.

Vesconite, which is used as low friction material for moving machinery parts, was more dimensionally stable and much stiffer and stronger in compression than Teflon. It had compressive strength of more than the required minimum value of 30 MPa. When polished by means of sand paper, its coefficient of friction was reduced. Vesconite was therefore chosen as the low friction medium to be used instead of brushes and Teflon. The friction coefficient was not measured, but indications are in the order of 0.1, roughly one order of magnitude higher than Teflon.

3.4 CONCLUSION

The design of experiments has been discussed. The size and geometry of the biaxial specimens were decided upon using FE analyses.

Comparisons were made between steel loading platens, steel brushes, Teflon and Vesconite. The reasons that led to the choice of Vesconite over steel brushes and Teflon were explained. The following chapter describes the experimental programme.

CHAPTER 4

EXPERIMENTAL PROGRAMME

4.1 INTRODUCTION

In order to carry out experiments on SHCC, various specimens were manufactured for different purposes: 1) Dumbbell shaped specimens were made from which simple (uni-axial) tensile properties of SHCC were to be determined; 2) Cylindrical and cubic specimens were made to determine uni-axial compressive properties and; 3) Square plates of SHCC specimens were made that were to be tested under biaxial compression conditions. The tests on dumbbell specimens and cylindrical specimens were done to verify the material strengths obtained from the biaxial tests, to determine the material's Elastic moduli, E in tension and in compression, as well as the ductility characteristics in uni-axial tension and in compression. The SHCC cubes were tested to verify compressive strengths obtained for cylindrical specimens.

4.2 MATERIALS

SHCC specimens were made of mixes comprising Ordinary Portland cement (CEM1-42.5N), fly ash (FA), fine sand, Polyvinyl Alcohol (PVA) fibres, Viscous agent (CHRYSO® Aquabeton ZA), Super-plasticiser (CHRYSO® Premia 100) and water. The details of each constituent are discussed below. Further information on these materials can be found in the thesis by Shang (2006).

4.2.1 PORTLAND CEMENT (CEM1-42.5N)

The type of cement used was Ordinary Portland cement of grade CEM1-42.5N. It was used as the main binder in the SHCC mix and made up 50% of the binder.

4.2.2 FLY ASH

The Fly Ash used, also known as DuraPozz®, was supplied by Ash Resources. Since it is a waste material produced in coal power stations, it was used as a cheap filler material. It formed, together with the cement, the total binder in the mix.

In the research work preceding this one, 5% of Ground Granulated Corex Slag (GGCS) by total mass of binder was used. This quantity of GGCS has now being replaced by the same amount of fly ash. This is to say that the binder material comprised only cement and fly ash in this research.

4.2.3 FINE SAND

The fine sand used was Consol no. 2 sand. This is a silica sand of average particle size smaller than 0.3 mm. It was the only aggregate used in the mix.

4.2.4 SUPER-PLASTICIZER

The type of the super-plasticizer used was CHRYSO® *Premia 100* manufactured and supplied by Chryso South Africa. The purpose of this constituent was to improve the workability of the SHCC mix so that a uniform mix was achieved and that even distribution of fibres was ensured.

4.2.5 VISCOUS AGENT

PVA fibres in fresh SHCC mix tend to group together forming lumps. These lumps are not desirable if good strain-hardening behaviour (including closely spaced multiple micro cracks) is to be achieved. The viscous agent is an admixture that aids in dispersing the fibres so that they are evenly distributed and lumps that could create points of weaknesses are avoided.

The viscous agent used was a white methyl cellulose powder called CHRYSO® Aquabeton ZA. It was produced and supplied by Chryso South Africa.

4.2.6 FIBRES

The fibres used were made of Polyvinyl Alcohol (PVA). Their properties were as follows:

- Length = 12 mm
- Diameter = 40 μm
- Ultimate tensile strength = 1600 MPa
- E-modulus = 40 GPa
- Ultimate strain = 6 %.

Figure 4.1 below shows all the dry raw materials in weighing bowls.



Figure 4.1 Dry raw materials for SHCC (Cement, fly ash, PVA fibres, Fine sand and Viscous Agent)

4.3 MIXING AND CASTING OF SPECIMENS

4.3.1 MIX DESIGN

The mix used was the standard SHCC mix developed at Stellenbosch University. It consisted of 550 kg/m³ Portland cement (CEM1-42.5N), 650 kg/m³ Fly Ash, 550 kg/m³ Fine sand (Consol no.2), Viscous agent (0.075 % of cement), Super-plasticizer (0.4 % of cement), 26 kg/m³ of PVA fibres (2 % by volume of mix) and 395 kg/m³ water. The details of each constituent are obtainable in the previous section.

Table 4.1 SHCC mix proportions

Item	Mass Kg/m ³	Relative Density
Water	395	1.0
Cement (CEM1-42.5N)	550	3.14
Fly Ash (DuraPozz®)	650	2.3
Fine Sand (Consol no.2)	550	2.0
PVA Fibre	26	1.3
Viscous agent (CHRYSO® Aquabeton)	0.4125	1.2
CHRYSO® Premia 100	2.2	1.3

A total of five batches of SHCC were made. Only one mix could be made per day due to the limited number of biaxial specimen moulds. This means that it took five days to make the five batches.

4.3.2 APPARATUS

- 30 kg Electronic scale
- Weighing bowls
- 250 ml Glass beaker
- Small measuring cylinder
- Large measuring cylinder

- 5 L plastic bucket
- 10L Kitchen mixer
- Stopwatch
- Scraper
- Scientific calculator

4.3.3 BATCHING PROCEDURE

The different materials were mixed using the following procedure:

- **Step 1:** A 10 L Hobart mixer with 3-speeds was used. The inside of the bucket was wiped clean by means of a damp cloth; this was to ensure that the sides of the bucket do not draw water from the mix and that any deleterious substances were removed.
- **Step 2:** All the materials were weighed according to the mix design (see table 4.1). The dry materials (powdery and fibres) were weighed in bowls. The liquid ones (that is, super-plasticizer and water) were weighed in glass beaker and plastic bucket, respectively.
- **Step 3:** The fine sand was first to be added to the bucket – only half of the total quantity of sand was added at this stage.
- **Step 4:** The cement, fly ash and the viscous agent (CHRYSO® Aquabeton ZA) were then added; that is, on top of the sand.
- **Step 5:** The remaining fine sand was added.
- **Step 6:** The mixer was then started and the dry ingredients were mixed for about 1 minute at slow speed (speed 1). If uniformity was not achieved, the mixing was extended beyond 1 minute until the mix was uniform.
- **Step 7:** Water was added slowly; taking care to avoid spillage. About 500 ml of water was left to be used at a later stage – it was to be mixed with the super-plasticizer for easy dispensing of the admixture.
- **Step 8:** The wet materials were allowed to mix at a faster speed (speed 2) for about 1 minute.
- **Step 9:** the mixer was stopped and the material at the bottom of the bucket was scraped using a scraper to ensure that the unmixed material

(that which could not be reached by the arm of the mixer) was brought to the top.

- **Step 10:** The mixer was run again until the mix was uniform.
- **Step 11:** The super-plasticizer (CHRYSO® Premia 100) was mixed with the remaining water in a glass beaker and then poured into the mixer.
- **Step 12:** The PVA fibres were the last to be added. It was done slowly to avoid spillages. The mixer was allowed to run until uniformity was achieved.
- **Step 13:** The final mixing was done by hand and using the mixer. The bottom of the bucket was scrapped again (as in step 9) to bring to the top the material that could not be reached by the arm of the mixer. The mix was also checked, by hand, for lumps of fibres. The mixer was run again until all the lumps were removed.

The SHCC mix was now ready for casting. Four different types of specimens were made: Square Biaxial specimens, Cylindrical specimens, Dumbbell (also known as Dog-bone) specimens and Cubes.

4.3.4 CASTING OF SPECIMENS

Materials and Equipment:

- 2 Biaxial specimen moulds (figure 4.2)
- 1 Cylindrical mould (figure 4.3)
- 3 Dumbbell moulds (figure 4.4)
- Spanners and Allen keys (for assembling moulds)
- Scoop
- Steel trowel
- Vibrating table
- Small paint brush (for applying mould oil)
- Mould oil
- Ear plugs (for the vibrating table noise)

- Latex gloves



Figure 4.2 Biaxial test specimen mould



Figure 4.3 Cylindrical specimen mould



Figure 4.4 Dumbbell specimen mould with lid

All the moulds were cleaned by scraping off unwanted material. They were then lightly oiled with mould oil by means of a paint brush to enable easy de-moulding. For dumbbell moulds, which had parts such as dowels and lids (see figure 4.4), the parts were also oiled.

Square Biaxial specimens: Two moulds were used for biaxial specimens. Each mould had 4 compartments (see figure 4.2). This means that 8 (4 x 2) specimens were made at a time (figure 4.5).

The casting procedure for the biaxial specimens was as follows:

- The wet SHCC mix was placed at the centre of each compartment by means of a scoop; so that when levelled by vibration, the mould compartments were filled to mid height.
- The vibrating table was switched on. The mould containing the mix was vibrated to allow trapped air to escape.
- More SHCC mix was added until all the compartments were filled to just above the brim of the mould. The mould was vibrated until most of the air had escaped (that is, no air bubbles were visible).
- Excess material was then scraped off. The exposed surface of the mix was then levelled and floated to flush with the top of the mould by means of a steel trowel.
- The vibrating table was switched off and the mould removed from the table.
- The moulded specimens were allowed to stand for about 1 hour, after which final floating was done.
- The two moulds were covered by a plastic sheet and then placed in a climate room. The conditions in the room were such that the temperature was about 25⁰C and the relative humidity was 65 percent.
- The hardened specimens were removed from the moulds after 24 hours, marked to show date of cast and specimen number. They were then

placed in a curing bath to cure. The temperature of the water in the bath was about 25°C.



Figure 4.5 Two biaxial specimen moulds on vibrating table

Cylindrical Specimens: the mould for cylindrical specimens had three compartments of 50 mm diameter by 100 mm high (figure 4.3). After ensuring that the wing nuts of the mould were tightened to prevent leakage of material, the casting of the cylindrical specimens was carried out as follows:

- Each compartment was filled with wet SHCC mix to one third height;
- The mould was placed on the vibrating table;
- The vibrating table was switched on and allowed to run until air bubbles could no longer be seen;
- The previous three steps were repeated until the mould was full. That is, more material was placed in the mould in increments of a third of the height. The exception to the last layer was that it was slightly overfilled.
- Excess material was scraped off and floated flush by means of a steel trowel. See figure 4.6.
- The mould was then placed in the climate room at temperature of about 25°C and relative humidity of 65 percent.

- The hardened specimens were removed from the moulds after 24 hours and similarly marked (as the biaxial ones). They were placed in the curing bath at temperature of 25°C.



Figure 4.6 Casting of cylindrical specimens

Dumbbell specimens: these specimens are also called Dog-bones at Stellenbosch University. Each mould had one compartment, two steel dowels to go into two holes near the ends of the moulds and a lid to help with the final compaction and levelling (see figure 4.4). The two dowels were to form holes in the specimen through which it was to be mounted to the testing machine.

The casting procedure for the dumbbell SHCC specimens was carried out as follows:

- The 2 dowels were fitted into the holes of each mould.
- The mould was placed on the vibrating table.
- The mix was first placed from centre of the mould and then outwards in the direction of the wider (outer) parts of the mould. That is, from the

narrow (central) part of the mould (see figure 4.7). This was to ensure that no flaws or points of weakness are created within this narrow strip.

- The mould was vibrated during casting until it was full. Vibration continued until no bubbles were visible on the surface of the mix.
- Excess material was scraped off and floated flush with the steel trowel.
- The mould and its contents were allowed to stand for about 1 hour, after which final floating was done. The lid was then placed on the mould.
- The moulds were placed in the climate room at temperature of about 25⁰C and relative humidity of 65 percent.
- The hardened specimens were removed from the moulds after 48 hours. Please note the importance of the curing time of at least 24 hours after casting for these type of specimens because they are easily damaged if they are inadequately cured; 48 hours curing time was allowed because of the mix having slower than anticipated early strength gain rate.
- The hardened specimens were marked accordingly and then placed in the curing bath with the biaxial and cylindrical specimens.



Figure 4.7 Casting of Dumbbell specimens

Cubes: the remainder of the SHCC mix was used to cast 100 x 100 x 100 mm cubes. They were to be tested in compression.

The cubes were made as follows:

- Standard concrete cube moulds were used;
- The moulds were cleaned and oiled;
- They were filled with wet SHCC mix up to one third of the height;
- The mould was vibrated on the vibrating table until air bubbles were no longer visible;
- The mould was then filled up in third layers, while being vibrated, until it was full;
- The last layer was slightly overfilled;
- Excess material was scrapped off and floated flush using steel trowel;
- The moulds were placed in the climate room at temperature of about 25 °C and relative humidity of 65 percent.
- The hardened cubes were removed from the moulds the following day;
- They were marked to show date of cast and specimen numbers.
- They were then placed in curing bath of temperature of about 25 °C.

4.4 TESTING OF SPECIMENS

4.4.1 BIAXIAL SPECIMENS

The testing of these specimens was carried out in the Heavy structures laboratory of the Department of Civil Engineering at Stellenbosch University. A total of 32 square specimens were tested between ages 23 and 33 days under biaxial compression-compression conditions. Prior to testing, all specimens were removed from the curing bath and each one was marked numbers 1 to 4 at their corners as shown in figure 4.8 below. Their masses and dimensions were determined in grams to the nearest 0.1 gram using an electronic scale and in millimetres to the nearest 0.05 mm respectively. The marking of the corners was done to ensure that the method used to take dimensions was consistent for all the specimens.

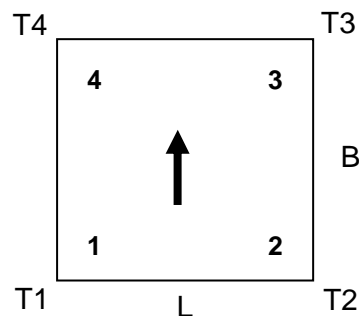


Figure 4.8 Dimensions of square specimens taken

The labels T1 to T4 in figure 4.8 represent the four thickness measurements corresponding to corners 1 to 4 respectively. The length L was measured along edge 1-2 while the breadth B along edge 2-3. The arrow denotes the upward or vertical direction of the specimen as it was placed in the testing frame so that edges 1-2 and 3-4 were horizontal whereas edges 2-3 and 1-4 were vertical. The average thickness of the specimen was calculated as the average of the four thicknesses T1, T2, T3 and T4. The areas for the computation of the applied vertical and horizontal stresses were calculated by multiplying the average thickness by length L and breadth B respectively.

Figure 4.9 shows the biaxial test frame with hydraulic jacks, loading platens and square test specimen. The Two vertical and horizontal Instron actuators (jacks) of 500 kN capacity were used to apply the biaxial forces at various ratios of the vertical load to the horizontal load. The applied load ratios were such that the applied stress paths made angles 0° , 15° , 30° and 45° with the line of action of the horizontal force. A system of four sets of roller bearings, details of which can be seen on figure 4.11, was used to help with self alignment of the loading system during testing as the material deformed. A weights and pulley system was used to counter balance the roller bearings.

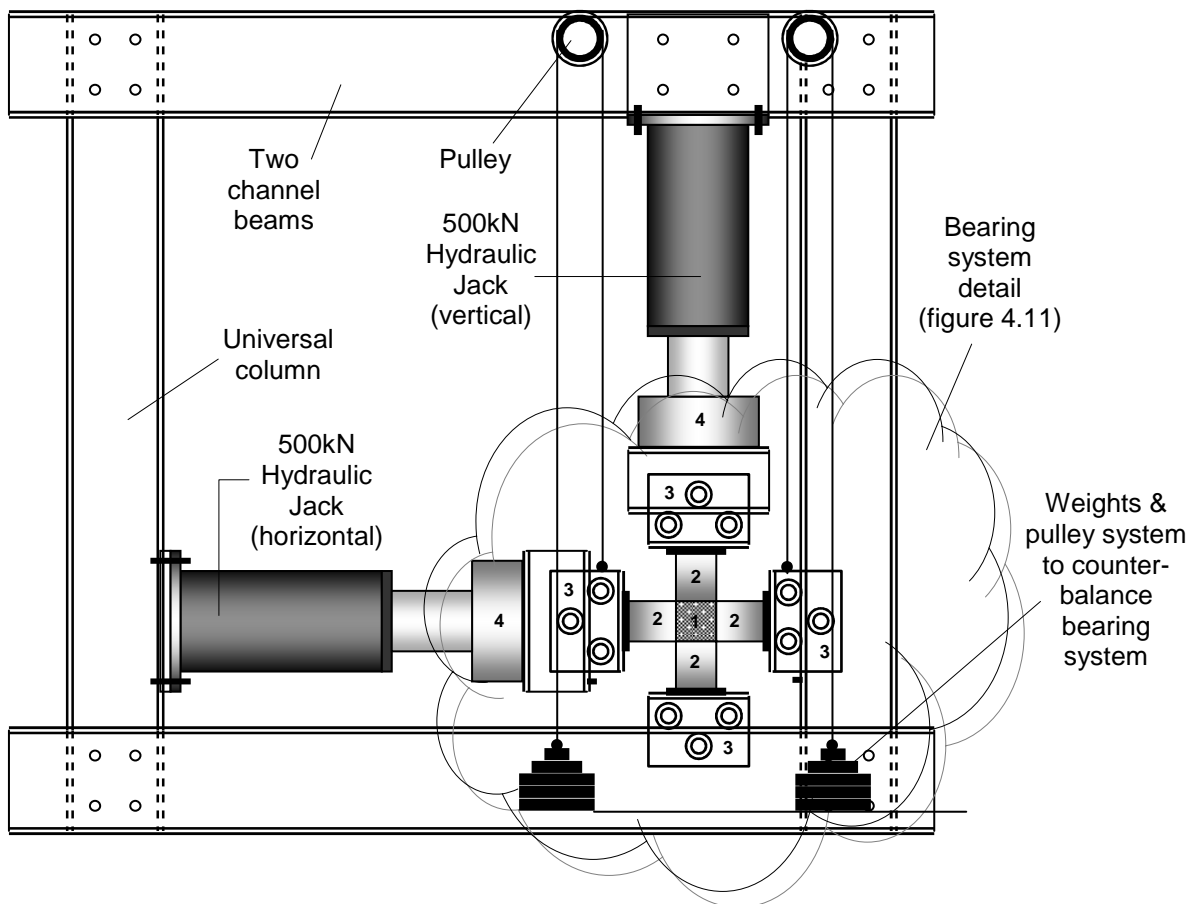


Figure 4.9 Biaxial test frame

The tests were performed under force control conditions. The basic loading rate was 0.355 kN/s in the major direction (horizontal) while the rate in the vertical

direction was a fraction of this basic loading rate. Load ratios corresponded to the stress path angles 0° , 15° , 30° and 45° . These ratios were determined by dividing the loading rate for the vertical actuator by the loading rate for the horizontal one. For example, the load ratios corresponding to angles 0° , 15° , 30° and 45° were 0 ($=0/0.355$), 0.268 ($=0.095/0.355$), 0.577 ($=0.205/0.355$) and 1.0 ($=0.355/0.355$) respectively. Table 4.2 below gives a summary of the loading rates and figure 4.10 an illustration of load ratios.

Table 4.2 Loading Rates for the biaxial tests

Stress Path Angle (degrees)	Load Ratio	Vertical Loading rate (kN/s)	Horizontal Loading rate (kN/s)
0	0.000	0.000	0.355
15	0.268	0.095	0.355
30	0.577	0.205	0.355
45	1.000	0.355	0.355

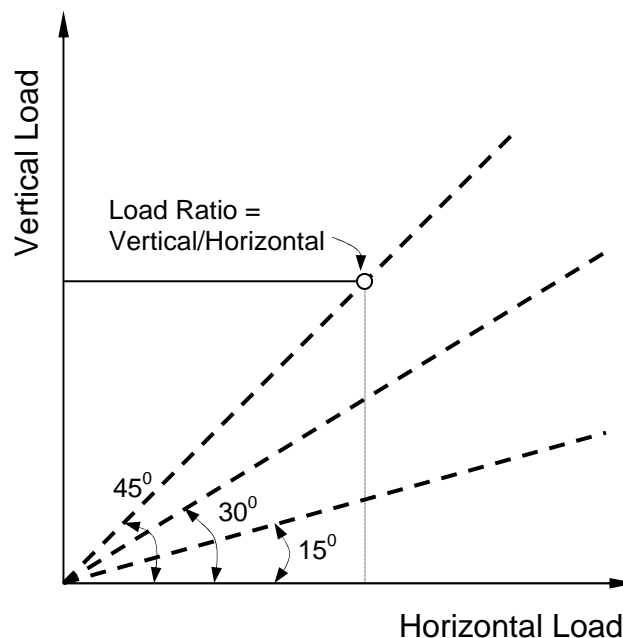


Figure 4.10 Illustration of applied load ratios

Application of loads: The loads were applied through loading platens mounted to a system of bearings (see figure 4.11). The purpose of the bearings was to act as rollers to allow for free movement of the platens and the specimen in the directions perpendicular to the loading direction during testing. For each load ratio, two sets of biaxial tests were done: with the load applied directly to SHCC specimens through solid steel platens and; with load applied through the same solid steel platens but with 2 mm Vesconite sheets between the steel and the specimen surface to reduce the restraining effect of the frictional force between SHCC and solid loading platens (see figure 4.12).

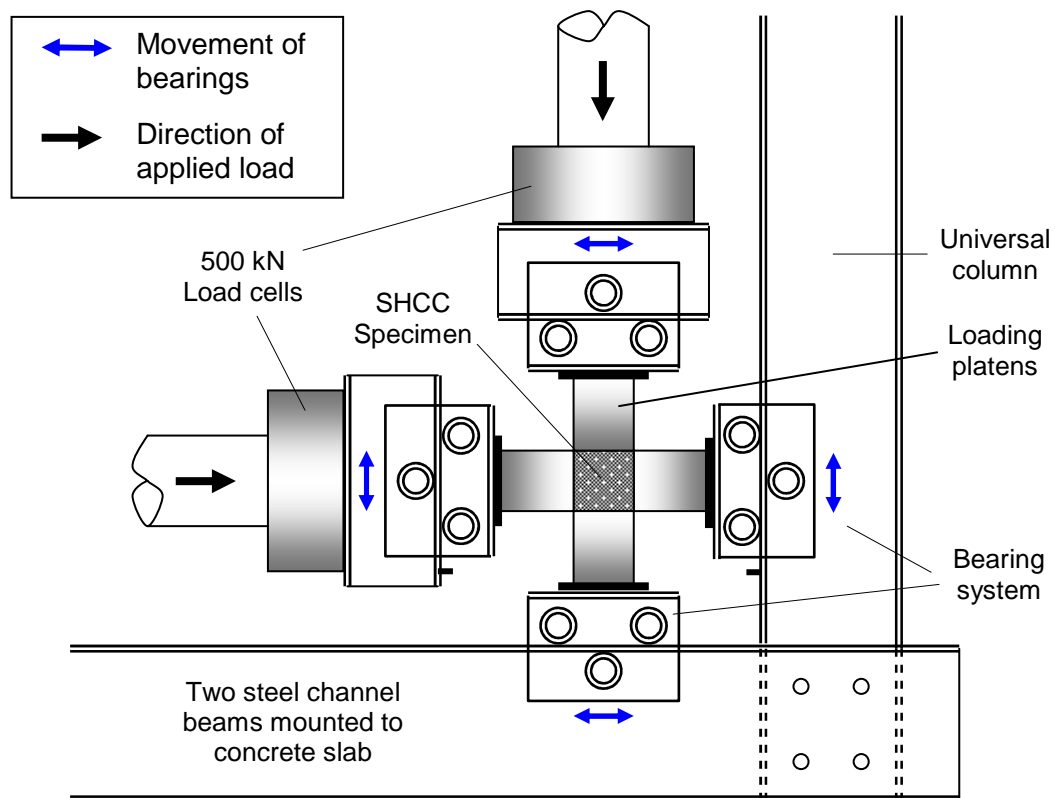


Figure 4.11 Biaxial test setup showing bearing system detail

The applied loads and their corresponding displacements of the actuator crossheads were recorded on a computer through the use of Instron software at a sampling rate of 25 Hertz. This software was also used to control the tests

through a Proportional Derivative Integration (PDI) controller. The recorded data was used to plot failure envelopes.

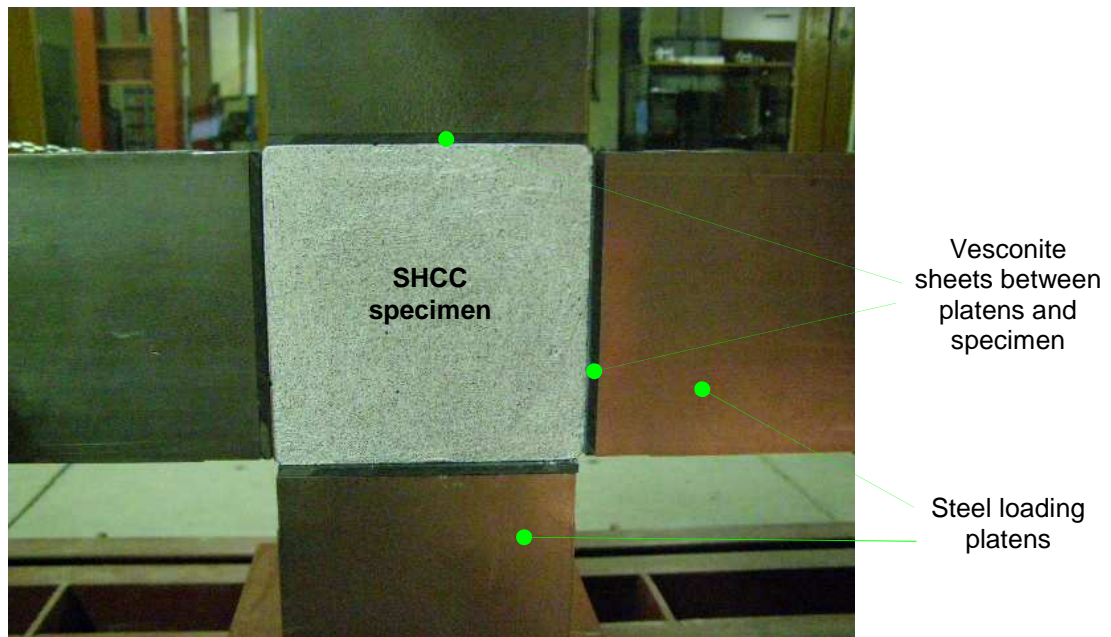


Figure 4.12 Vesconite between loading platens and specimen to reduce friction

Deformation measurement: The deformations were measured using a system of two cameras mounted onto an adjustable tripod, a computer and software called ARAMIS (manufactured by GOM Optical Measuring Techniques). The system captured photographs using the two cameras simultaneously and then used the images to calculate deformations. For this to be done, it was required that the surfaces of the specimens be prepared by forming a speckle pattern of black dots on a white background. The pattern was formed by applying a film of a viscous solution of chalk and water using a painting brush. The wet chalk was dried by blowing the specimens with compressed air. When the chalk was nearly dry, a pattern of fine, evenly distributed dots was formed by means of black spray paint. The technique of spraying was such that only fine dots of paint (like mist) were applied. This was ensured by spraying at a very low height and from a distance of about 0.5 m away from the specimen as shown in figure 4.13.

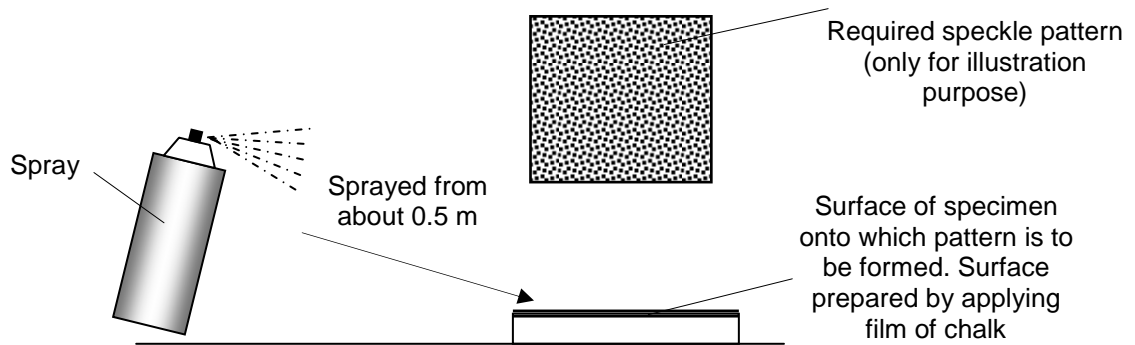


Figure 4.13 Preparation of speckle pattern for deformation measurement

Figures 4.8 to 4.13, including associated text described various components of making up the biaxial test. The following section will give a description of the whole biaxial test of each specimen. Figure 4.14 shows a layout of how the individual components were linked to form one test setup.

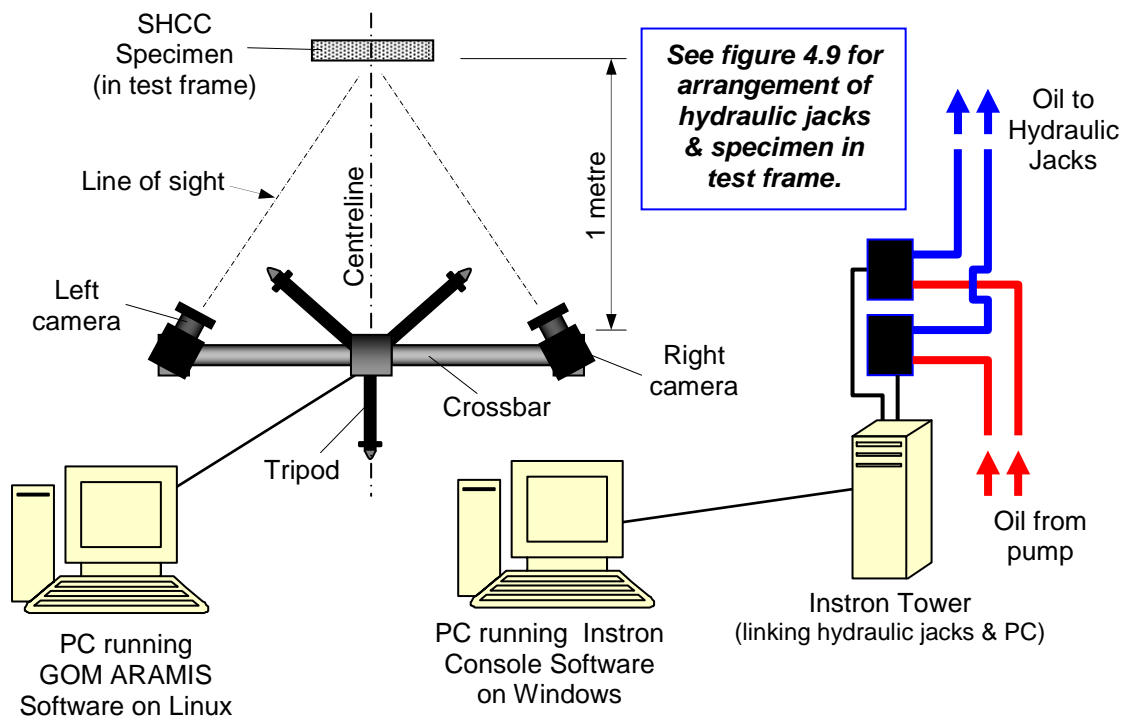


Figure 4.14 Layout of Biaxial test equipment (*cameras and specimen in plan view*)

Once the specimen was placed in the test setup and was ready to be tested, the capturing of the photographs using ARAMIS software was started and then followed by the application of the loads using the hydraulic actuators. The reason for following this sequence was to ensure that the first photographs were taken to mark the starting point of measurement (ie. the datum or zero values for calculation of deformations in ARAMIS). The photographs were taken, using two cameras situated at 1 m away from the face of the specimen (see figure 4.14), at a sampling rate of one image per second (ie. 1 Hz). The maximum number of images that could be taken was set to 350.

The images were recorded in what are called stages; with the first images denoting stage 0. Each stage had two images: one from the left hand camera and the other one from the right hand camera. Focus areas called masks were created for each set of test results. Masks are areas within which the computer program computes whatever information that may be required by the user. This information could be deformations or various kinds of strains. In this case, the deformations were then computed from the recorded images.

In order to be selective about areas where information is sought, and to reduce the amount of data that can be downloaded for the purpose of further analysis and presentation, the user may create points or sections of interest on the masked area. It can then be chosen to download required information at the points or along the sections created. Since it was required to compute deformations and hence strains from the image data, six sections were created in ARAMIS for each set of test results at 30 mm apart in the vertical and horizontal direction of the global ARAMIS coordinate system (figure 4.15). The distance between the sections was to be used as the gauge length in the computation of strains due to applied vertical and horizontal stresses.

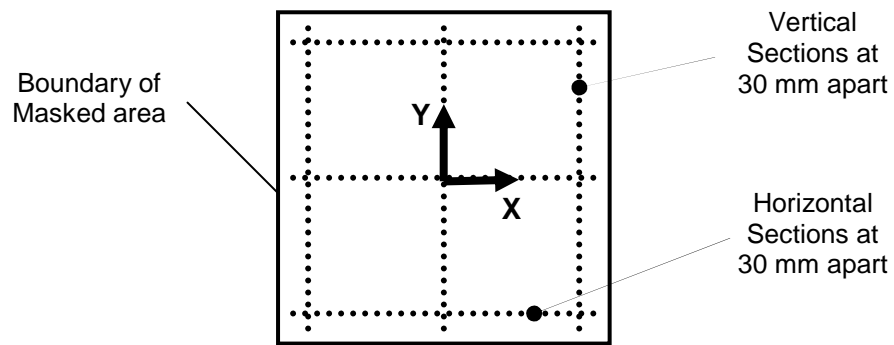


Figure 4.15 ARAMIS sections in global coordinate system

The section data were downloaded as text files which could then be imported into Microsoft Excel for further analysis and presentation.

4.4.2 Cylindrical Specimens

These specimens were subjected to compressive load until failure occurred.

The compressive loads were applied at the rate of 1 mm/min using Zwick Z250 testing machine, which was situated in the PPC laboratory of the Department of Civil Engineering at Stellenbosch University. The testing apparatus consisted of a load cell, two LVDTs, LVDT frame, the Zwick machine connected to a PC to apply the loads and Spider8 data logger connected to a PC to collect and store data from the LVDTs and the load cell. Figure 4.16 shows the apparatus for the test.

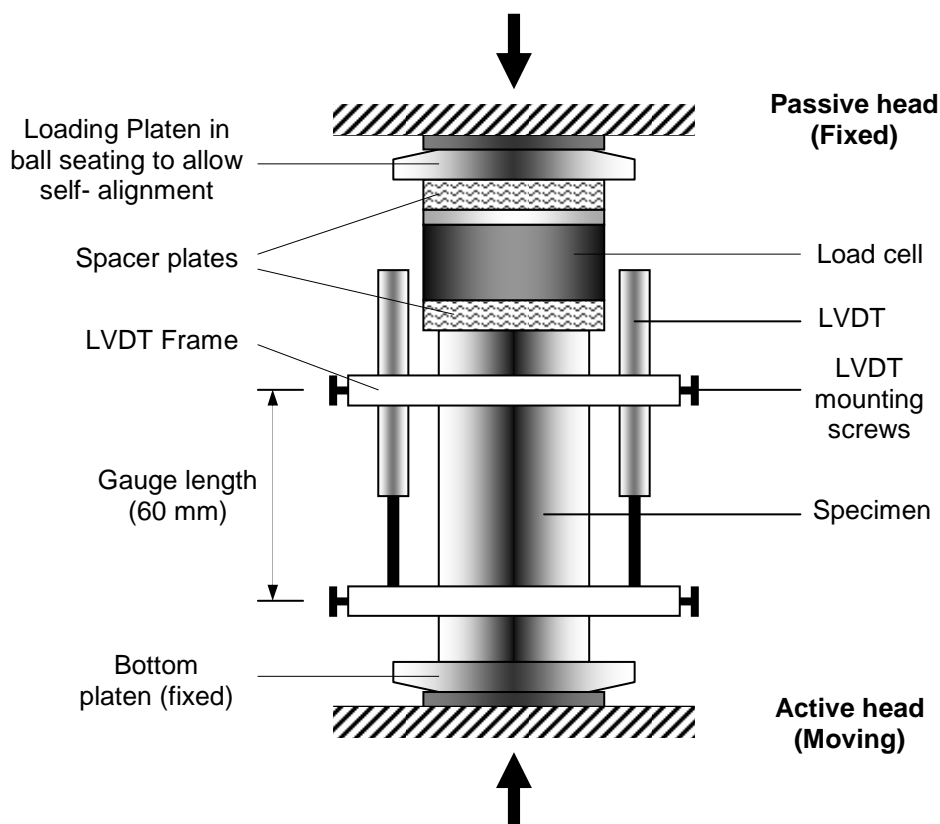


Figure 4.16 Apparatus for Cylindrical specimens

The test procedure, which must be read in conjunction with figure 4.16 and 4.18, was carried out as follows:

- A batch of three specimens was removed from the curing bath on the day of testing;

- A very thin slice was cut off their tops using a concrete cutting saw to ensure that the surfaces onto which the loads were to be applied were parallel and smooth;
- Their masses were determined using an electronic scale and then recorded on a pre-printed form in grams to the nearest 0.1 gram;
- The heights and diameters were measured using a veneer callipers and recorded on the form in millimetres to the nearest 0.05 mm;
- The top and bottom loading platens were fixed to the Zwick Z250 machine passive head and active head (crosshead) respectively;
- A pre-saved test program to run the test was opened in the computer. The settings for the Zwick Z250 machine and the test program were checked for correctness. Adjustments were made where necessary;
- The crosshead position appropriate for the size of the specimen was set;
- Spider8 data logger was connected to a PC with Catman software; The PC and the Spider8 were switched on;
- Load cell and two LVDTs were connected to the Spider8 data logger;
- Catman software was then setup as per manual to connect and setup the load cell and LVDTs;
- LVDTs and the frame were mounted onto the cylindrical specimen. The mounting screws were tightened;
- The two vertical elements of the LVDT's frame used to maintain the correct gauge length between the top and bottom of the frame were removed. The gauge length was 60 mm;
- The Catman software was run to start capturing data and then followed by the running of the test program in Zwick to start the test;
- The specimen was tested until failure occurred;
- The capturing of data was stopped. Data was then exported as text file, which was then imported into Microsoft Excel for further processing at a later stage;
- The remaining two specimens were tested following the same procedure described above.

4.4.3 Dumbbell Specimens

The testing of Dumbbell specimens was done under tensile loading as shown in figure 4.17 below..

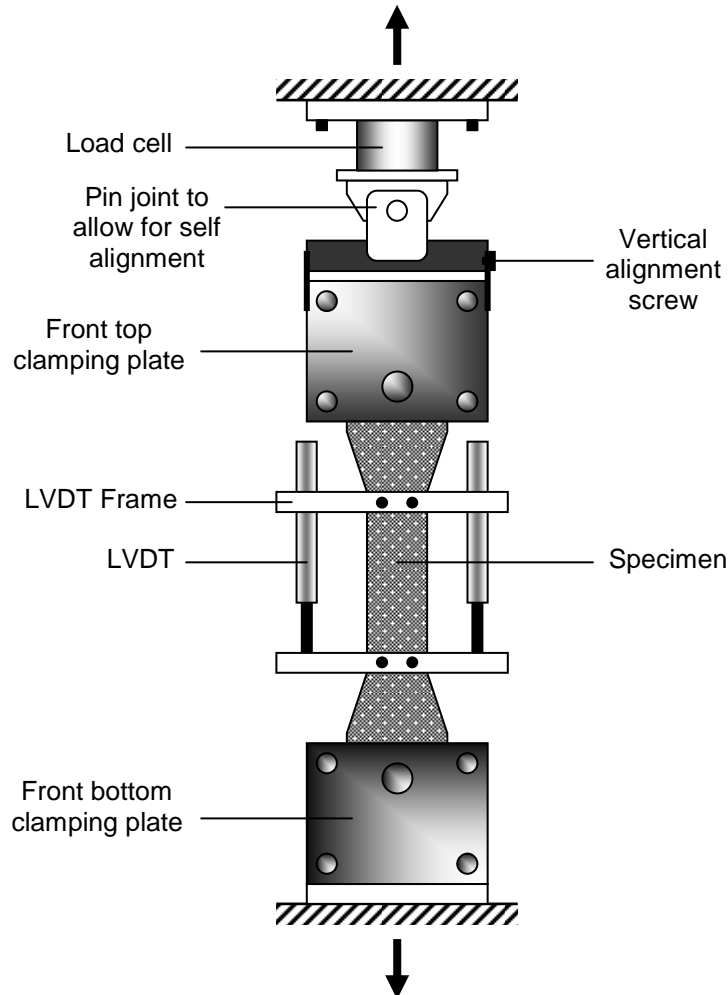


Figure 4.17 Apparatus for Dumbbell specimens

Even though the dumbbells were different from the cylinders and that they were subjected to tensile loading instead of compressive loading, the general testing procedure was similar. The dumbbell specimens were tested in the following manner:

- Four specimens were removed from the curing bath on the day of the test;
- The edges of the specimens were cleaned by means of a pair of scissors so that there was no unwanted material extending beyond them;

- The thickness and width were measured at the narrow part of the specimen using a veneer callipers and recorded on the form in millimetres to the nearest 0.05 mm;
- The top and bottom loading units onto which the specimen was to be clamped were fixed to the Zwick Z250 machine passive head and active head respectively. The top unit included a load cell;
- A pre-saved test program to run the test was opened in the computer. The settings for the Zwick Z250 machine and the test program were checked for correctness. Adjustments were made where necessary;
- The crosshead position appropriate for the standard dumbbell specimen was set;
- Spider8 console (data logging device) was connected to a PC with Catman software; The PC and the Spider8 were switched on;
- Load cell and two LVDT's were connected to the Spider8 data logger;
- Catman software was then setup as per manual to connect and setup the load cell and LVDT's;
- LVDT's and the frame were mounted onto the dumbbell specimen. The mounting screws were tightened;
- The two vertical elements of the LVDT frame used to maintain the correct gauge length between the top and bottom of the frame were removed. The gauge length was 80 mm;
- The Catman software was run to start capturing data and then followed by the running of the test program in Zwick to start the test;
- The specimen was tested until failure occurred;
- The capturing of data was stopped. Data was then exported as text file, which was to be imported into Microsoft Excel for further processing at a later stage;
- The remaining three specimens were tested following the same procedure described above.

Figure 4.18 below shows the general layout of the test set up for the dumbbell and cylindrical specimen tests on the Zwick machine.

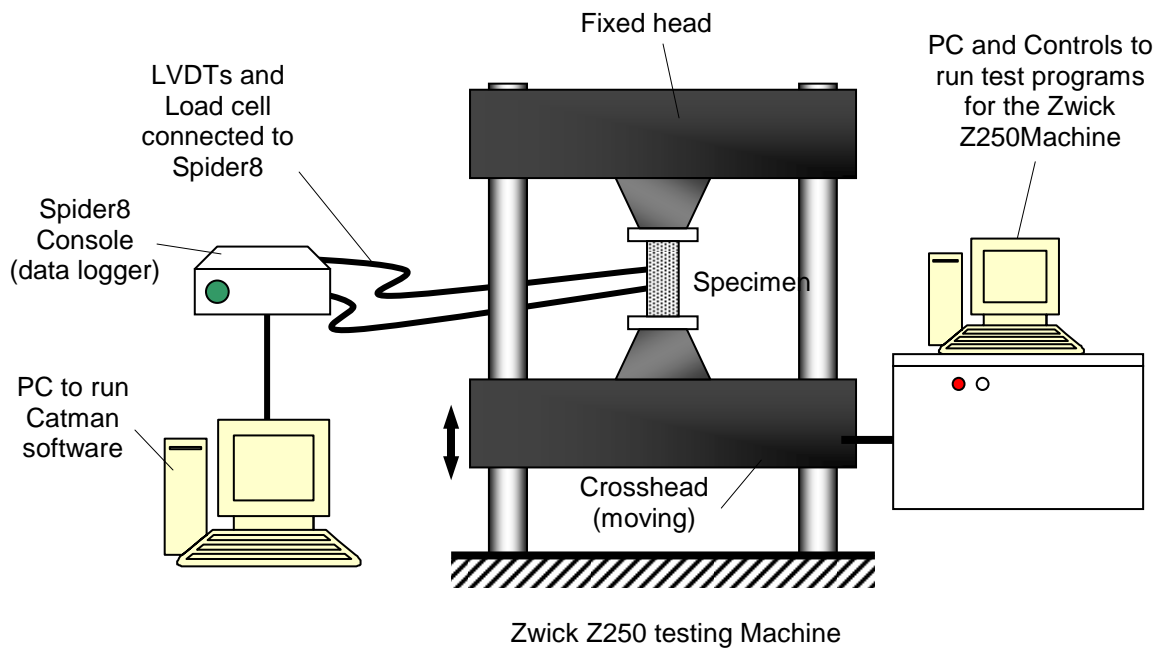


Figure 4.18 Zwick Z250 testing machine, Spider8 console and PC for Catman software

4.4.4 Cubes

The cubes tested were 100 x 100 x 100 mm. There were three specimens per batch. They were tested under compression until failure occurred using the Contest Machine (type GD10 Grade A) in concrete laboratory of the Department of Civil Engineering at Stellenbosch University. The testing ages were 33, 28, 27 and 23 days respectively.

The tests were performed as follows:

- Three cubic specimens were removed from the curing bath;
- Excess water was wiped off using a damp cloth;
- Their masses were determined using an electronic scale and then recorded on a pre-printed form;
- The dimensions were determined using a veneer calliper and recorded on the same form;

- Each cube was placed centrally in the machine so that the surface that was floated was facing the direction of the machine operator;
- The cubes were tested under compression until failure occurred;
- Maximum force (for each specimen) was recorded in Newtons.

4.5 CONCLUSION

The experimental programme followed in this study has been presented in this chapter. The constituents used for making the SHCC material that was tested were described. Mixing, casting and testing of SHCC specimens of various shapes for different purposes were discussed. The specimens manufactured and tested were cylindrical, cubic, dumbbell and square plates. The cylindrical and cubic specimens were tested to determine the properties of SHCC under uni-axial compressive loading. The dumbbell specimens were tested to determine the properties under direct tensile loading while the square plate specimens were tested to determine behaviour of SHCC under biaxial compression. The results obtained from the tests are presented in Chapter 5.

CHAPTER 5

EXPERIMENTAL RESULTS

5.1 INTRODUCTION

In this Chapter, the results obtained from the experiments described in Chapter 4 are presented. First, the results obtained from the testing of cylindrical and dumbbell specimens under simple uni-axial compressive and tensile loading are presented. Cube test results are also presented for the purpose of having figures that can be compared to the cylindrical ones. The tensile strengths, compressive strengths and Elastic Moduli obtained from dumbbell and cylindrical specimens are obtainable.

However, the results from testing of the cubes and the cylindrical specimens showed irregularities in strength. It was expected for the results showing strengths to decrease with decreasing testing age. This was not found to be the case with these specimens. It is suspected that the specimens were either mixed or an error occurred in the mixing stage of the batches.

Furthermore, the results obtained from the biaxial testing of SHCC are presented in the form of failure envelope and stress-strain curves. Crack patterns are included in the next chapter to aid in the discussion of the obtained results.

5.2 CYLINDRICAL SPECIMENS

The specimens were tested under simple uni-axial compressive loading. Results obtained from testing of specimens made from four batches are shown in tables 5.1 and 5.2, and graphically in figure 5.1. There were three specimens

per mix. Table 5.2 shows averages of failure strengths, Elastic moduli and densities.

As it was already mentioned in the introduction to this chapter, the results obtained from the testing of these specimens showed irregularities. This is evident from the high standard deviation of 6.14 MPa for batch 3 (table 5.2). Figure 5.1 also show batch 3, which was 27 days old at testing, to have an average strength of 31.54 MPa. This is higher than the strength of batch 1 and 2 at ages 32 and 28 days respectively. A recommendation is made in chapter 7 to investigate the rate of strength gain for SHCC for up to 90 days.

Figure 5.2 show a typical load-displacement curve for cylindrical specimens tested under compressive loading. The curve shows softening after maximum stress was reached.

Table 5.1 Results obtained from testing of cylindrical specimens

Batch	Specimen Number	Age (days)	Density (kg/m³)	Ultimate Strength (MPa)	Elastic Modulus (MPa)
1	11	32	1942	31.13	16446
	12	32	1933	28.68	15746
	13	32	1902	25.71	11249
2	21	28	1912	27.95	14495
	22	28	1936	28.35	12405
	23	28	1953	28.74	24387
3	31	27	1919	33.99	13404
	32	27	1952	36.08	20617
	33	27	1960	24.56	11463
4	41	23	1910	-	-
	42	23	1937	27.76	16896
	43	23	1924	25.14	29333

The results for Specimen 41 could not be obtained because the specimen was damaged prior to testing.

Table 5.2 Summary of results from Compressive tests

	Batch 1	Batch 2	Batch 3	Batch 4
Age (days)	32	28	27	23
Ultimate Strength (MPa)				
Mean	28.51	28.35	31.54	26.45
Standard deviation	2.71	0.39	6.14	1.85
Elastic Modulus (MPa)				
Mean	14480	17096	15161	23114
Standard deviation	2820	6400	4823	8794
Density (kg/m³)				
Mean	1926	1934	1944	1924
Standard deviation	21	21	22	13

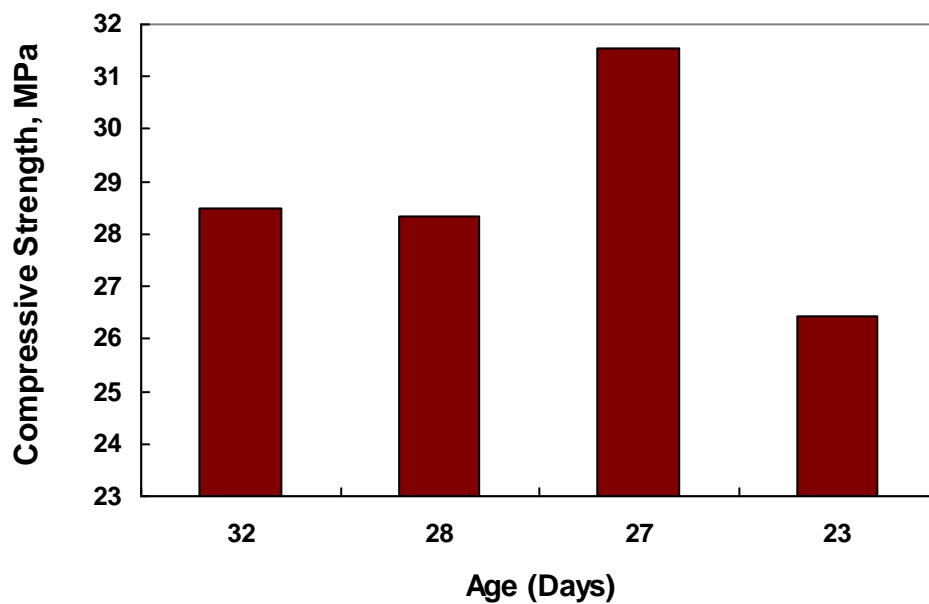


Figure 5.1 Mean Compressive strengths of Cylindrical specimens

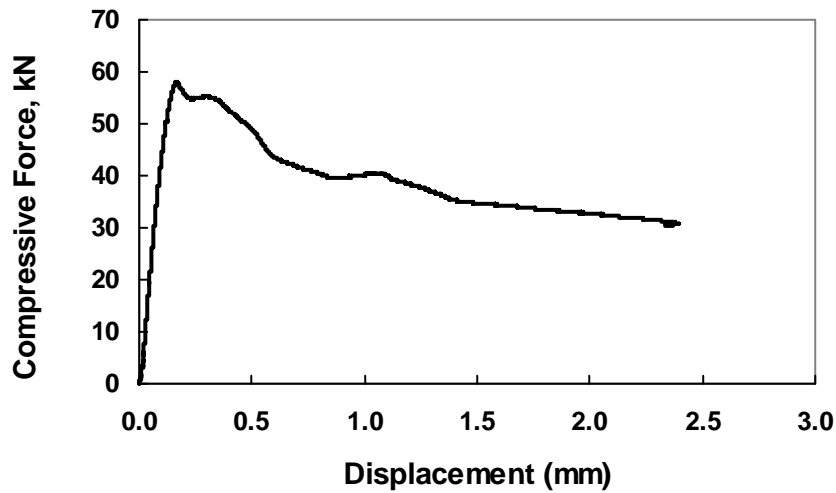


Figure 5.2 Typical Load-displacement curve for Cylindrical Specimens

The variability in E-modulus may be due to measurement irregularity and/or variability of physical properties. Although the LVDT frame was carefully attached, and fixing screws were locked in position by lock nuts, the variability in E-modulus may indicate very small movement of the frame. On the other hand, entrained air is known to strongly influence the E-modulus of cement-based materials. Air content of the fresh mix was not measured, as the viscosity renders standard air content measurement methods inappropriate. Varying air content could also explain irregularities in compressive strength.

5.3 DUMBBELL SPECIMENS

These specimens were tested under simple uni-axial tensile loading. Four batches consisting of four specimens each were tested. The results are presented in tables 5.3 and 5.4 and graphically in figure 5.3.

Table 5.3 Results obtained from testing of Dumbbell Specimens

Batch	Specimen No.	Age (days)	Ultimate Strength (MPa)	Elastic Modulus (MPa)
1	11	32	3.89	18167
	12	32	3.71	19767
	13	32	3.83	5502
	14	32	3.55	4572
2	21	28	4.19	19535
	22	28	4.10	8065
	23	28	2.65	10993
	24	28	2.71	14465
3	31	27	1.57	7327
	32	27	2.36	4012
	33	27	3.18	7925
	34	27	3.56	9506
4	41	23	3.00	8616
	42	23	2.72	5636
	43	23	2.88	10761
	44	23	2.36	8807

Table 5.4 shows averages of results for the dumbbell specimens. The average tensile strengths as depicted by table 5.4 and figure 5.3 show increasing strengths with increasing ages as expected. The standard deviations for the strength were below 1 MPa.

It can also be seen from figure 5.4, which is a typical load-displacement curve for dumbbell specimens subjected to tensile loading, that the material showed strain hardening behaviour.

Table 5.4 Summary of results obtained from Tensile tests

	Batch 1	Batch 2	Batch 3	Batch 4
Age (days)	32	28	27	23
Ultimate Tensile Strength (MPa)				
Mean	3.75	3.41	2.67	2.74
Standard deviation	0.15	0.85	0.89	0.28
Elastic Modulus (MPa)				
Mean	12002	13264	7192	8455
Standard deviation	8078	4931	2311	2115

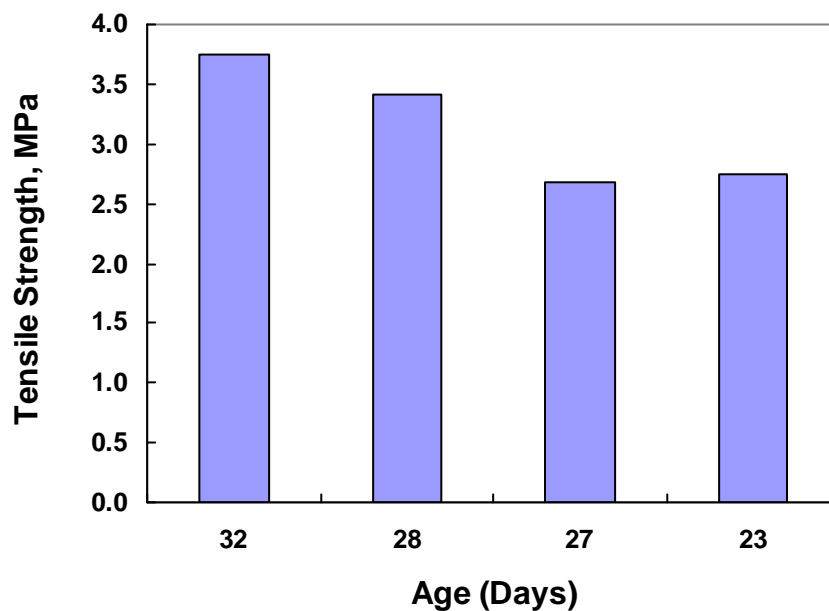


Figure 5.3 Mean tensile strengths of Dumbbell Specimens

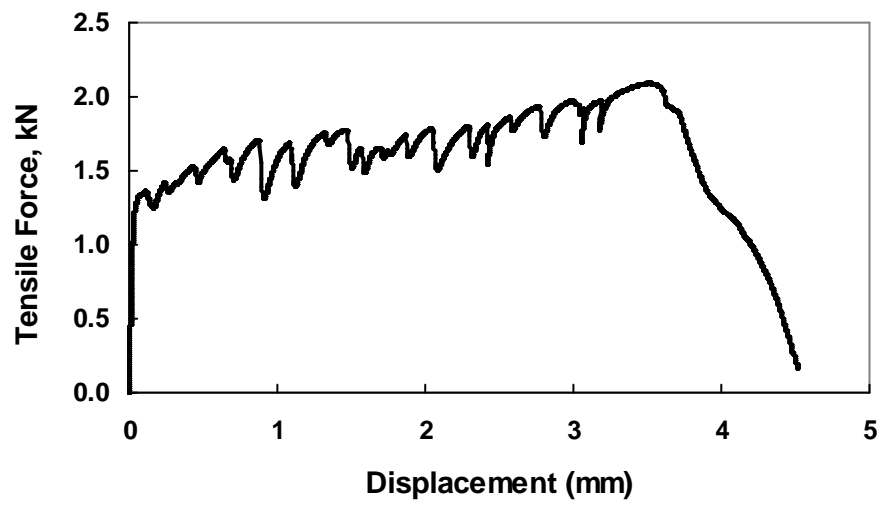


Figure 5.4 Typical Load-displacement curve for Dumbbell Specimens

5.4 CUBIC SPECIMENS

These specimens were tested under compressive loading. The tested specimens were made from the same four batches as it was done for Dumbbell and Cylindrical specimens. The results are shown in tables 5.5 and 5.6, and graphically in figure 5.5.

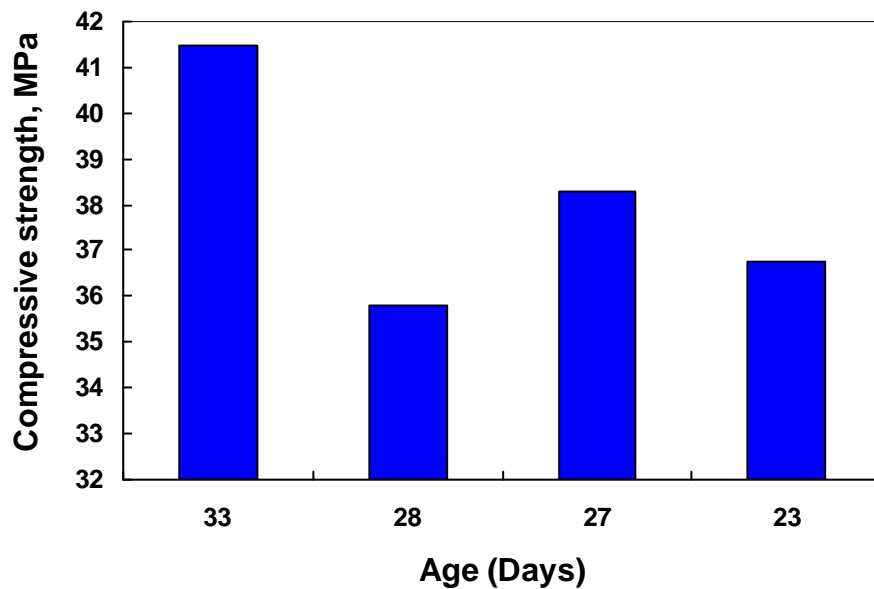
Table 5.5 Results obtained from testing of Cubic Specimens

Batch	Specimen No.	Age (days)	Density (kg/m ³)	Ultimate Strength (MPa)
1	11	33	1911	40.63
	12	33	1926	42.10
	13	33	1904	41.67
2	21	28	1914	36.22
	22	28	1916	34.84
	23	28	1899	36.29
3	31	27	1899	36.86
	32	27	1901	39.67
	33	27	1903	38.29
4	41	23	1909	35.00
	42	23	1879	38.36
	43	23	1919	36.86

Although the standard deviations for the results were low, ranging between 0.75 and 1.68 MPa, specimens made from mix 2 yielded lower results at 28 days than those made from mixes 3 and 4 at 27 and 23 days respectively (figure 5.5). This reaffirms the assumption that the specimens were mixed or the making of the mixes was inconsistent.

Table 5.6 Summary of results obtained from crushing of Cubes

	Batch 1	Batch 2	Batch 3	Batch 4
Age (days)	33	28	27	23
Ultimate Strength (MPa)				
Mean	41.47	35.78	38.27	36.74
Standard deviation	0.75	0.82	1.41	1.68
Density (kg/m³)				
Mean	1914	1910	1901	1902
Standard deviation	11	9	2	21

**Figure 5.5** Mean compressive strengths of Cubic Specimens

5.5 SQUARE BIAXIAL PLATE SPECIMENS

The square plate specimens of dimensions 102.6 x 102.6 x 20.6 mm were tested under biaxial compressive loading until failure occurred. A total of 32 specimens were subjected to four load ratios as explained in chapter 4. This means that there were eight specimens per load ratio. Of the eight specimens for each load ratio, four were tested directly by applying loads through steel platens while for the other four, the loads were applied through Vesconite sheets (see figure 4.12).

Table 5.7 below shows averages of maximum vertical and horizontal stresses obtained from the testing of the square biaxial plates for different stress path angles or ratios, and loading medium (steel or Vesconite). The stresses were obtained by dividing the maximum forces obtained by the loaded areas of the specimens. The loaded areas were computed using the measured dimensions of the specimens. These results are also shown graphically in figure 5.6a and 5.6b.

Table 5.7 Summary of Biaxial test results

Stress Path Angle (degrees)	Mix No.	Age (days)	Loading Details	Max. Vertical Stress (MPa)		Max. Horizontal Stress (MPa)	
				Mean	Std. Dev.	Mean	Std. Dev.
0	2	28	Steel	0.00	0.00	25.70	2.54
15	3	27	Steel	9.60	0.44	34.53	1.56
30	4	23	Steel	16.43	0.94	26.82	1.76
45	1	33	Steel	34.61	2.99	33.98	2.90
0	2	28	Vesconite	0.00	0.00	23.82	2.98
15	3	27	Vesconite	8.75	0.95	28.10	2.28
30	4	23	Vesconite	15.26	0.66	25.36	1.97
45	1	34	Vesconite	31.29	2.16	30.36	2.07

It can be seen from table 5.7 and figure 5.6a that the maximum stresses for specimens tested with Vesconite between steel and the specimen were lower

than for those tested directly through steel platens. The maximum stress reduction (as percentage of results from steel platens) for stress paths angles 0° , 15° , 30° and 45° were 7 %, 19 %, 5 % and 11 % respectively.

Figure 5.6a shows the normalised biaxial stress envelope for specimens tested using steel platens directly and those tested using Vesconite sheets. Each data point was obtained by dividing the mean biaxial test results shown in table 5.7 by the corresponding strengths obtained from testing of cylindrical specimens. The data points shown are for the results obtained from testing all specimens and the corresponding averages for specimens tested using steel and Vesconite. The blue circular hollow markers, the square solid markers, the diamond red markers and the magenta triangular markers represent data for all specimens tested using steel, average results for specimens tested using steel, data for all specimens tested using Vesconite and averages of results obtained from specimens tested using Vesconite respectively.

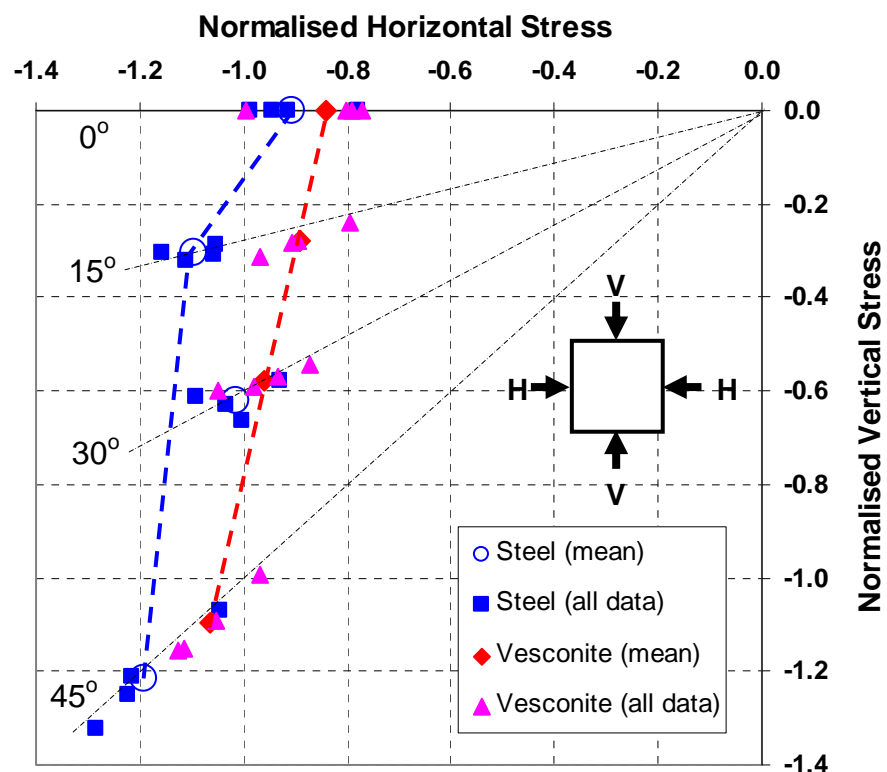


Figure 5.6a Normalised Biaxial stress envelope (using Cylinder strengths)

In figure 5.6a, the blue dashed line is drawn through mean points of stresses for tests done using steel platens only (except for point corresponding to 30^0 stress path angle) while the red dashed line is drawn through mean points for stresses obtained from tests done using Vesconite. These lines mark the failure envelopes for SHCC under biaxial compression-compression for specimens tested with and without Vesconite. The sign convention adopted: compression was negative.

It can be seen from figure 5.6a that the values for the uni-axial condition (stress path angle 0^0) are less than 1. This is because the strengths of cylindrical specimens used were slightly higher than the uni-axial strengths for square plate specimens. In order to clearly show relative magnitudes of biaxial stress envelope results, the results shown in figure 5.6a were processed further by dividing each data point by the normalised average strength of specimens tested using Vesconite for the stress path angle of 0^0 (uni-axial condition) of 0.84. The resulting graph is shown in figure 5.6b, which shows normalised average uni-axial strength of specimens tested using Vesconite to be equal to unity.

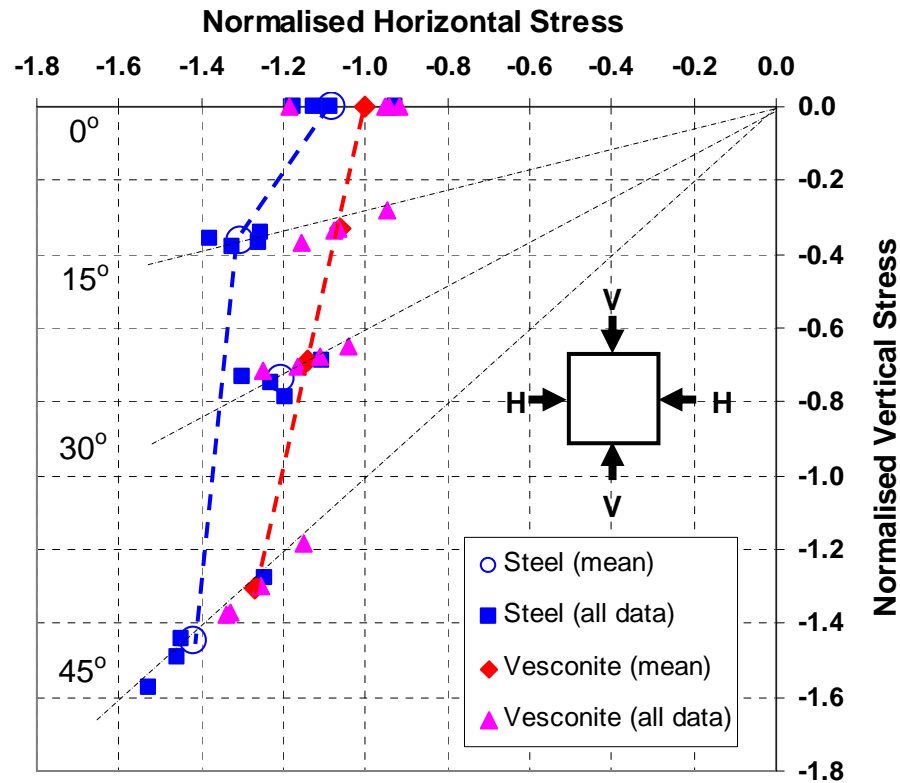


Figure 5.6b Normalised Biaxial stress envelope (using Vesconite uni-axial strength)

5.6 STRESS-STRAIN RELATIONSHIPS

In order to be able to analyse and discuss the biaxial behaviour of SHCC under biaxial stresses, the specimen displacements measured using the GOM ARAMIS system had to be processed and synchronised with the forces recorded by the Instron system (see figure 4.14).

Recall that in section 4.4.1, it was mentioned that six *sections* were drawn at distances of 30 mm apart on the masked area of the GOM ARAMIS image. That is, three horizontal and the remainder vertical as shown in figure 4.15. These sections were to be used as lines of reference to enable computation of strains due to applied loads. Each section consisted of data points ranging between 70 and 80 in number depending on the size of the mask. For each

data point and hence section, deformed and undeformed (marking original positions) Cartesian coordinates were recorded. All data were exported from GOM ARAMIS software as text files and then imported into Microsoft Excel for processing.

In order to reduce the data into manageable sizes and also to leave relevant data for the computation of strains, the data for the middle sections in the vertical and horizontal directions were removed. This left the original distance between sections in either direction of 60 mm; this was used as the gauge length in the computation of strains. The removed sections (red centreline type lines) and those used for calculating strains are shown in figure 5.7 below. In figure 5.7, the red (dashed) lines represent the middle sections for which data were removed; the green (solid) horizontal lines represent the positions of sections used for calculating deformations in the vertical direction; and the blue (solid) vertical lines represent the positions of sections used for calculating deformations in the horizontal direction.

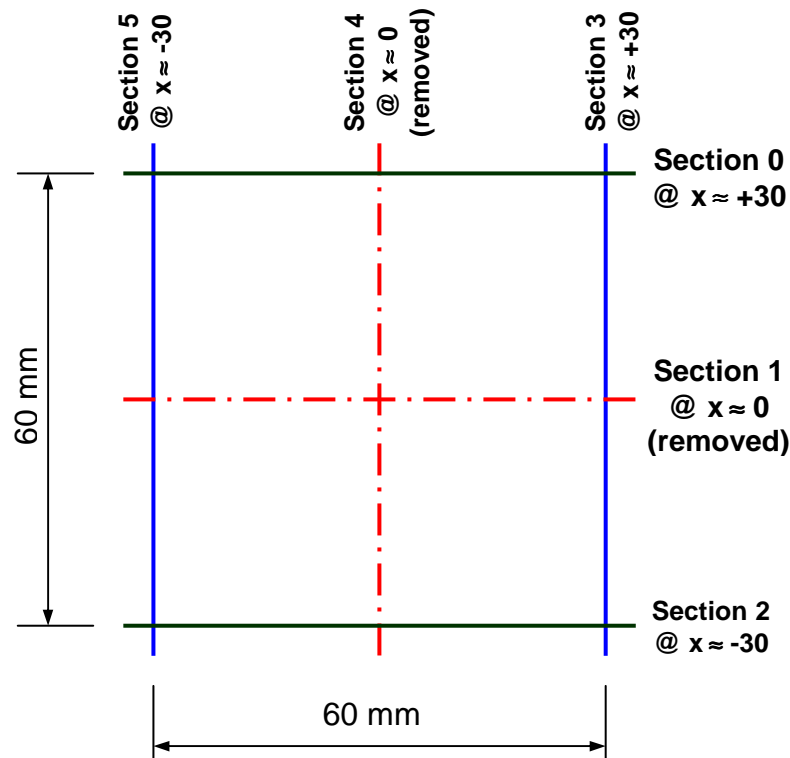


Figure 5.7 Sections used for calculating strains

Since there were about 80 data points along each section or line, the positions of the sections corresponding to each stage or captured image were determined by computing the averages of the data points. This gave single values of deformed and undeformed coordinates for each section and stage. The strains were then computed by dividing the change in length, which was calculated by determining the difference between the averages of deformed and undeformed coordinates in millimetres, by the original length of 60 mm.

The calculated strains (ARAMIS) were then synchronised with the corresponding calculated stresses (Instron) for each data set obtained from the testing of one specimen. The synchronised data were then used to plot stress-strain relationships for tests done using steel platens directly and Vesconite for various stress ratios as depicted by graphs in figures 5.8 and 5.9 respectively. The sign convention adopted was positive for tensile strains and negative for compressive strains. In both figures, each line represents results for one specimen (corresponding to a particular stress ratio) that was selected as the one representing all data for that stress ratio. This explains why some of the maximum stresses in figures 5.8 and 5.9 are higher or lower than the average values shown in table 5.7. The results for mix 4 corresponding to stress path angle of 30° and ratio of 0.57/1 were not included because the ARAMIS deformations for this stress ratio were erroneous as the result of poor calibration of the system.

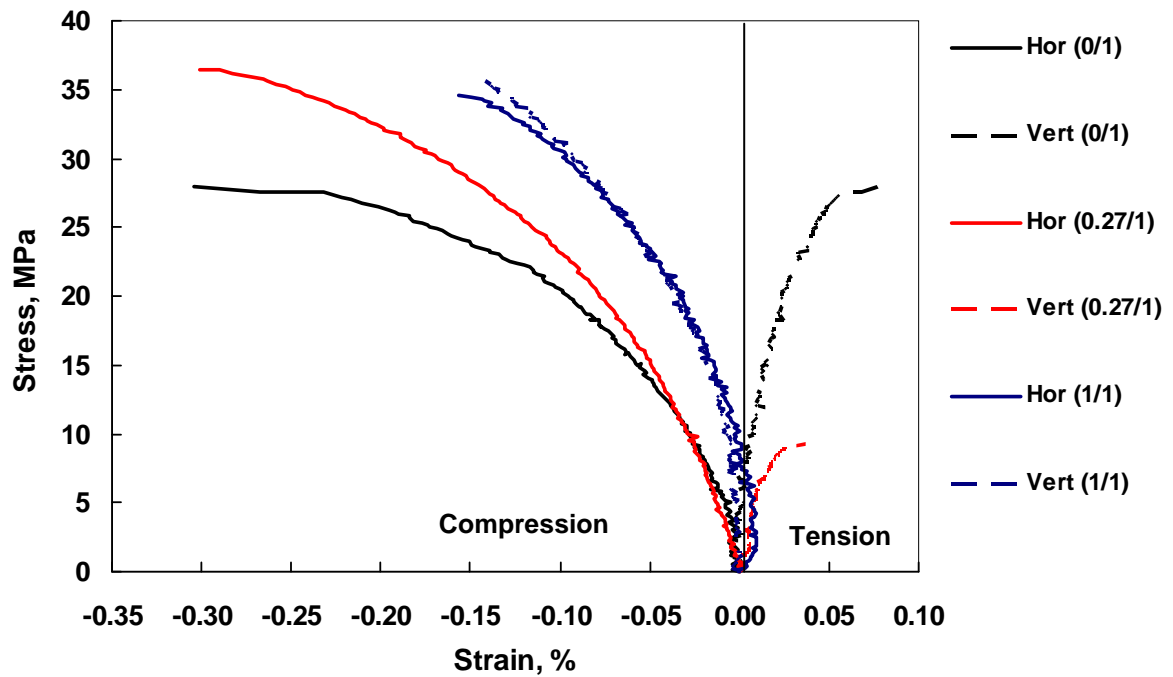


Figure 5.8 Stress-strain relationships for specimens loaded using steel platens

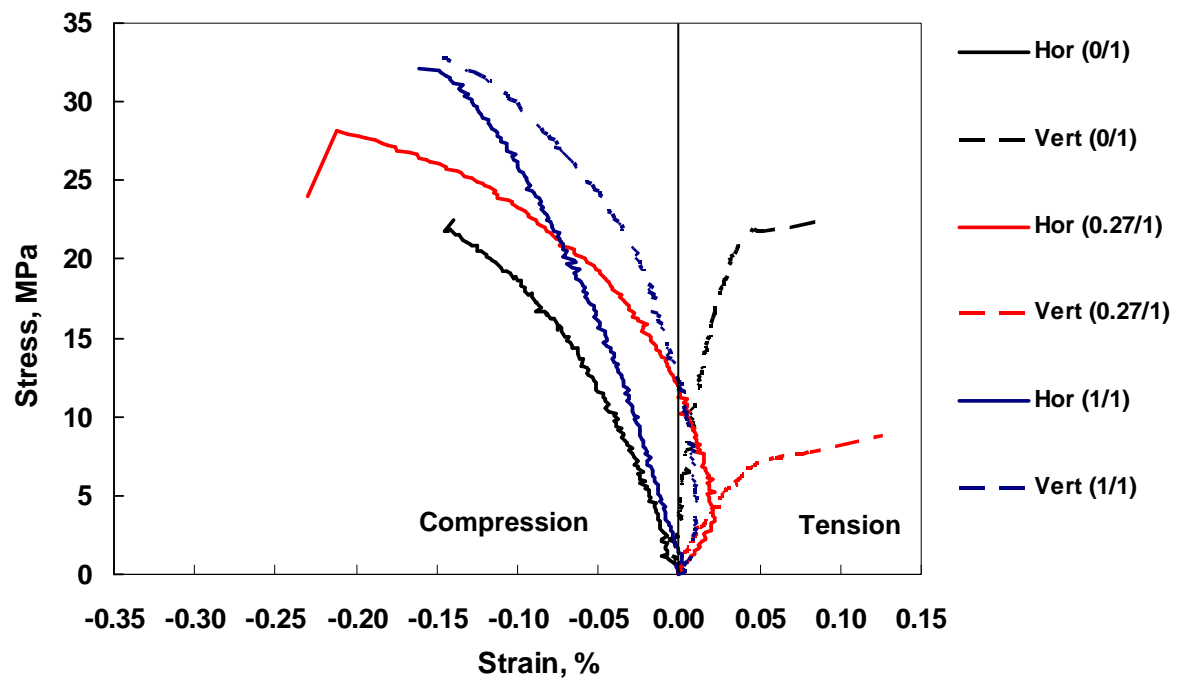


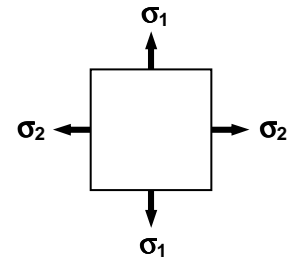
Figure 5.9 Stress-strain relationships for specimens loaded using Vesconite

5.7 POISSON'S RATIO

Graphs of vertical strains against horizontal strains were plotted for the data used in Figures 5.8 and 5.9 (see figures 5.10 and 5.11).

General expressions for the ratios of the vertical strains to horizontal strains in terms of the applied stress ratios and Poisson's ratio were derived from material law expressions.

Let r be the applied stress ratio. That is, $r = \sigma_1 / \sigma_2$



For plane stress situation, the strains due to vertical and horizontal stresses σ_1 and σ_2 respectively are given by (Megson, 1996):

$$\varepsilon_1 = \frac{1}{E}(\sigma_1 - \nu\sigma_2) \quad (5.1)$$

$$\varepsilon_2 = \frac{1}{E}(\sigma_2 - \nu\sigma_1) \quad (5.2)$$

Dividing (5.1) by (5.2) yields

$$\begin{aligned} \frac{\varepsilon_1}{\varepsilon_2} &= \frac{\sigma_1 - \nu\sigma_2}{\sigma_2 - \nu\sigma_1} \\ &= \frac{\sigma_1 / \sigma_2 - \nu}{1 - \nu \cdot \sigma_1 / \sigma_2} \\ &= \frac{r - \nu}{1 - \nu \cdot r} = m \end{aligned} \quad (5.3)$$

Therefore,

$$\varepsilon_1 = \left(\frac{r - \nu}{1 - \nu \cdot r} \right) \varepsilon_2 \quad (5.4)$$

$$\varepsilon_1 = m\varepsilon_2 \quad (5.5)$$

This is the general equation for the strains with respect to applied stress ratio and Poisson's ratio. The part $(r - \nu)/(1 - \nu r)$ in equation 5.4 represents the slope of the graph of vertical strains against horizontal strains. This means that the slope is influenced by the applied stress ratio and Poisson's ratio. In the previously derived expressions, an assumption is made that the Elastic moduli in compression is the same as in tension and that the material is isotropic.

For the stress ratio of 0 (0/1), equation 5.4 or 5.5 becomes

$$\varepsilon_1 = -\nu\varepsilon_2 \quad (5.6)$$

This is the equation for the uni-axial stress case. The slope of the graph of vertical strains against horizontal strains m becomes $-\nu$, which is negative of the Poisson's ratio. In order to determine the value of Poisson's ratio for SHCC, the slopes of the graphs plotted from uni-axial data for both steel and Vesconite, were determined by using linear regression analysis. The slopes of the best fit straight lines obtained in this manner were substituted into equation 5.5. The resulting expressions relating the strains are shown in tables 5.8 and 5.9.

Recall from equation 5.3:

$$m = \frac{r - \nu}{1 - \nu \cdot r}$$

By rearranging the equation for slope we get:

$$\nu = \left(\frac{m - r}{mr - 1} \right) \quad (5.7)$$

This is the derived equation for Poisson's ratio and the values for stress path angles of 0° and 15° are obtainable in table 5.8 and 5.9. The values for the stress path angle of 45° were not included because the equation of Poisson's ratio derived gives a meaningless result for this case.

Table 5.8 Expressions for strains for specimens tested using steel

Stress Path angle (degrees)	Stress Ratio r	Slope $m = \left(\frac{r - \nu}{1 - \nu \cdot r} \right)$	Expression $\varepsilon_1 = \left(\frac{r - \nu}{1 - \nu \cdot r} \right) \varepsilon_2$	Poisson's Ratio $\nu = \left(\frac{m - r}{mr - 1} \right)$
0	0.00	-0.2562	$\varepsilon_1 = -0.2562\varepsilon_2$	0.2562
15	0.27	-0.0885	$\varepsilon_1 = -0.0885\varepsilon_2$	0.35
45	1.00	1	$\varepsilon_1 = 1.0\varepsilon_2$	--

Table 5.9 Expressions for strains for specimens tested using Vesconite

Stress Path angle (degrees)	Stress Ratio r	Slope $m = \left(\frac{r - \nu}{1 - \nu \cdot r} \right)$	Expression $\varepsilon_1 = \left(\frac{r - \nu}{1 - \nu \cdot r} \right) \varepsilon_2$	Poisson's Ratio $\nu = \left(\frac{m - r}{mr - 1} \right)$
0	0.00	-0.3139	$\varepsilon_1 = -0.3139\varepsilon_2$	0.31
15	0.27	-0.2404	$\varepsilon_1 = -0.2404\varepsilon_2$	0.48
45	1.00	1	$\varepsilon_1 = 1.0\varepsilon_2$	--

The values of Poisson's ratio calculated using uni-axial data were different for steel and Vesconite: the value for steel was lower than for Vesconite. This could be because of the restraining effect of the steel platens resulting in an apparently "stiffer" material. The values of Poisson's ratios calculated from the derived equation were also different from the uni-axial values. This could be because of the assumption that there were not stresses in the out-of-plane direction. This assumption was made because it was assumed initially that the fibres were to be randomly aligned in the plane of the applied loads, resulting in a plane stress situation. However, there is a possibility that there was a considerable amount of fibres aligned in the out-of-plane direction giving rise to stresses in that direction as the fibres provided resistance to deformations. This possible triaxial stress state can render the expressions used for estimating

Poisson's ratio invalid. See the equations 5.8 and 5.9 below relating strains and stresses to Elastic modulus and Poisson's ratio for plane stress or 2-dimensional case.

Plane stress:

$$\{\varepsilon\} = \frac{1}{E} \begin{bmatrix} 1 & -\nu & 0 \\ -\nu & 1 & 0 \\ 0 & 0 & 2(1+\nu) \end{bmatrix} \{\sigma\}, \quad (5.8)$$

or inversely

$$\{\sigma\} = \frac{E}{(1-\nu^2)} \begin{bmatrix} 1 & \nu & 0 \\ \nu & 1 & 0 \\ 0 & 0 & \frac{1-\nu}{2} \end{bmatrix} \{\varepsilon\} \quad (5.9)$$

Figure 5.10 and 5.11 show graphs of vertical strains against horizontal strains for specimens tested using steel directly and those tested using Vesconite respectively. The straight lines in both figures were plotted from the expressions for strains in tables 5.8 and 5.9. It can be seen that the results for steel platens followed the trends of the straight lines while the ones for Vesconite did not.

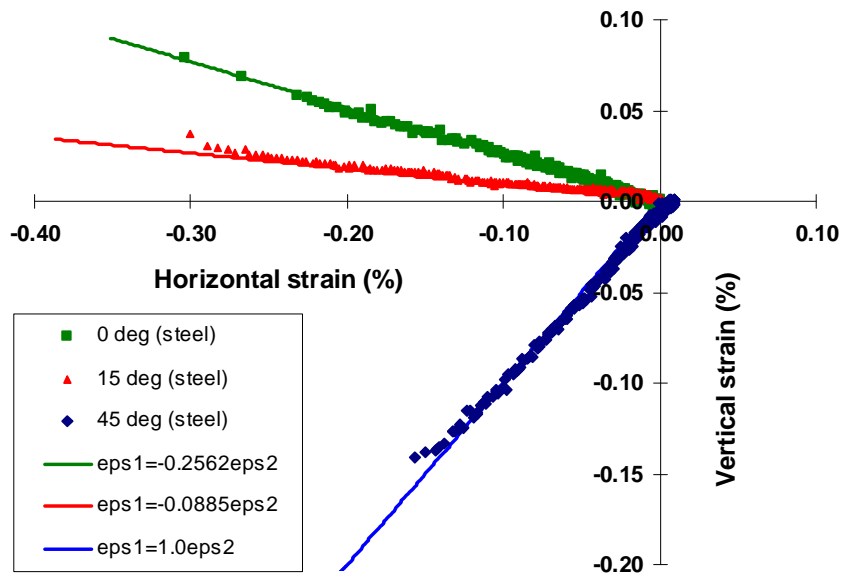


Figure 5.10 Vertical strain against horizontal strain for specimens tested using steel

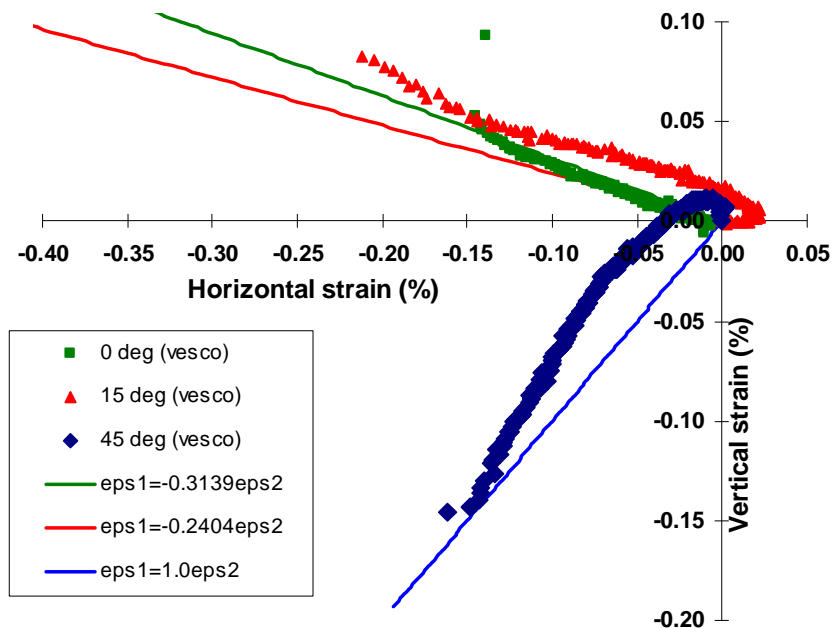


Figure 5.11 Vertical strain against horizontal strain for specimens tested using Vesconite

5.8 CONCLUSION

The results for all the experiments conducted were presented. It was found that the results obtained from the testing of cylindrical and cubical specimens had irregularities. However, the results obtained from testing of dumbbell and square biaxial plate specimens followed expected trends; with strengths decreasing with decreasing testing ages. The points used to plot the failure envelope also showed irregularities because they were normalised using the strengths obtained from cylindrical specimens.

Additionally, the strengths obtained from testing of square biaxial plate specimens were lower for specimens tested using Vesconite than those tested using steel directly. Thus, the use of Vesconite did reduce the restraining effect of the frictional force between the specimen and steel loading platens.

The value of Poisson's ratio was also estimated from the derived expressions. These expressions made the assumption that the Elastic moduli in tension and compression were the same and that the problem dealt with was a plane stress one. The values obtained were different for stress path angles of 0^0 and 15^0 , and for specimens tested using steel and Vesconite. The possibility of triaxial stress state exists.

Lastly, the stress-strain relationships were plotted from the synchronised ARAMIS and Instron data. In the following chapter, the results presented in this chapter will be analysed and discussed.

CHAPTER 6

ANALYSIS AND DISCUSSION OF RESULTS

6.1 INTRODUCTION

This part of the thesis will be concerned with the analysis and discussion of the results obtained previously in Chapter 5. The discussion will form the basis for the recommendations and conclusions in Chapter 7.

In this chapter, the main concern will be the results obtained from biaxial tests: the failure envelope, stress-strain relationship and observed crack patterns.

6.2 FAILURE ENVELOPE

According to the study conducted by Yin et. al. (1990), in which they studied the behaviour of fibre reinforced concretes (FRC) of different fibre compositions under biaxial compression, it was found that the addition of fibres did not have an effect on the uniaxial strength of FRC while the effect was significant under biaxial compression. In this study, no comparison was made between SHCC and normal concrete. However, comparison was made between two loading media: steel and Vesconite.

It would be expected under desirable conditions that the normalised stress under uni-axial loading (ie. stress ratio 0/1 or angle 0^0) in figure 5.6 would be equal to unity, signifying equal average cylinder strength to biaxial plate strength. This is not the case because of varying cylinder strengths used for normalising the biaxial results. If it is assumed that this problem was absent in

the results, and also considering the relative magnitudes of the normalised stresses for specimens loaded using steel directly and those tested using Vesconite, it can be seen that the results from specimens tested using Vesconite were lower than those obtained from testing using steel platens only.

In normal concrete, the strength under biaxial stresses is higher than under simple uniaxial stresses (Kupfer et. al, 1973). Similarly, the strength of SHCC under biaxial compression was also found to be higher than that under uni-axial compression. For specimens tested using steel platens only, the ratio of the applied stress to the average cylinder strength ranged from roughly 0.9 to 1.2 for stress path angle 0° to 45° respectively. For those tested using Vesconite, it ranged roughly between 0.85 and 1.05 for stress path angles 0° to 45° respectively.

6.3 BIAXIAL STRESS-STRAIN RELATIONSHIPS

The stress-strain relationships of tests done for SHCC plates are shown in figures 5.8 and 5.9 for steel and Vesconite respectively. In the two figures, the stresses are plotted against the corresponding strains for all stress ratios except for the one for the uni-axial case (ratio 0/1 or path 0°). In the case of stress ratio of 0/1, the stress-strain curve for the principal direction perpendicular to that of loading was obtained by plotting major principal stresses against the minor principal strains. That is, while there corresponding stresses and strains that can be plotted against one another for all other stress ratios in both directions of loading, this was not the case for the uni-axial case. The applied stress was in one direction only while the resulting strains in both directions. Since there were no stresses applied in the minor axis direction for the uniaxial case, it would make no sense to plot the resulting strains with zero stress; so it was decided to plot the applied uni-axial stresses against the resulting tensile strains.

Additionally, the stress-strain curves showing tensile strains in the minor principal direction show slight indication of strain-hardening, which is typical of SHCC. This behaviour could not be clearly seen because of the very low sampling rate of the GOM ARAMIS system that was used to measure deformations relative to that of the Instron system. The sampling rate of GOM ARAMIS was 1 Hz while that of Instron 25 Hz.

Furthermore, the stress-strain relationships shown in figures 5.8 and 5.9 can be improved by coupling the data logging of the applied loads and the measured resulting deformations. It would therefore be advisable that this is taken into consideration in the future biaxial experimental work.

6.4 OBSERVED FAILURE MODES

While the results obtained from biaxial compressive testing did not show particular characteristics that can be attributed to the SHCC material, the observed crack or failure patterns showed interesting characteristics, namely multiple cracking in the thickness direction (unloaded direction). Typical crack patterns are shown in table 6.1 for stress path angles of 0° , 15° , 30° and 45° for steel and Vesconite.

In table 6.1, the crack patterns for specimens tested using steel platens directly are shown by sketches a), c), e) and g). For those tested using Vesconite, typical crack patterns are shown by sketches b), d), f) and h). When comparing the sketches for patterns of specimens tested using steel and those of specimens tested using Vesconite, it can be seen that the observed crack patterns did not differ noticeably due to different loading media for a particular stress path angle or ratio. The salient feature for all the patterns is the presence of multiple hair line cracks along the thickness of the plates in the direction perpendicular to that of loading accompanied by shear slip type of failure as opposed to single wide cracks and tensile splitting type of failure for normal

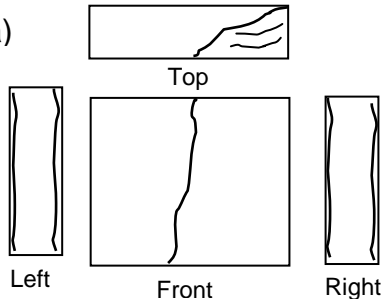
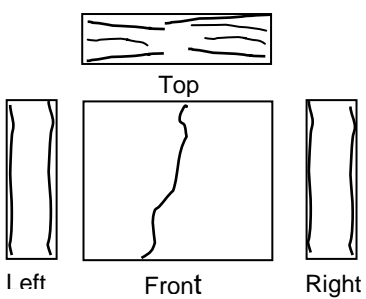
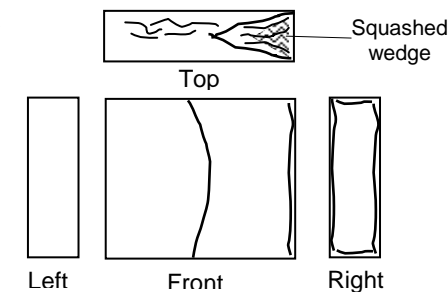
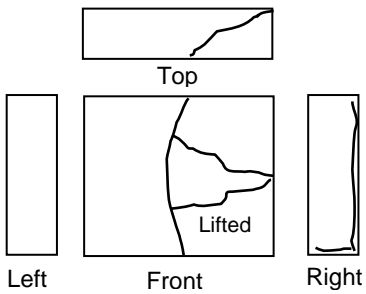
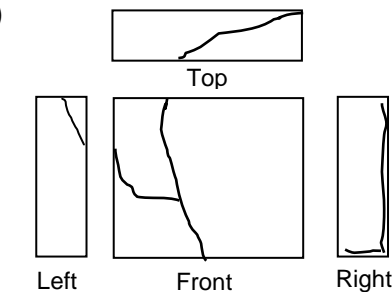
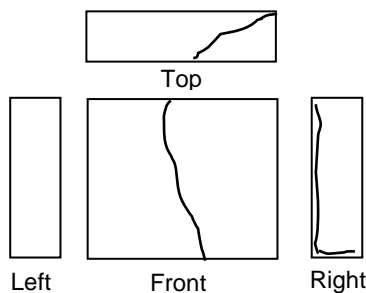
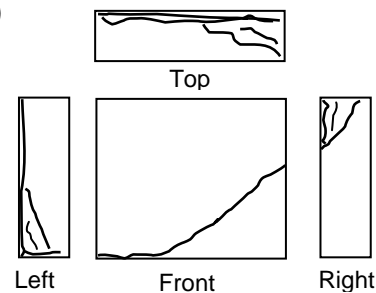
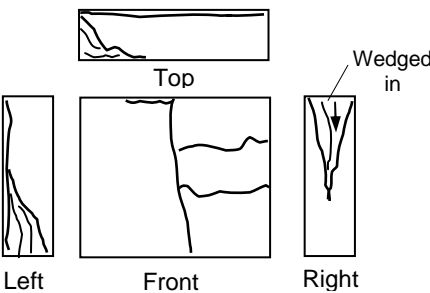
concrete (Yin et. al., 1990). This behaviour, which can be attributed to SHCC, was due to the tensile strains in thickness or transverse direction (out-of-plane) that resulted from the biaxial compressive stress state in the plane of the applied loads. It would therefore be advisable to measure strains in the out-of-plane direction in order to be able to accurately describe biaxial behaviour of SHCC in future work.

The sketches in table 6.1 show four views of the plate specimen: top, left, front and right views. The bottom and rear views were not included because they were similar to the top and front views respectively. For the uni-axial case (stress path 0°), the specimens tested using steel and Vesconite show vertical cracks in front view. These cracks were perpendicular to the direction of loading (major principal stress). Also, multiple micro-cracking could be seen on the top view of the specimens for this stress ratio. This feature could not be seen on the left and right hand views because of the relatively high load causing friction that prevented straining on these edges.

For the other stress path angles, the cracks on the front view showed to deviate from vertical with increasing stress path angle. That is, the inclination angles of the front cracks with the vertical increased slightly from vertical to almost diagonal from stress path 0° to 45° respectively. The shear slip type of failure was evident in all failure patterns. This was seen by the clearly visible wedges that appeared on the edges perpendicular to the ones onto which the major principal stresses were applied for stress path angles 0° , 15° and 30° directions; and on all the edges for stress path 45° .

Also important to notice were the diagonal cracks that formed wedges on the edges of the specimens: their ends coincided with the front vertical and near diagonal cracks showing that there were bodies of material that were sliding against another as the specimens failed. This is also indicative of shear type of failure.

Table 6.1 Typical crack patterns

Angle	Steel	Vesconite
0°	<p>a)</p>  <p>Top</p> <p>Left Front Right</p> <p>Major principal stress – horizontal.</p>	<p>b)</p>  <p>Top</p> <p>Left Front Right</p> <p>Major principal stress – horizontal.</p>
15°	<p>c)</p>  <p>Top</p> <p>Left Front Right</p> <p>Squashed wedge</p> <p>Major principal stress – horizontal.</p>	<p>d)</p>  <p>Top</p> <p>Left Front Right</p> <p>Lifted</p> <p>Major principal stress – horizontal.</p>
30°	<p>e)</p>  <p>Top</p> <p>Left Front Right</p> <p>Major principal stress – horizontal.</p>	<p>f)</p>  <p>Top</p> <p>Left Front Right</p> <p>Major principal stress – horizontal.</p>
45°	<p>g)</p>  <p>Top</p> <p>Left Front Right</p> <p>Major principal stress – both directions.</p>	<p>h)</p>  <p>Top</p> <p>Left Front Right</p> <p>Wedged in</p> <p>Major principal stress – both directions.</p>

6.5 CONCLUSION

The results obtained from the biaxial compressive testing of SHCC plates have been analysed and discussed. The biaxial envelope for specimens tested using steel platens yielded higher results than those tested using Vesconite. The biaxial stress-strains relationships showed increased stiffness of the material with increasing stress path angles for compressive strains. The reverse was seen where tensile strains were measured.

The observed crack patterns showed evidence of multiple micro-cracking due to tensile strains in the unloaded direction of the specimens. These patterns further showed that all specimens failed by shear slip type mechanism.

The following chapter will focus on the observations and conclusions made from this experimental work; and recommendations for future researchers who will be doing extensions to this study.

CHAPTER 7

RECOMMENDATIONS AND CONCLUSIONS

7.1 INTRODUCTION

This is the final chapter of the thesis. Chapter 1 was introduction in which the overview, background and literature study for this work were explained. Chapter 2 focused on the known properties of SHCC for the benefit of the novice on the subject matter.

In Chapters 3 through 6, all aspects of the experiments that were conducted were discussed. That is, the experimental design, experimental programme, experimental results; and analysis and discussion of results.

In this chapter observations made from the results obtained (numerical and visual) will be discussed. It will be from this that conclusions on the behaviour of SHCC under biaxial compressive stresses will be made. Since these were the first biaxial experiments done on SHCC at postgraduate level at Stellenbosch University, there were a number of problems that only became evident after obtaining the results. Such problems included the unanticipated limitations of and inadequate knowledge of testing equipment, the choice of equipment for measuring deformations, the chosen ages of testing and the adverse effect of using uncoupled systems to apply forces and to measure deformations. However, the observations herein will serve to inform future researchers who will be conducting further biaxial testing on the SHCC material. Parts of this research could therefore, to some extent, be considered as pilot work for biaxial testing of SHCC.

7.2 OBSERVATIONS

With respect to the testing age of SHCC under simple uni-axial tensile, compressive and biaxial loading condition, the material was found to be very sensitive to increase of strength at different ages. This could be attributed to the use of fly ash in the mix whose delayed reaction could have been activated from ages 20 to 28 days and thereby continuing the gain in strength between those ages.

Under biaxial compression stress state, the strain-hardening characteristic of SHCC could not be seen in the plane of loading but there was evidence of multiple micro-cracking on the specimens in the out-of-plane direction. The multiple micro-cracking phenomenon was accompanied by formation of wedges and shear slip type of failure. Recall that the strain-hardening characteristic of SHCC is dominant in tension.

Stress-strain relationships for specimens subjected to stress ratios such that tensile strains were experienced in the minor principal direction, showed slight evidence of strain hardening. In the tensile straining range, the material was found to increase in stiffness with decrease in stress path angle. In contrast, it was seen from the results that under biaxial compressive straining, the stiffness of the material increased with increasing stress path angles.

7.3 RECOMMENDATIONS

In view of the observations made from this experimental work, the following recommendations are made:

- The study of the strength gain of the SHCC material developed at Stellenbosch University must be undertaken for tensile and compressive strengths for up to say 90 days by testing dumbbell and cylindrical specimens

respectively. This will inform researchers on the right age to conduct biaxial testing where strength gain is minimal.

- The systems applying the forces and measuring deformations must be coupled by using a common data logger to ensure that the correct force is associated with the correct corresponding displacement at any particular time.
- Capacitance transducers such as LVDT's that can be attached directly to the specimens must be used instead of GOM ARAMIS images to measure deformations because of the ease with which they can be connected to a data logging system like Spider8 and that data obtained from them does not require extensive processing, which could lead to human error, as it is the case for ARAMIS data. However, the ARAMIS system may still be used for studying local behaviour of specific areas of specimens.
- The loading rates must be reduced to lengthen each experiment so that strain-hardening behaviour can be observed in the tensile straining ranges of biaxial stress-strain relationships. This must also be accompanied by the sampling rate of at least 10 Hz for both load and displacement measurement systems.

7.4 CONCLUSIONS

SHCC was designed to have strain-hardening behaviour under simple uni-axial tensile loading after occurrence of first crack; accompanied by multiple micro-cracking. The formation of numerous closely spaced hair-line cracks is a good characteristic in a cementitious composite in that ingress of harmful substances into materials in harsh environments can be minimised thereby improving durability of reinforced concrete infrastructure incorporating SHCC as an outer layer.

In this study, the behaviour of SHCC under biaxial compression was investigated through experimentation. It was found that under complex stress

state, aspects of strain-hardening could not be seen in the plane of loading and in stress-strain relationships where compressive strains were measured.

However, the following features that could be attributed to the known behaviour of SHCC were:

- Slight evidence of strain hardening in stress-strain relationships where tensile strains were measured;
- Appearance of closely spaced multiple micro-cracks which were parallel to the applied loads on the edges of specimens.
- The wedging in of the displaced bodies of material in the direction of maximum principal stresses. This could have been purely due to the material being fibre reinforced or the way in which the material was cast that influenced the direction of the fibres to be dominantly randomly aligned in the plane of loading.
- In contrast to the tensile splitting failure mechanism observed in normal concrete, the general failure mechanism for SHCC under biaxial compression was shear slip type.
- The direction of cracks appearing in front of SHCC plate specimens were vertical to near diagonal for stress paths angles 0° through 45° ;
- Although plane stress situation was assumed, the possibility of triaxial stress state exists.
- The strengths of SHCC under biaxial compression were higher than for uni-axial cases. The biaxial strengths for specimens tested using steel platens directly were higher than that for those tested using Vesconite.

REFERENCES

Boshoff, WP. and van Zijl, GPAG. (2007) A computational model for strain-hardening fibre-reinforced cement-based composites. *J SAICE*, 49(2) 24-31.

Boshoff, WP. and van Zijl, GPAG. (2008), FRC in South Africa - application fields, new developments and outlook, Proceedings ICCX 2008 Sun City, South africa.

Diana (2009). User Manual for Diana finite element software, version 9.3.

Ehm, C. and Schneider, U. (1985) The high temperature behaviour of concrete under biaxial conditions, *Cement and Concrete Research*, Vol. 15, pp. 27-34, Pergamon Press, USA.

Hussein, A. and Marzouk, H. (2000) Behavior of High-Strength Concrete under Biaxial Stresses, *ACI Materials Journal*, Volume 97, No. 1, pp 27-36.

Kupfer, HB. and Gerstle, KH. (1973), Behaviour of concrete under biaxial stresses, *Journal of the Engineering Mechanics Division*, pp 853-866.

Li, VC. (2002), Reflections on the Research and Development of Engineered Cementitious Composites (ECC), Proceedings of the JCI International Workshop on Ductile Fibre Reinforced Cementitious Composite (DFRCC) – Application and Evaluation (DFRCC-2002), Takayama, Japan.

Li, VC. (2002), Advances in ECC Research, ACI Special Publication on Concrete: Material Science to Applications, SP 206-23, pp. 373-400.

Megson, THG. (1996), Structural and stress analysis, Butterworth Heinemann, United Kingdom.

Shang, Q. (2006), Shear behaviour of Engineered Cement-based composites, Master of Science (Engineering) Thesis, Stellenbosch University.

Van Zijl, GPAG. (2007), Improved mechanical performance: Shear behaviour of strain hardening cement-based composites (SHCC). Cement and Concrete Research, 37(8), pp. 1241-1247.

Van Zijl, GPAG. (2009). Constitutive model for fibre-reinforced strain-hardening cement composites (SHCC), Concrete / Beton, Journal of the Concrete Society of Southern Africa, November 2009 issue.

Yin, WS., Eric, C., Su, M., Mansur, MA. Hsu, TC. (1990), Fiber-reinforced concrete under biaxial compression, Engineering Fracture Mechanics, Vol 35, No. 1/2/3, pp. 261-268, Great Britain.

BIBLIOGRAPHY

Adendorff, CJ. Boshoff, WP. van Zijl, GPAG. (2009), Characterisation of crack distribution of Strain-hardened Cement Composites (SHCC) under imposed strain, *Advances Cement-Based Materials*, pp. 215-221, CRC Press, London.

Boshoff WP and van Zijl GPAG. (2007), Time-dependent response of ECC: Characterisation of creep and rate dependence. *Cement and Concrete Research*, 37, pp. 725-734.

Coates, RC. Coutie, MG. Kong, FK. (1988), *Structural Analysis*, Third edition, Chapman and Hall, United Kingdom.

Collins, MP. Mitchell, D. Adebar, P. Vecchioni, FJ. (1996), A general shear design method, *ACI Structural Journal*, Volume 93, No. 1, pp 36-45.

Matsumoto, T. and Mihashi, H. (2002), JCI-DFRCC Summary Report on DFRCC Terminologies and Application concepts, *Proceedings of the JCI International Workshop on Ductile Fibre Reinforced Cementitious Composite (DFRCC) – Application and Evaluation (DFRCC-2002)*, Takayama, Japan.

Stander, H. 2007, *Interfacial Bond Properties For ECC Overlay Systems*, Master of Science (Engineering) Thesis, Stellenbosch University.

Van Mier, J. (1984), *Strain-softening of concrete under multiaxial loading conditions*, PhD Thesis, Netherlands.

Van Zijl, GPAG. (2008), Mechanisms of creep in fibre-reinforced strain-hardening cement composites (SHCC), accepted for *Proceedings of 8th International Conference on Creep, Shrinkage and Durability of Concrete and Concrete Structures (CONCREEP 8)*, Oct 2008, Ise-Shima, Japan.

Visser, C. (2007), Mechanical and Structural characterization of Extrusion moulded SHCC, Master of Science (Engineering) Thesis, Stellenbosch University.

Wikipedia, Concrete, <http://en.wikipedia.org/wiki/Concrete>, accessed on 13 October 2010.

APPENDICES

A. SHCC FE MODELS SHOWING SHEAR STRESSES

Figures A1 to A5 are contour plots of shear stresses of SHCC FE models corresponding to the normal stresses shown in figures 3.7a-e.

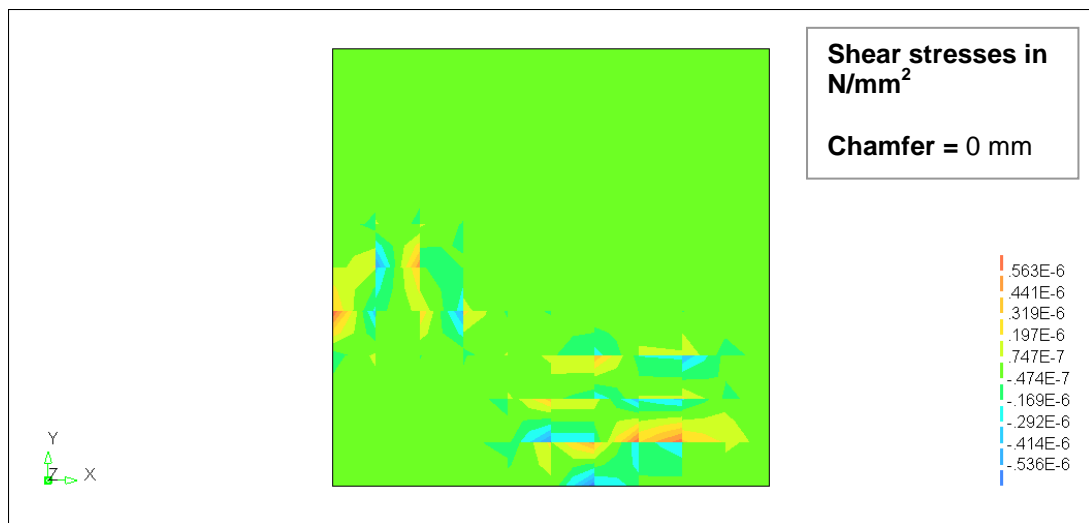


Figure A1 Shear stresses S_{xy} for model without chamfers (Diana 9.3)

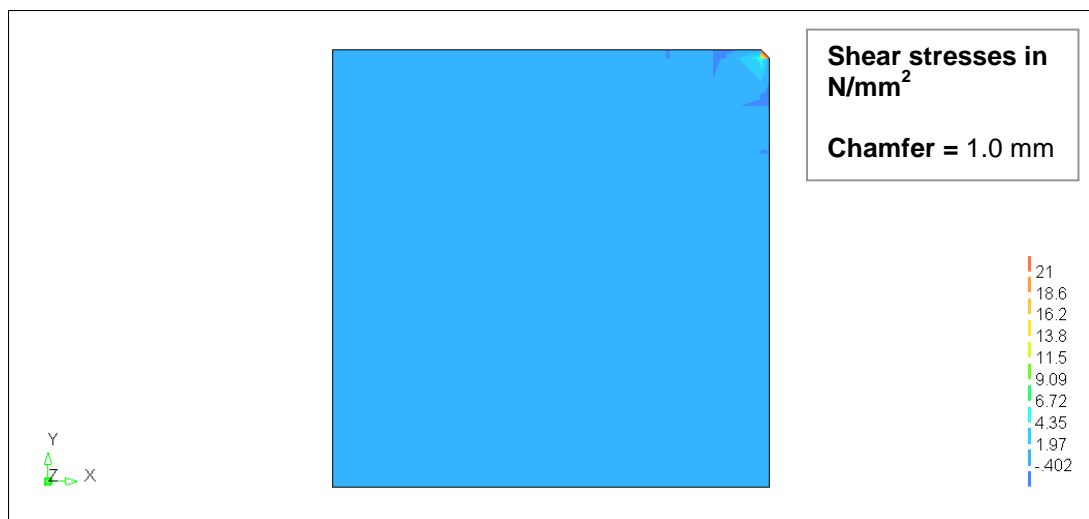


Figure A2 Shear stresses S_{xy} for model with 1 mm chamfer (Diana 9,.3)

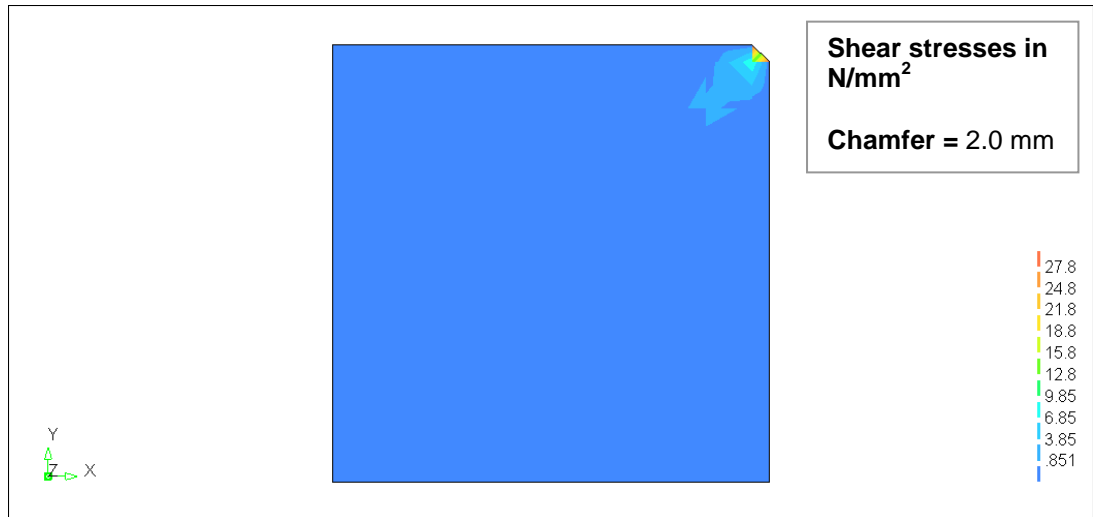


Figure A3 Shear stresses S_{xy} for model with 2 mm chamfer (Diana 9,.3)

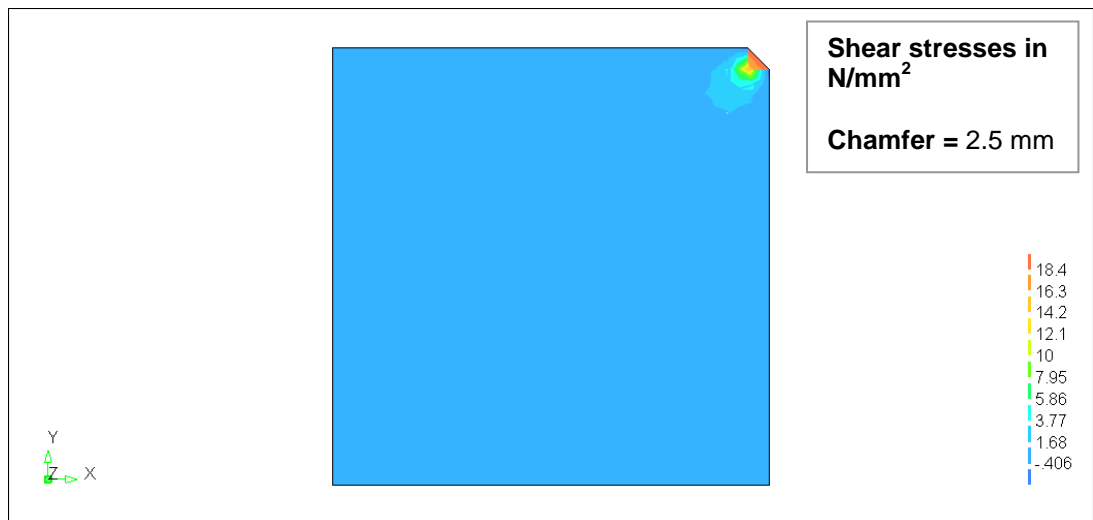


Figure A4 Shear stresses S_{xy} for model with 2.5 mm chamfer (Diana 9,.3)

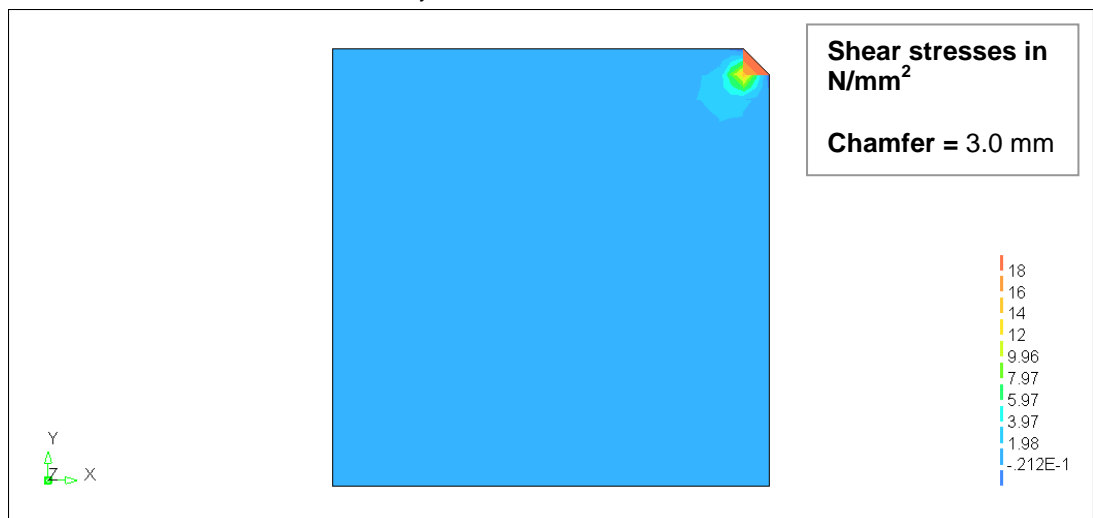


Figure A5 Shear stresses S_{xy} for model with 3 mm chamfer (Diana 9,.3)

B. STRESS-STRAIN CURVES FOR SHCC IN DIRECT TENSION

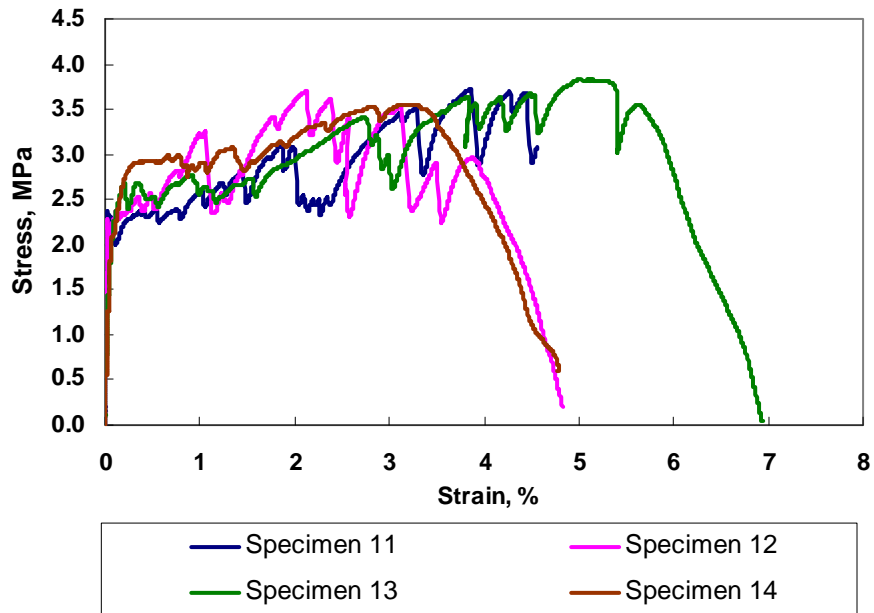


Figure B1 Tensile stress-strain curves for Dumbbells from Batch 1

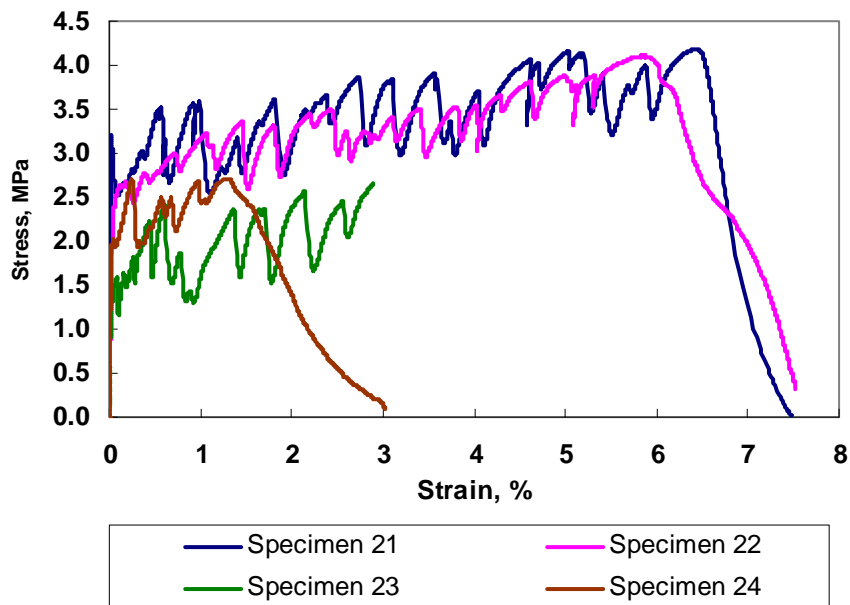


Figure B2 Tensile stress-strain curves for Dumbbells from Batch 2

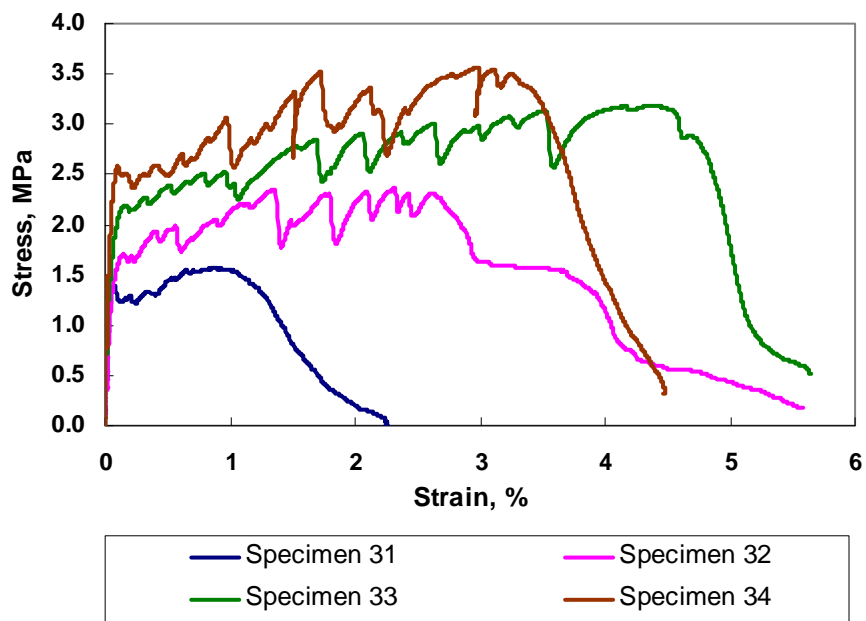


Figure B3 Tensile stress-strain curves for Dumbbells from Batch 3

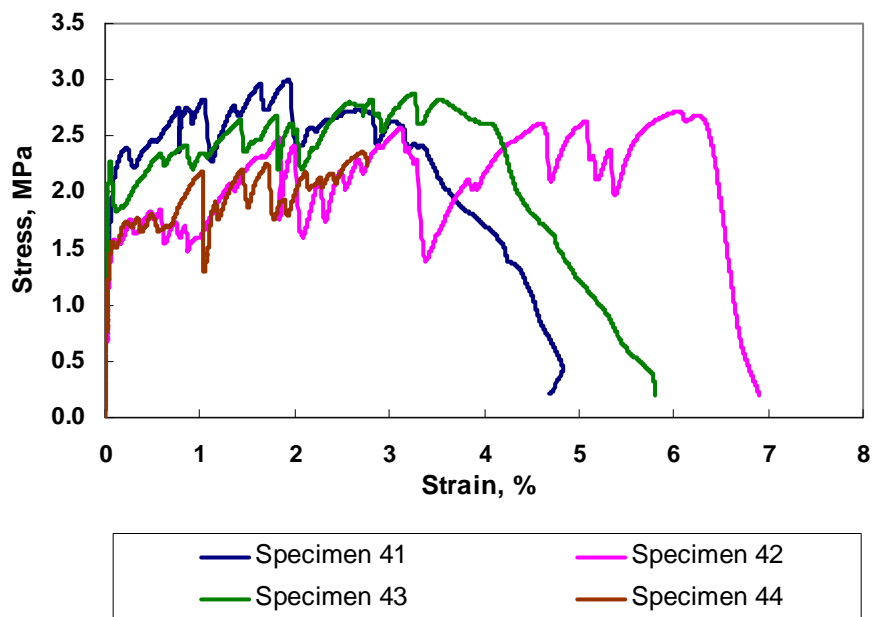


Figure B4 Tensile stress-strain curves for Dumbbells from Batch 4

C. STRESS-STRAIN CURVES FOR SHCC IN DIRECT COMPRESSION

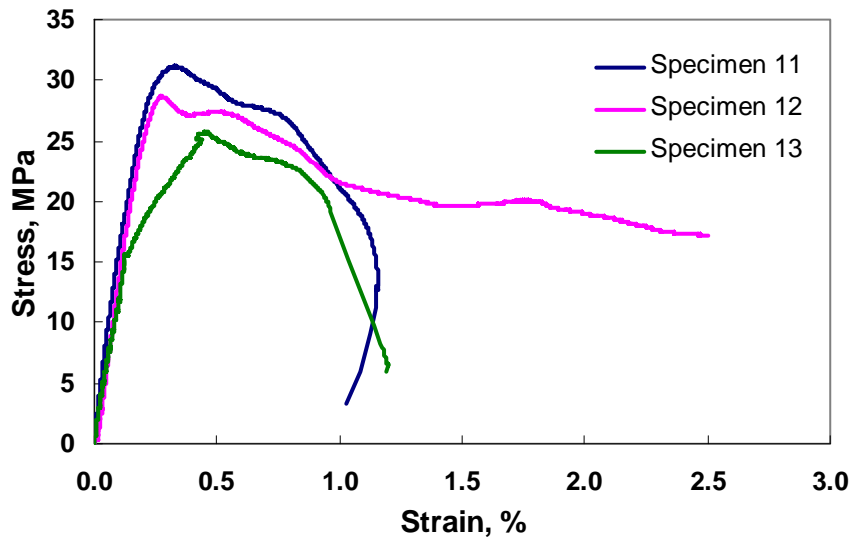


Figure C1 Compressive stress-strain curves for Cylinders from Batch 1

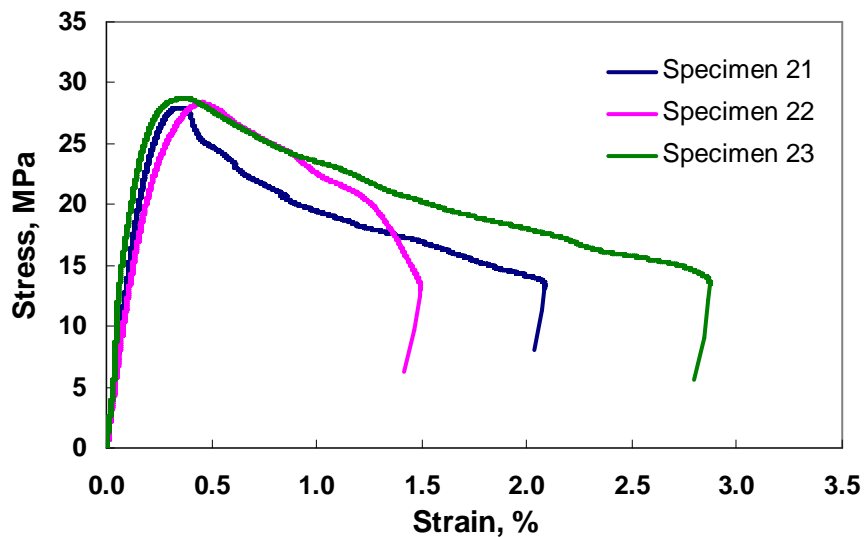


Figure C2 Compressive stress-strain curves for Cylinders from Batch 2

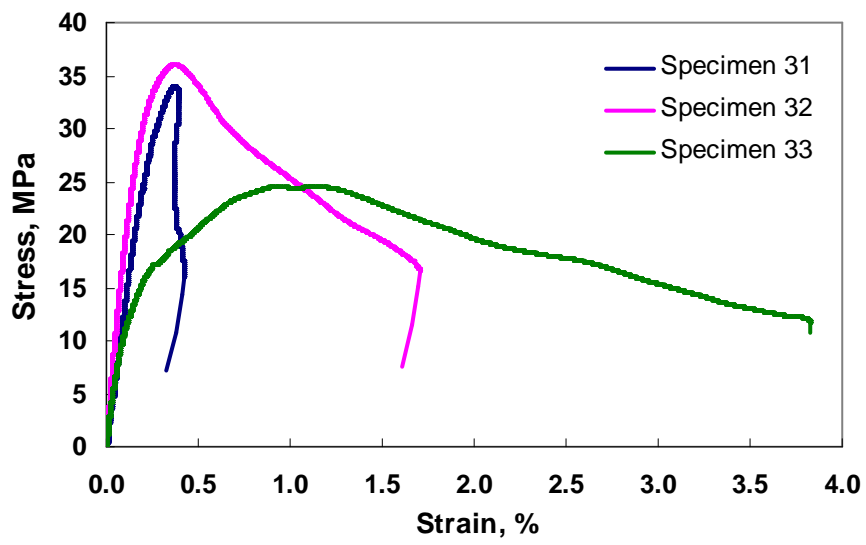


Figure C3 Compressive stress-strain curves for Cylinders from Batch 3

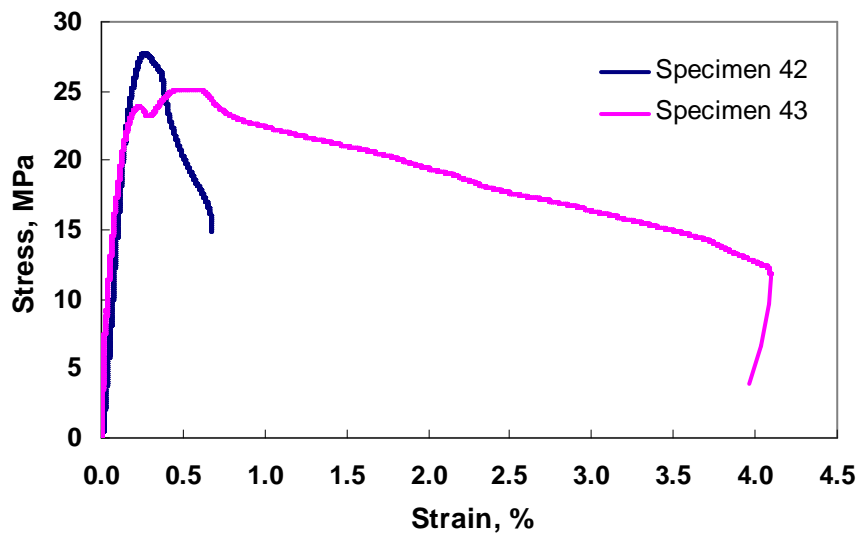


Figure C4 Compressive stress-strain curves for Cylinders from Batch 4

D. BIAXIAL RESULTS: GRAPHS OF VERTICAL LOADS AGAINST HORIZONTAL LOADS

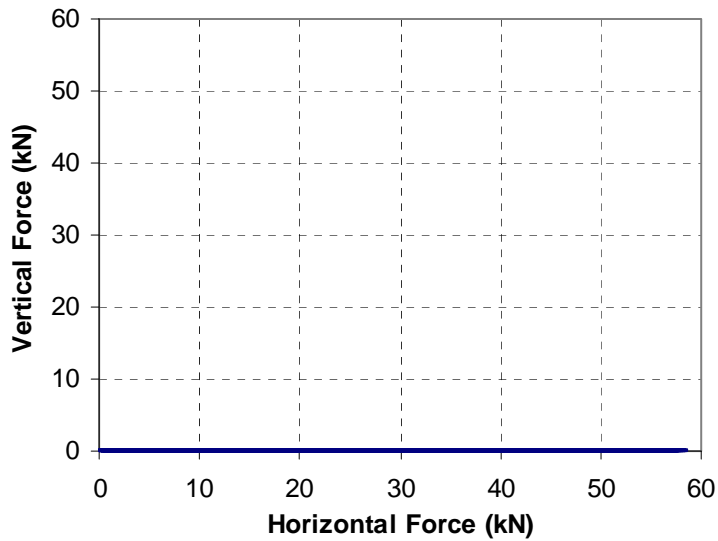


Figure D1 Typical graph of vertical force vs horizontal force for stress ratio of 0 (0°)

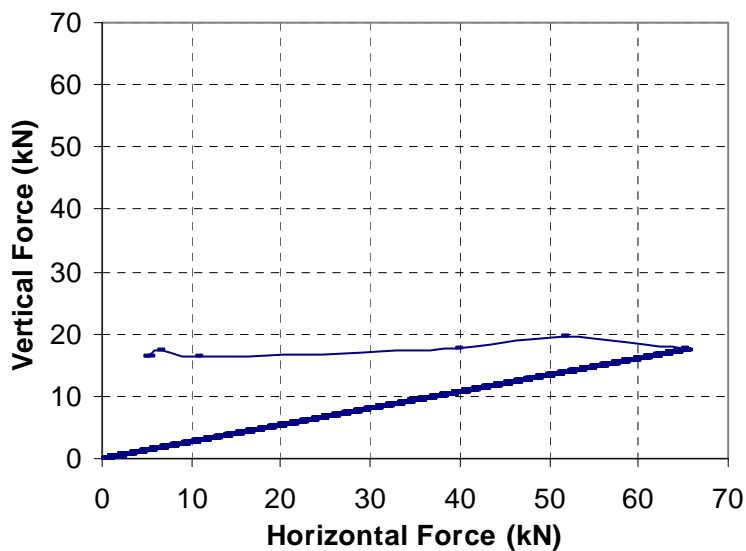


Figure D2 Typical graph of vertical force vs horizontal force for stress ratio of 0.27 (15°)

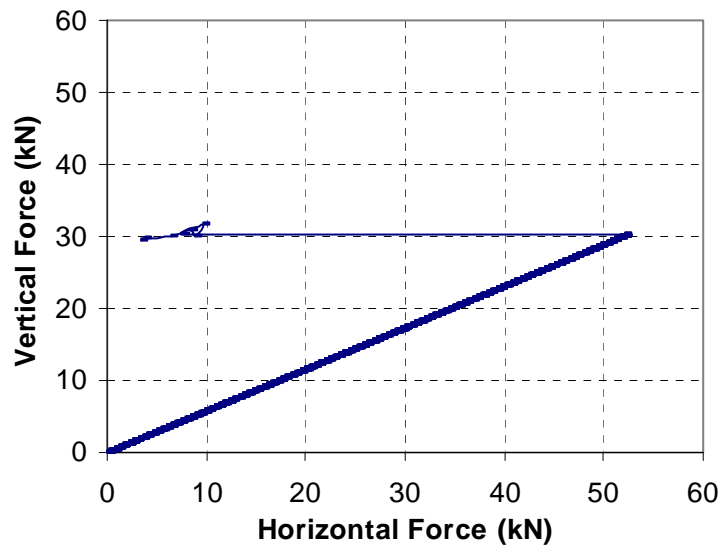


Figure D3 Typical graph of vertical force vs horizontal force for stress ratio of 0.58 (30°)

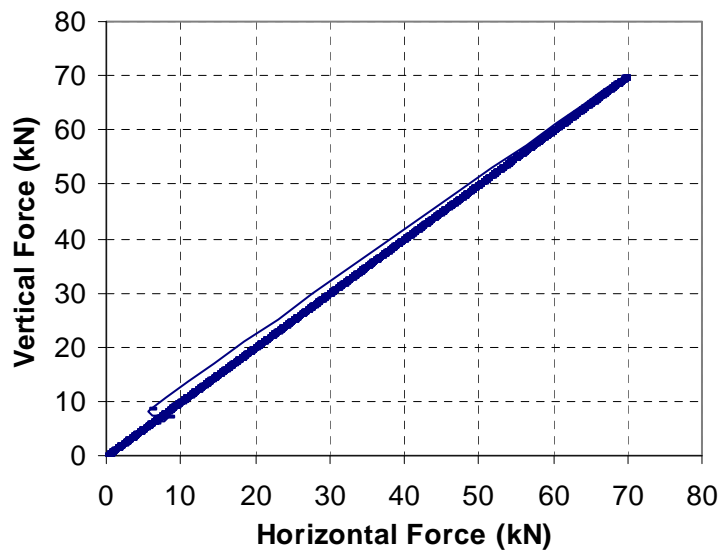


Figure D4 Typical graph of vertical force vs horizontal force for stress ratio of 1.0 (45°)

E. BIAXIAL RESULTS: LOAD-DISPLACEMENT CURVES (INSTRON)

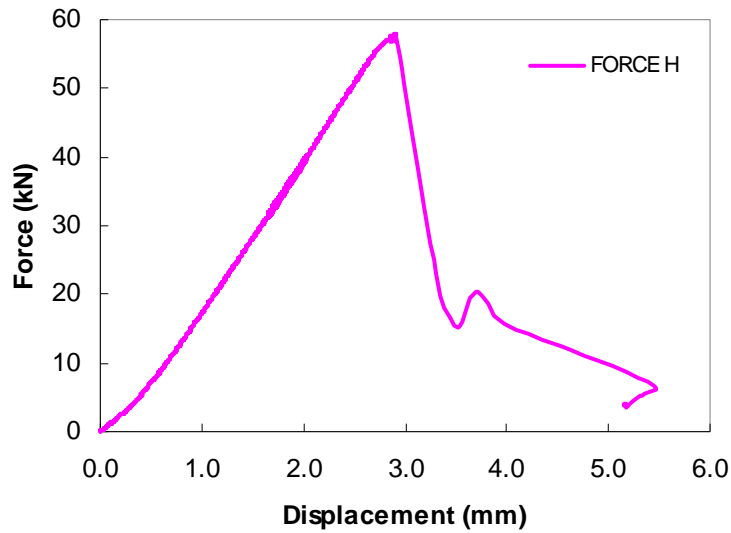


Figure E1 Typical Load-displacement curve for stress ratio of 0 (0°)

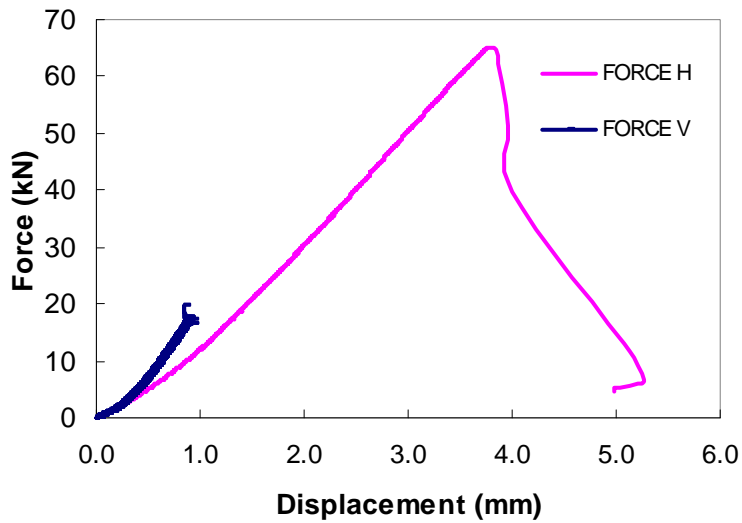


Figure E2 Typical Load-displacement curve for stress ratio of 0.27 (15°)

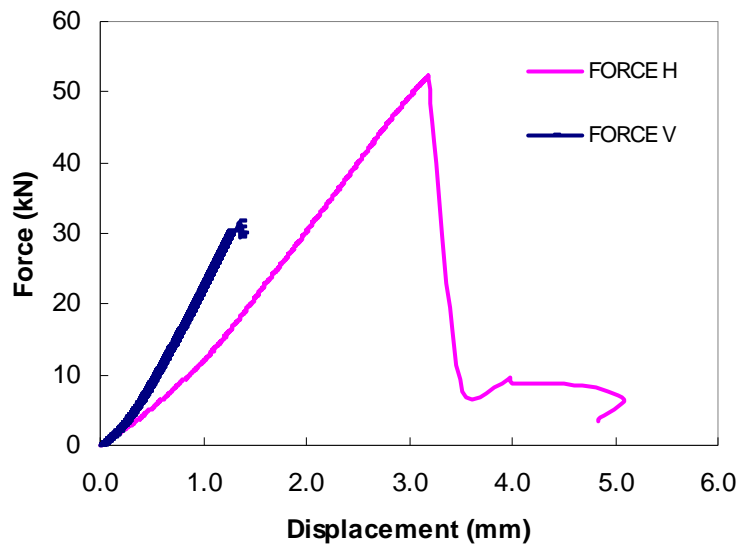


Figure E3 Typical Load-displacement curve for stress ratio of 0.58 (30°)

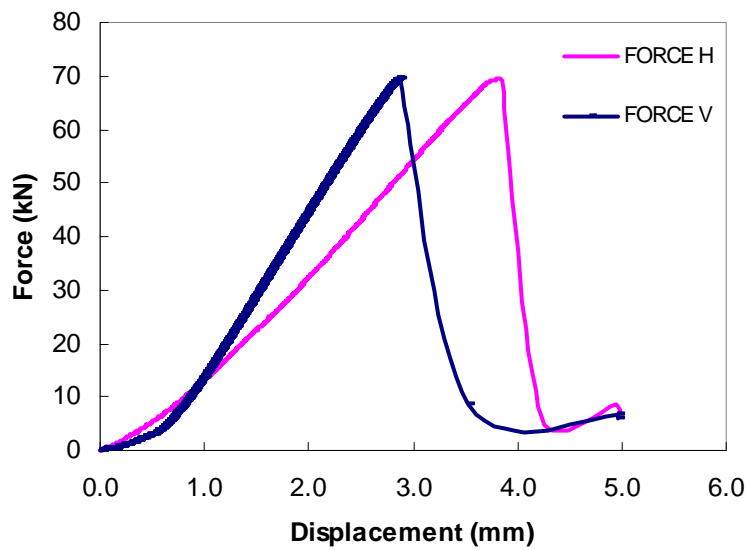


Figure E4 Typical Load-displacement curve for stress ratio of 1.0 (45°)

F. BIAXIAL TEST SETUP (PHOTOGRAPHS)

The figure below shows the picture of the biaxial setup. In the picture the following can be seen: the square plate specimen, the steel loading platen, bearing roller system, horizontal hydraulic jack, weights hanging on pulleys and GOM ARAMIS cameras mounted on tripod.

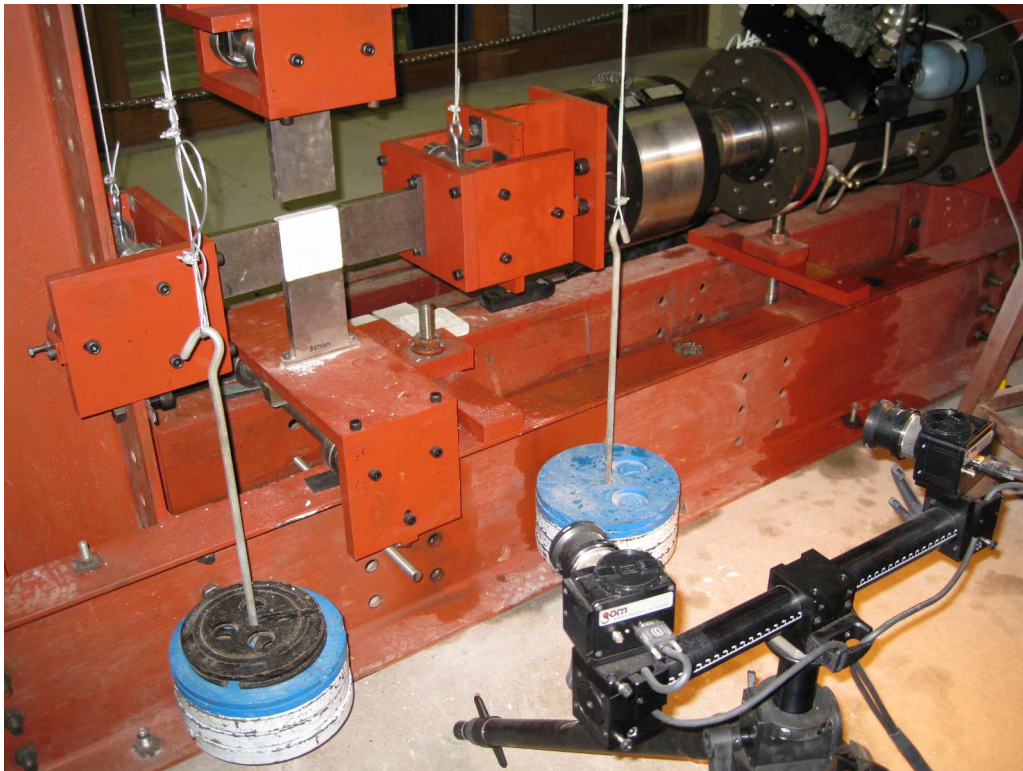


Figure F1 Picture of biaxial setup